# Effects of Variable Wind Stress on Ocean Heat Content

by

Kelly Klima

B.S. Mechanical Engineering
California Institute of Technology, 2003

M.S. Aeronautics and Astronautics
Massachusetts Institute of Technology, 2005

SUBMITTED TO THE DEPARTMENT OF EARTH, ATMOSPHERE, AND PLANETARY SCIENCE
IN PARTIAL FULFILLMENT OF THE REQUIREMENTS FOR THE DEGREE OF
MASTER OF SCIENCE IN EARTH, ATMOSPHERE, AND PLANETARY SCIENCE
AT THE
MASSACHUSETTS INSTITUTE OF TECHNOLOGY

SEPTEMBER 2008



Signature of Author……..……..
Department of Earth, Atmosphere, and Planetary Science
August 2008

Certified by……..……..
Peter Stone
Professor of Earth, Atmosphere, and Planetary Science
Thesis Supervisor

Accepted by……..……..……..
Maria T. Zuber
E.A. Griswold Professor of Geophysics
Head, Department of Earth, Atmospheric & Planetary Sciences

**Effects of Variable Wind Stress on Ocean Heat Uptake**

by

Kelly Klima

Submitted to the Department of Earth, Atmosphere, and Planetary Science
on August 8, 2008 in Partial Fulfillment of the
Requirements for the Degree of Master of Science in
At the Massachusetts Institute of Technology in
Earth, Atmosphere, and Planetary Science

## ABSTRACT

Ocean heat content change (ocean heat uptake) has an important role in variability of the Earth's heat balance. The understanding of which methods and physical processes control ocean heat uptake needs improvement in order to better understand variability in the Earth's heat balance, improve the simulation of present-day climate, and improve the understanding and projection of future climate. Wind stress can play a strong role in ocean heat uptake on all timescales, and short timescale wind stress effects have not been well studied in the literature. This study for the first time examines short timescale spatial and temporal patterns of global variable wind stress datasets in a coupled atmosphere-ocean climate model.

NCEP wind stress dataset was characterized for years 1978 to 2007. NCEP monthly means and monthly standard deviations are of the same magnitude, and strong wind stress events (tropical cyclones) are observed. A variety of metrics cannot reliably identify significant timescales or spatial patterns of the variable wind stress.

Model behavior with and without variable wind stress is studied. This study uses the MIT IGSM, a 4°×11 vertical level zonal atmospheric model coupled at the four hour timestep to a 2°×2.5°×22 vertical level ocean model with the K profile parameterization. Ocean properties in a no forcing scenario are sensitive to variable wind stress. In a weak forcing scenario (observed forcing over the last century), ocean properties are sensitive to variable wind stress, and internal modes of variability (such as an equatorial Pacific oscillation) are observed. In a global warming scenario (1% $CO_2$ rise per year or a business as usual emissions scenario), the strong forcing overwhelms the more subtle responses due to the differences in variable wind stress forcing. Regardless of forcing, the high frequency variable wind stress (monthly or less) variable wind stresses can force a low frequency response. Hence the major source of annual variability of the MOC in this coarse resolution model is surface wind variability.

Thesis Supervisor: Peter Stone
Title: Professor of Earth, Atmosphere, and Planetary Science

**ACKNOWLEDGEMENTS**

*The mind is its own place, and in itself, can make a Heaven of Hell, a Hell of Heaven.*
~ John Milton

I am truly grateful for all those who contributed to make a Heaven of Hell.

Foremost, I thank Professor Peter Stone for refining my skills, developing my cognitive abilities, and teaching me how to formulate problems and solutions. I am especially thankful for his attention to detail, which has helped me improve my writing style.

Next I would like to thank Jeff Scott. He was instrumental to my success, and I greatly appreciate his willingness to further my research. He also always bolstered my spirits, and was willing to step in whenever I needed help.

I also would like to thank all those who contributed ideas and/or data to this work. Special thanks go out to Raffaele Ferrari, Kerry Emanuel, Chris Forest, Andrei Sokolov, Stephanie Dutkiewicz, Patrick Heimbach, Chris Hill, and many others for their expert advice.

I also would like to thank the MIT Joint Program on the Science and Policy Global Change. Your existence (and free lunches) helped me make the transition to this field, for which I am truly grateful.

Next I would like to thank all the members of PAOC who made my time a memorable one. Thanks Mary, Cegeon, Brian T., Angela, Dan, Yang, Bill, Masa, Roberto, Dave, Mauro… I shall always remember you guys.

Finally I would like to thank my family, the MIT Women's Volleyball Club, the Thirsty Ear, Joyce, Emily, Leeland, Mike, and all those who have supported me through this process.

Thank you.

**CONTENTS**

## LIST OF FIGURES

## LIST OF TABLES

**NOMENCLATURE**

| | |
|---|---|
| $t$ | time (seconds) |
| $x$ | zonal component, sometimes longitude value |
| $y$ | meridional component, sometimes latitude value |
| $z$ | depth component, sometimes depth value |
| $C_D$ | drag coefficient in wind stress equation |
| $C_p$ | specific heat of water (4000 J/kgK) |
| $H$ | specific ocean depth (usually thermocline 700m, or full ocean 3000m) |
| $N$ | number of datapoints |
| $Q$ | ocean heat content (J) |
| $\dot{Q}$, $\Delta$Q, $\partial Q$ | ocean heat uptake (J/s) |
| $T$ | ocean water temperature (K) |
| $\vec{U}$ | wind velocity (m/s) |
| $V$ | volume of the fluid ($m^3$) |
| $X_i$ | particular value of the datapoint, |
| $\theta$ | latitude (degrees) |
| $\varphi$ | longitude (degrees) |
| $\rho$ | ocean water density ($kg/m^3$) |
| $\rho_{AIR}$ | surface air density (1 $kg/m^3$) |
| $\vec{\tau}$ | wind stress (Pa) |
| $\lvert\tau\rvert$ | wind stress magnitude (Pa) |
| $\overline{\vec{\tau}}$ | interpolated wind stress (Pa) |
| $\vec{\tau}'$ | variable wind stress (Pa) |

**GLOSSARY**

| | |
|---|---|
| AR4 | IPCC Fourth Annual Assessment Report |
| CLM | Community Land Model |
| $CO_2$ | carbon dioxide |
| ECMWF | European Centre for Medium-Range Weather Forecast |
| GCM | General Circulation Model |
| GISS | Goddard Institute for Space Studies |
| H5 | category 5 hurricane |
| IGSM | MIT Integrated Global System Model |
| MOC | meridional overturning circulation |
| NCAR | National Center for Atmospheric Research |
| NCEP | National Center for Environmental Prediction |
| NEM | Natural Emissions Model |
| OHU | ocean heat uptake |
| TEM | Terrestrial Ecosystem Model |

# CHAPTER 1: INTRODUCTION

Due to its heat capacity and mass, the ocean is the largest heat reservoir in the climate system (Wunsch and Ferrari, 2004, Peixoto & Oort 1992). Furthermore, ocean heat content change accounts for most of the energy change in the climate's system; from 1993-2003 (1961-2003), ocean heat content change at depths 0-700m (0-3000m) have accounted for 91% (89%) of the Earth's global energy content change (IPCC Fourth Assessment Report 2007, or AR4). Therefore ocean heat content change (ocean heat uptake) has an important role in variability of the Earth's heat balance.

Our understanding of ocean heat uptake is complicated due to large temporal, regional, and depth variations (IPPC 4th Annual Assessment Report, Forest et al 2002, Pierce et al. 2005). Figure 1 shows the location of major AOGCMs on a probability distribution function of ocean heat uptake and climate sensitivity. All models underestimate ocean heat uptake in the simulation of the present day climate.

Uncertainty is magnified in the long-term response of climate warming scenarios (Forest et al 2005, 2008). This occurs because the slow processes that mix heat into the deep ocean, and therefore characterize the ocean's thermal inertia, are poorly understood (Church et al., 2001). For instance, these processes could reduce the meridional overturning circulation, resulting in either abrupt climate change or an unknown recovery time to present day climate (AR4).

In conclusion, the understanding of which methods and physical processes control ocean heat uptake needs improvement in order to better understand variability in the Earth's heat balance, improve the simulation of present-day climate, and improve the understanding and projection of future climate. Let us explore ocean heat uptake further.

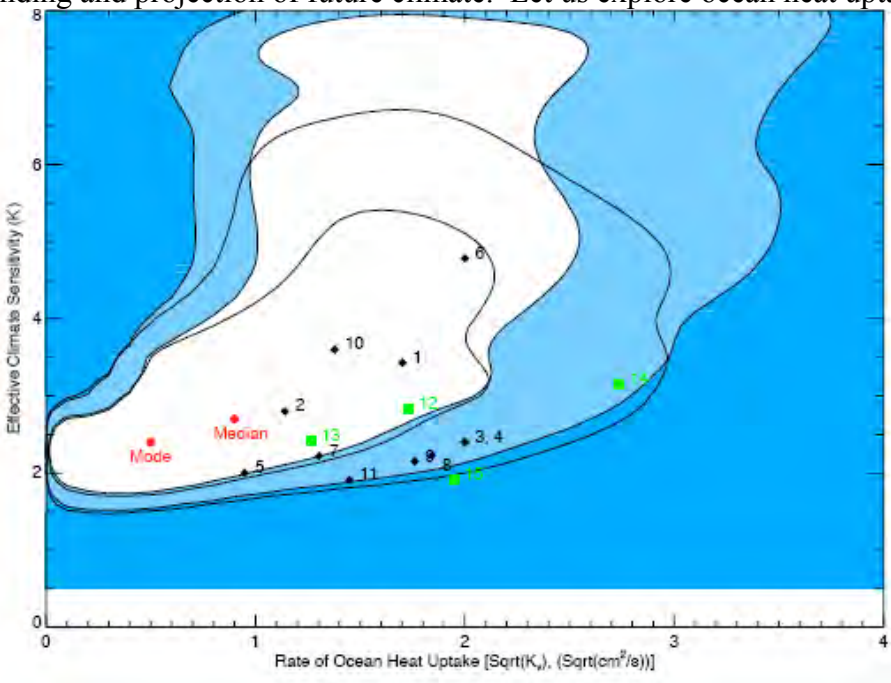


**Figure 1 - Marginal posterior PDF. The shading denotes rejection regions for the 10% and 1% significance levels, light to dark, respectively. The 10%, and 1% boundaries for the posterior with expert prior on S are shown by thick black contours. The positions of AOGCMs [from Sokolov et al., 2003] represent the parameter values required in the MIT 2D model to match the transient response in surface temperature and thermal expansion component of sea-level rise. Forest (2008)**

## 1.1. STATE OF KNOWLEDGE

Basic knowledge of ocean heat uptake exists. Table 1 lists a variety of commonly referenced ocean heat uptake analyses. Figure 2 shows two time series of global ocean heat content for the 0 to 700 m layer of the World Ocean for 1955 to 2005 (Ishii et al. 2006, Levitus et al. 2005) and a time series for 0 to 750 m for 1993 to 2005 (Willis et al. 2004). These studies use the World Ocean Database 2001, the Global Temperature and Salinity Profile Program, the World Ocean Circulation Experiment, Argo data, sea surface salinity compiled by the IRD (L'Institut de Recherche pour le Développement, Numea, France). Results are uncertain; Gouretski & Koltermann (2007) identify a positive bias in the expendable bathythermographs measurements which would reduce trends by 37%, while another new analysis indicates that trends should be increased by 30% (Forest et al, 2008 references C. Domingues, personal communication).

In all cases, the mean global rate of ocean heat uptake has displayed a significant upward trend over 50 year timescales. The surface ocean depth range (0-700m) has proportionally more ocean heat uptake than the full ocean depth range (0-3000m), indicating that heat is slowly transported down through diffusion, turbulent mixing, convective mixing, and vertical movement into the deep ocean. However, significant temporal fluctuations exist, indicating interesting regional/temporal dynamics.

| Date Range | 1955-1998 | 1961-2003 | 1961-2003 | 1993-2003 |
|---|---|---|---|---|
| Depth Range (m) | 0-3000 (full ocean) | 0-3000 | 0-700 (thermocline) | 0-700 |
| Total Ocean Heat Uptake ($10^{22}$J) | 14.2 | 14.5 | ~12 | 8.11 |
| Mean Temperature Increase (C) | 0.037 | 0.038 | 0.1 | 0.067 |
| Ocean Heat Uptake Rate ($W/m^2$) per unit area of Earth's total surface area | 0.20 | 0.21 | ~0.17 | 0.12 |
| Ocean Heat Uptake Rate ($W/m^2$) per unit area of Earth's ocean surface area | 0.28 | 0.30 | 0.24 | 0.17 |

**Table 1 – Commonly referenced ocean heat uptake measurements. Values adapted from Levitus 2005 and AR4.**

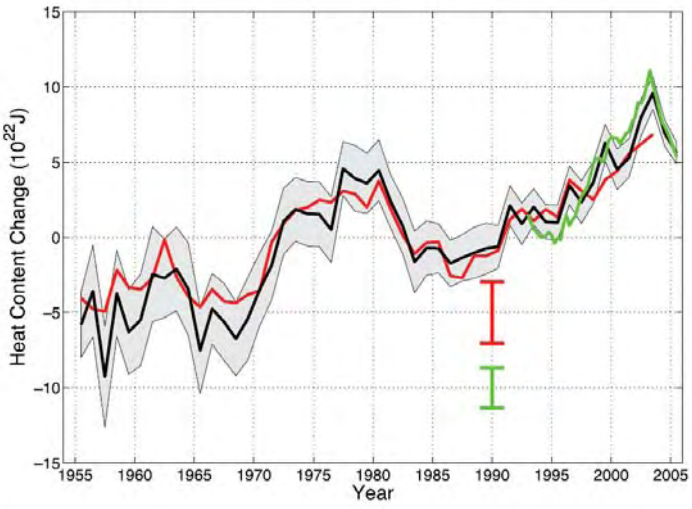


**Figure 2 – Taken from IPCC AR4. Time series of global annual ocean heat content ($10^{22}$ J) for the 0 to 700 m layer. The black curve is updated from Levitus et al. (2005a), with the shading representing the 90% confidence interval. The red and green curves are updates of the analyses by Ishii et al. (2006) and Willis et al. (2004, over 0 to 750 m) respectively, with the error bars denoting the 90% confidence interval. The black and red curves denote the deviation from the 1961 to 1990 average and the shorter green curve denotes the deviation from the average of the black curve for the period 1993 to 2003.**

A closer examination of ocean heat uptake (regionally and temporally) indicates that local values can be an order of magnitude larger than global values. Hence local ocean heat uptake processes must be fully understood and explained to correctly obtain global values. First let us examine the depth differences. Figure 3 shows the linear trend from 1955 to 2003 of zonally averaged temperature in the upper 1,500 m of the water column (linear trend of ocean heat content is shown in Figure 4). As previously surmised, heat is gradually being transported down from the surface to the depths through turbulent mixing, convective overturning, and mean vertical motion, (Hartmann, 1994). However, the resolved structures raise more questions. Why does the Atlantic have a dipole structure? Why are the other oceans losing heat at 20°S b at ~250m depth?

Figure 5 shows a latitude/longitude plot of the observed columnar ocean heat uptake trends. Here the Atlantic dipole appears more clearly. The pattern in the Pacific Ocean might indicate a transfer of heat from the east to the west. Researchers believe these and other regional/ depth variations are due to interannual and inter-decadal variability superimposed on the longer-term trend (AR4, Hartmann 1994, Pexioto & Oort 1992). Some further conclude that the mid- and high-latitude oceans should respond to atmospheric driving only on multidecadal time scales (Wunsch & Heimbach, 2008). Possible phenomenon include the North Atlantic Oscillation (NAO), the Atlantic Meridional Oscillation (AMO), the El Niño Southern Oscillation (ENSO), the Pacific Decadal Oscillation (PDO), the Interdecadal Pacific Oscillation (IPO), and the Southern Annular Mode (SAM). Note, some are controversial and lack an accepted mechanistic explanation.

- The positive (negative) phase of the NAO is also associated with a cold (warm) sea surface temperature anomaly in the subpolar Northern Atlantic, a warm (cold) anomaly in midlatitudes, and a cold (warm) anomaly between the equator and 30° North. (AR4). This index appears to have a 20-30 year timescale whose magnitude has increased over time.
- The (controversial) AMO is a 65-70 year timescale associated with a 0.4C warming of sea surface temperatures in the Atlantic Ocean (AR4).
- ENSO is a general term for the closely linked El Niño (ocean) and Southern Oscillation (atmosphere) patterns. El Niño (La Niña) is characterized by a warming (cooling) of tropical Pacific surface waters on the west coast of South America, weakened (strengthened) SST gradient across the equatorial Pacific, and a shifting of major precipitation events eastward (westward). El Niño events occur ~ 3 to 7 years (AR4).
- The PDO and IPO are measures of variability in the Pacific Ocean. In a positive (negative) phase of the PDO, the west Pacific becomes cool (warm) and the eastern ocean warms (cools). PDO events occur about every 20 to 30 years in the northern Pacific Ocean (AR4). IPO events are similar to PDO but occur in both northern and southern hemispheres on 15-30 year timescales.
- The positive SAM is associated with low pressure west of the Antarctic Peninsula leading to increased poleward flow, reduced sea ice, and a noticeable sea level rise (AR4, Liu et al., 2004). This index appears to have a 20-30 year timescale, but has been increasing in recent years.

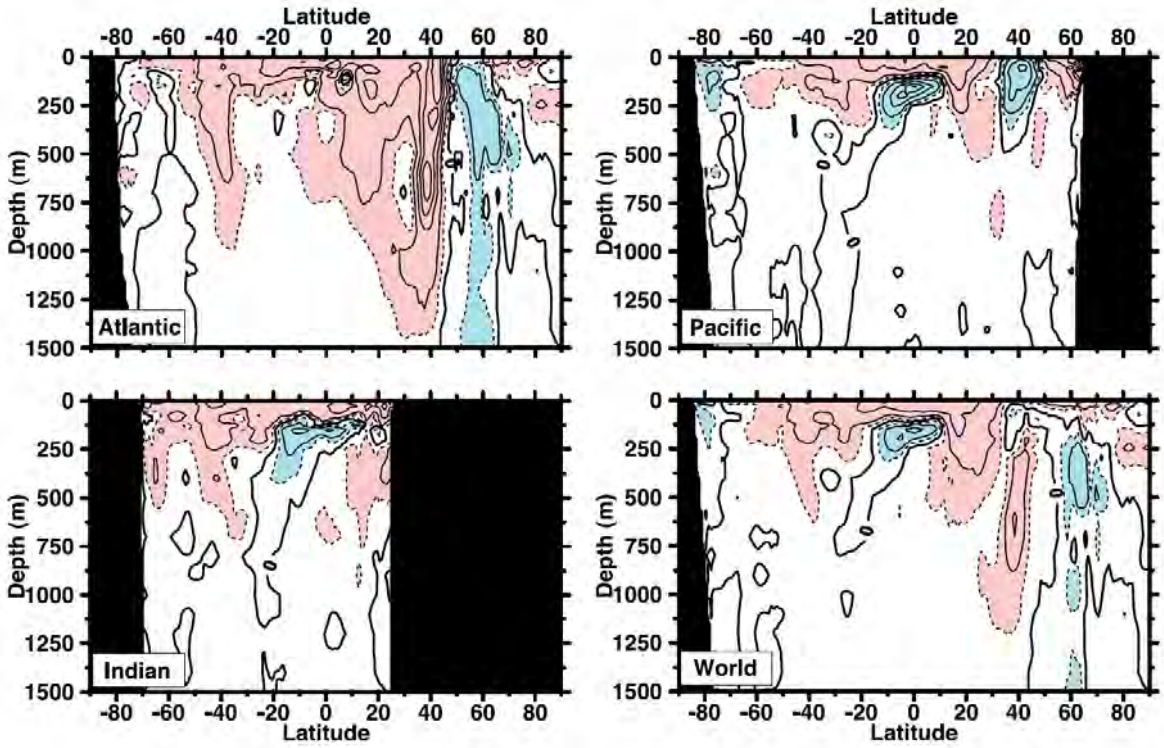


**Figure 3 – Taken from AR4, based on the work of Levitus et al. (2005). Linear trend (1955–2003) of zonally averaged temperature in the upper 1,500 m of the water column of the Atlantic, Pacific, Indian and World Oceans. The contour interval is 0.05°C per decade, and the dark solid line is the zero contour. Red shading indicates values equal to or greater than 0.025°C per decade and blue shading indicates values equal to or less than –0.025°C per decade.**

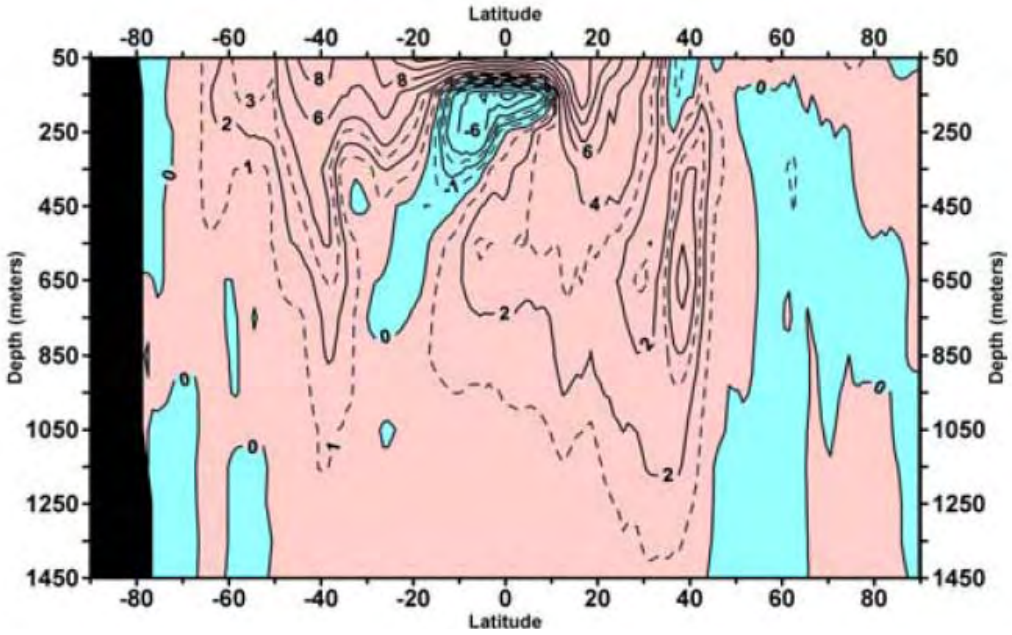


**Figure 4 – Linear trend (1955-2003) of the zonally integrated ocean heat content of the world ocean in 1° latitude belts for 100-m thick layers. Heat content values are plotted at the midpoint of each 100-m layer. Contour interval is $2\times10^{18}$ J/(1° latitude*100 meter*year). Taken from Levitus et al. 2005.**

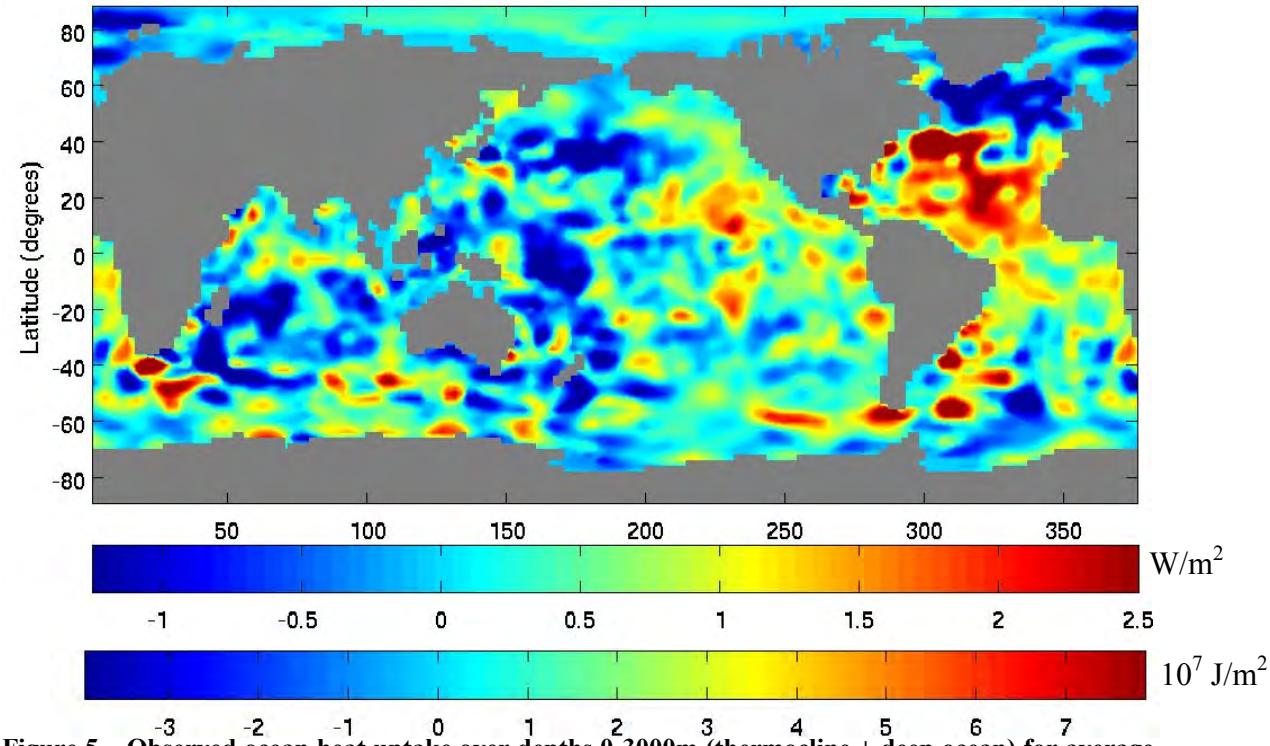


**Figure 5 – Observed ocean heat uptake over depths 0-3000m (thermocline + deep ocean) for average 1994-1998 minus average 1955-1959 from the World Ocean Atlas 2001, units of annual average W/m$^2$ or $10^7$ J/m$^2$. Depths 0-700m (thermocline only) yield similar spatial patterns to depths 0-3000m (but smaller magnitudes).**

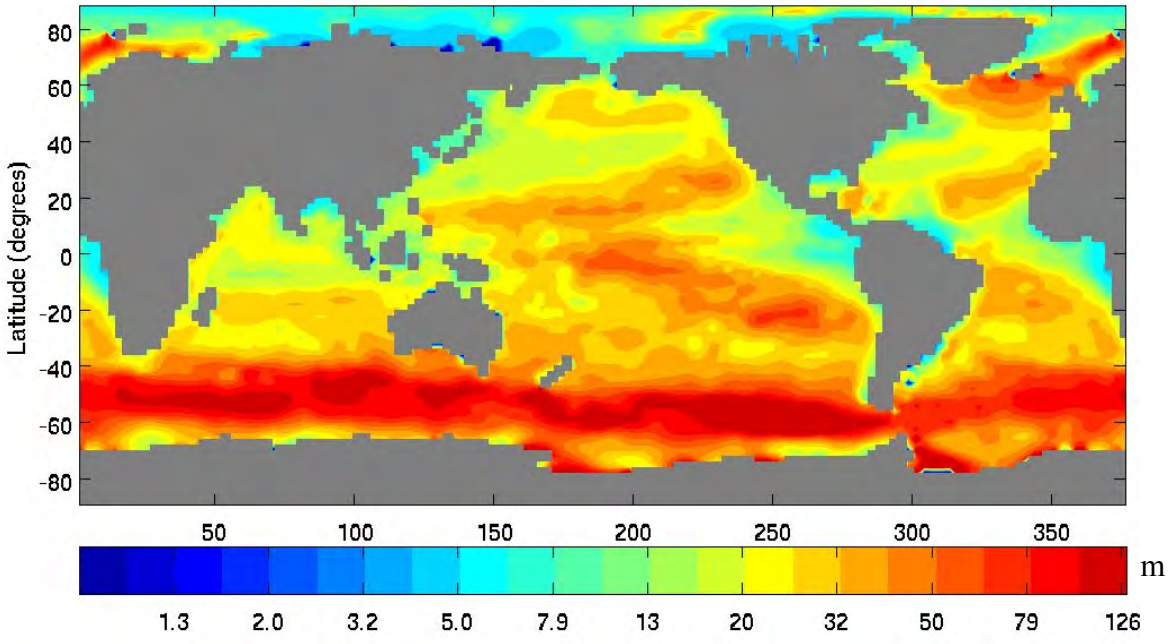


**Figure 6 – Mixed layer depth (m). Calculated from Levitus climatological temperature and salinity (1955-2003).**

Short timescale processes can also cause significant fluctuations. Jones & Toba (1992) give an extended discussion on several short timescale disturbances: mesoscale eddies, synoptic processes, diurnal processes, internal tides, waves, etc. Most of these processes are caused by surface forcing and move surface properties vertically or horizontally. On short timescales, these changes to the surface heat do not have time to communicate with deep ocean heat. Consequently, the mixed layer becomes highly important. The climatological mixed layer depth (years 1955-2003) is shown in Figure 6.

The ocean mixed layer is defined as the surface layer where convection and turbulent mixing cause temperature, salinity, and other properties of seawater to be almost independent with depth (Hartmann). Changes in local buoyancy can lead to convection. For instance, in the winter (or nighttime), air temperatures decrease and the surface is cooled strongly. Cold, dense water rests on warmer deeper water, leading to convection and a deepening of the mixed layer. In the summer (or midday), air temperatures warm the water, convection ceases, and the mixed layer becomes shallower. Kamenkovich (2005) suggests that daily fluctuations have the biggest effect on the mixed layer structure (and therefore the time-mean temperature).

Strong evaporation/precipitation can similarly affect local buoyancy changes and alter convection. In addition to convection, turbulent mixing can sustain a boundary layer. Increased wind stress increases turbulent mixing and, depending on the relative strength of convection and turbulent mixing, can cause the entrainment of cool, dense water. For instance, Figure 7 shows sea surface temperatures following a September 1996 tropical cyclone event. Sea surface temperatures are decreased due to turbulent mixing from high wind stresses that penetrated below the mixed layer depth and entrained cooler water.

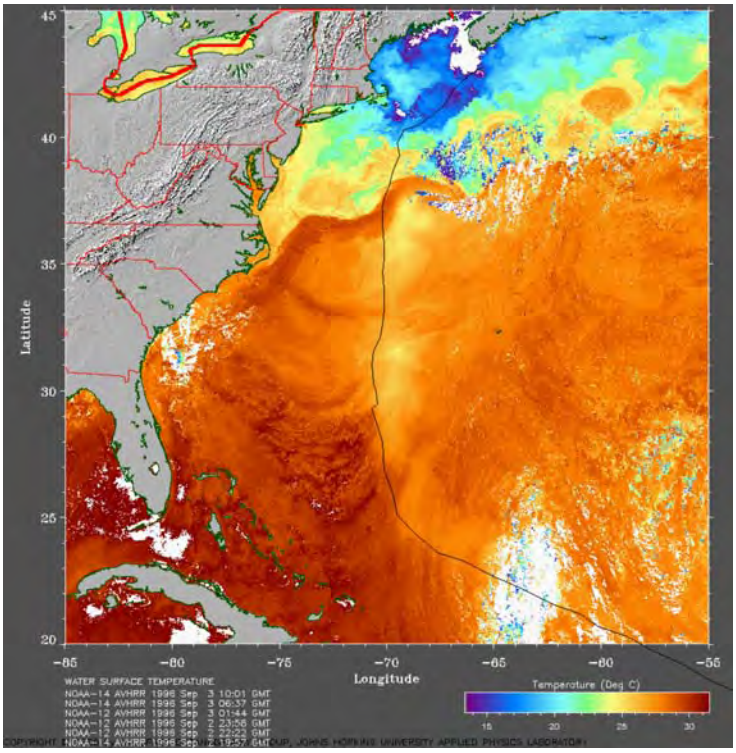


**Figure 7 - Seas surface temperature following a 1996 tropical cyclone event. Note the cooler waters in the wake of the tropical cyclone (marked by the black line). Emanuel, 2005.**

Communication between the mixed layer and the thermocline is described via a mechanism informally known as "Stommel's demon" (Pedlosky). In the summer, storms and Ekman layers can penetrate below the shallow convective mixed layer depth and temporarily communicate with the thermocline (i.e. the demon at the base of the mixed layer permits exchange). However, the winter convective mixed layer deepens quickly and overtakes the previously subducted summer fluid (and its communicated properties). Therefore only the mixed layer properties at the maximum mixed layer depth (end of winter) will permanently communicate its properties to the thermocline. "Stommel's demon" is overcome only when turbulent mixing from very strong summer/fall storm systems (e.g. tropical cyclones) can penetrate below the winter convective mixed layer depth.

Aside from changes to the mixed layer depth, the effects of short timescale processes on ocean heat uptake are not well understood.

## 1.2. WIND STRESS IN OCEAN HEAT UPTAKE

Many of the processes discussed above are still poorly understood. However, wind stress can play a strong role in ocean heat uptake on all timescales (Wunsch & Ferrari, 2004). Here we will briefly discuss mean and variable wind stresses.

Much research exists on the effect of mean wind stress on the ocean. Two different regimes of wind stress exist (Jones & Toba, 2001). Small wind stresses (wind velocity, $\vec{U}$<60 m/s) interact with the ocean through interfacial drag ($\vec{U}^2$), and result in Ekman pumping, currents, western boundary layer, wind-waves, and set the mixed layer depth. Large wind stresses ($\vec{U}$>60 m/s) interact with the ocean through sea spray drag ($\vec{U}^4$) and result in sea spray, two-phase flow, breaking/cresting/etc waves, depressed mixed layer. The maximum wind velocities in the 1º×1º National Center for Environmental Prediction (NCEP) reanalysis data are ~35 m/s (interfacial drag regime).

Most variable wind stress studies have focused on long timescales, yielding discussions on the NAO, AMO, PDO, etc (Wunsch & Heimbach, 2008). Some fewer studies have focused on short timescale processes. Although they did not relate transient diapycnal diffusion to variable wind stress, Boos et al. (2004) found that transient diapycnal diffusion could theoretically affect the instantaneous meridional overturning circulation and other ocean properties. Kamenkovich (2005) examined the effect of daily wind stress (from NCEP) on mixed layer depth and sea surface temperature in the Southern Ocean (in an ocean GCM). He found that daily wind stress strengthens and deepens wind-generated turbulent mixing, and can slow wintertime convection. Lozier et al (2008) first examined the relation between large-scale patterns of heat content and variable wind stress. Using both NCEP and European Centre for Medium-Range Weather Forecast (ECMWF) data, Lozier et al. found that the gain in heat content over the North Atlantic subtropical gyre is primarily a consequence of short-timescale wind-induced circulation changes (short-timescale gyre changes). They ignore other effects such as increased turbulence or a deepening of the mixed layer.

In summary, studies indicate that our understanding of the relation between short timescale wind stress variability and ocean heat uptake is important and needs improvement.

## 1.3. THESIS STATEMENT

This study for the first time examines global variable wind stress datasets for short timescale spatial and temporal patterns. Note Jones and Toba (2001) and Large et al (2008) indicate that daily or hourly timescales are necessary to resolve most transient processes. Data is available in six hour timescales, so processes on finer time scales will be left to future studies.

Questions include:

- Can we identify patterns in the NCEP variability data that might relate to processes we should study further, parameterize, and put in the model?
- Are ocean properties (i.e. ocean heat content) sensitive to changes in the variable wind stress? If yes, is correct wind stress variability important for predictions of the ocean mean state?
- In a coarse resolution model, can variable wind stress be the major source of variability of the MOC (and other ocean metrics)?

CHAPTER 2: will describe the datasets and model used. First we will define variables and metrics used through the study. Then we will characterize the mean and variable wind stress using the finest resolution global wind stress dataset available. Here we specifically attempt to identify spatial patterns and timescales in the data that might relate to processes or limitations we should study further. Finally, we describe the computationally efficient ocean model with a good mixed layer depth parameterization which we will use in this study.

CHAPTER 3: will use the datasets and model to characterize the effects of variable wind stress on ocean properties in a coarse resolution model. First we examined whether variable wind stress would change the mean state of the ocean in our coarse resolution model. Next we tested our models' responses to a weak forcing scenario, a current climate scenario. Finally we tested our models' response to strong forcing scenarios, two global warming scenarios (our probable future).

CHAPTER 4: will contain a summary of conclusions and topics for future work.

# CHAPTER 2: DATA AND MODEL DESCRIPTION

Before proceeding with our discussion, we note that several quantities are ill-defined in the literature. Hence Section 2.1 will define variables and metrics used through the study.

Next we must acknowledge the lack of literature characterizing variable wind stress. Therefore we must characterize the mean and variable wind stress using the finest resolution global wind stress dataset available. At the time of this research, this dataset could be calculated from either the National Center for Environmental Prediction (NCEP) or the European Centre for Medium-Range Weather Forecast (ECMWF) wind velocity datasets. Since Lozier et al (2008) indicate that results using NCEP and ECMWF are qualitatively similar, we limit this study to the NCEP dataset. Section 2.2 describes and characterizes the NCEP dataset. Additionally, we attempted to identify spatial patterns and timescales in the data that might relate to processes or limitations we should study further. Section 2.2 concludes with a brief note on how well NCEP captures tropical cyclone variability.

Finally, this study requires a computationally efficient ocean model with a good mixed layer depth parameterization. A variety of models would be appropriate; one is the coupled 2D atmosphere 3D ocean model with the K profile parameterization (KPP) developed at the National Center for Atmospheric Research (NCAR, Large et al 1994). Section 2.3 describes this model.

## 2.1. DEFINITIONS

For the purposes of this research, we will use wind stress, variable wind stress, ocean heat uptake, and mixed layer depths. Our definitions follow.

### *2.1.1. Wind Stress Vector*

For small wind velocities ($\vec{U}$ < 60m/s), the wind stress ($\vec{\tau}$ , Pa) is defined as

$$\vec{\tau} \equiv \rho_{AIR} C_D \left|\vec{U}\right| \cdot \vec{U} \qquad (1)$$

where $\rho_{AIR}$ is the surface air density (1 kg/m$^3$) and $C_D$ is the drag coefficient. Common parameterizations for $C_D$ are either independent of or a linear function of the wind velocity at large wind velocities (Köhl & Heimbach, 2007). Therefore at large wind velocities, the wind stress approaches a function of $\vec{U}^2$ or $\vec{U}^3$. The standard NCEP approximation for the drag coefficient is a constant $C_D$=0.0013 (i.e. wind stress is proportional to the square of the wind velocity), which may cause the wind stress values to be underestimated at high wind velocities (Köhl & Heimbach, 2007). The Trenberth approximation for $C_D$ is a complicated function of $\vec{U}$ (i.e. wind stress is proportional to the cube of the wind velocity, Trenberth et al, 2001).

### *2.1.2. Variable Wind Stress*

To calculate variable wind stress, we adopted the same procedure as that used by the model described in Section 2.3. Climatological wind stress is defined as the monthly mean wind stress further averaged over all years in the dataset (usually 1978-2007). Hence there are twelve climatological wind stress datasets, one for each month. We further define the interpolated wind stress ($\overline{\vec{\tau}}$) at time *t* to be the wind stress interpolated

from the twelve climatological wind stress datasets[1]. Given these definitions, we then define variable wind stress ($\vec{\tau}'$) as the time anomaly from the interpolated wind stress, or:

$$\vec{\tau}'(\theta,\phi,t) \equiv \vec{\tau}(\theta,\phi,t) - \overline{\vec{\tau}}(\theta,\phi,t) \quad (2)$$

where $\theta$ is the latitude (degrees), $\varphi$ is the longitude (degrees), and $t$ is the time (seconds).

The standard deviation is one good measure of variability. In this case, we calculate standard deviation as:

$$STD = \sqrt{\frac{1}{N-1}\sum_{1}^{N}\left(X_i - \overline{X}\right)^2}$$

where $N$ is the number of data points, $X_i$ is a particular value of the data point, and the overbar indicates the average over all the data points. The standard deviation may span a month, a season, a year, or multiple years as appropriate.

*2.1.3. Ocean Heat Uptake*

Since oceanic kinetic energy & geothermal heating are small compared to the overall change in energy (Wunsch and Ferrari, 2004), most of the energy change comes from the change in temperature. Therefore to first order, we can relate ocean heat content ($Q$, J) and ocean heat uptake ($\Delta Q$, J/s) to temperature, or

$$Q = c_p \rho V T$$
$$\partial Q = c_p \rho V \partial T + c_p V T \partial \rho \quad \text{(Haney 1971, Sun et al 2003, Vallis 2005)} \quad (3)$$

where $C_p$ is the specific heat of water (4000 J/kgK), $\rho$ is the ocean water density (kg/m$^3$), $V$ is the volume of the fluid parcel (m$^3$), and $T$ is the ocean water temperature (K). Since ocean water is nearly incompressible ($(T\partial\rho) < (\rho\partial T)$, confirmed by inspection of the data), then Eq. 3 becomes

$$\partial Q \approx c_p \rho V \partial T \quad (4)$$

In the real ocean, heat exchange is continuous and a vector quantity. However, models discretize ocean water into well-mixed spatial and temporal boxes, and therefore heat fluxes are defined only at box boundaries. Hence Eq. 4 becomes

$$\Delta Q \approx c_p \rho V \Delta T \quad (5)$$

To obtain the columnar ocean heat content ($Q_z$, J/m$^2$), we can vertically integrate over discrete boxes from sea level to a specified depth $H$ (m), or

$$Q_z = \sum_{n=0}^{H} c_p \rho \Delta T_n \Delta z_n \ .$$

Typical depth ranges are the ocean depth ranges 0-700m and 0-3000m.

*2.1.4. Mixed Layer Depth*

The mixed layer is the uppermost layer of the ocean where temperature, salinity, and tracers are nearly invariant with depth. Strict definitions of mixed layer depth vary; here we define the mixed layer depth as the shallowest depth where the density is 0.125 kg/m$^3$ larger than the surface density.

In a model, we first calculate the density of each box as a function of temperature and salinity. From these depths and densities, we can linearly interpolate the mixed layer depth.

[1] This interpolated wind stress has a smooth seasonal cycle, similar to that achieved from a 30-day filter.

## 2.2. NCEP WIND VELOCITY DATA

NCEP reanalysis data was provided by the National Oceanic and Atmospsheric Administration/Cooperative Institute for Research in Environmental Sciences Climate Diagnostics Center (Boulder, Colorado) from their website at http://www.cdc.noaa.gov/ . The NCEP/NCAR project uses a state-of-the-art analysis/forecast system to perform data assimilation using past data from January 1, 1948 to the present. Spatial coverage is 2.5°×2.5° from 90°S to 90°N, 0°E to 357.5°E (73×144 points). Temporal coverage is every 6 hours (0Z, 6Z, 12Z, and 18Z). We calculated the wind stress (using Equation 1) from the zonal and meridional wind magnitudes at the 0.995 sigma level (approximately the 10m-height wind stress).

I did not use all the NCEP data. Figure 8 shows the introduction of some major datasets to the NCEP reanalysis process. The major changes of 1978 (addition of satellite data) cause a step function in the standard deviations (not shown), so for this study we restrict our dataset to 1978-2007 only.

### *2.2.1. Description*

Before any analysis can begin, we must first understand the general characteristics of the dataset. Therefore here we present monthly, zonal, and global means and standard deviations for the NCEP data set. Note that to allow comparison to other datasets, the NCEP data set was converted to 2°×2.5°, 4 hour values. Also note that since the meridional components of mean and variable wind stress are relatively small, we restrict our characterization to the zonal components only.

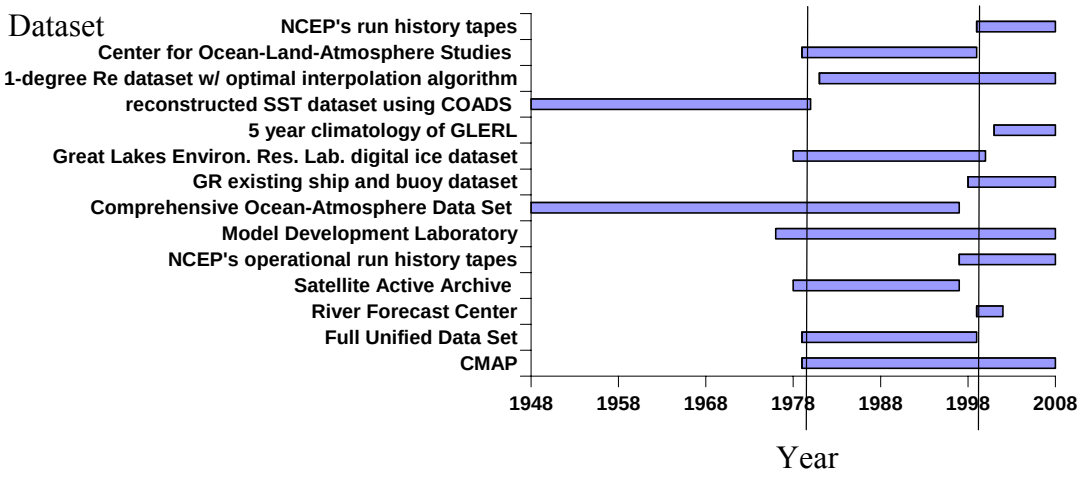


**Figure 8 - Introduction of datasets into NCEP reanalysis. Vertical lines indicate years 1979 and 2000.**

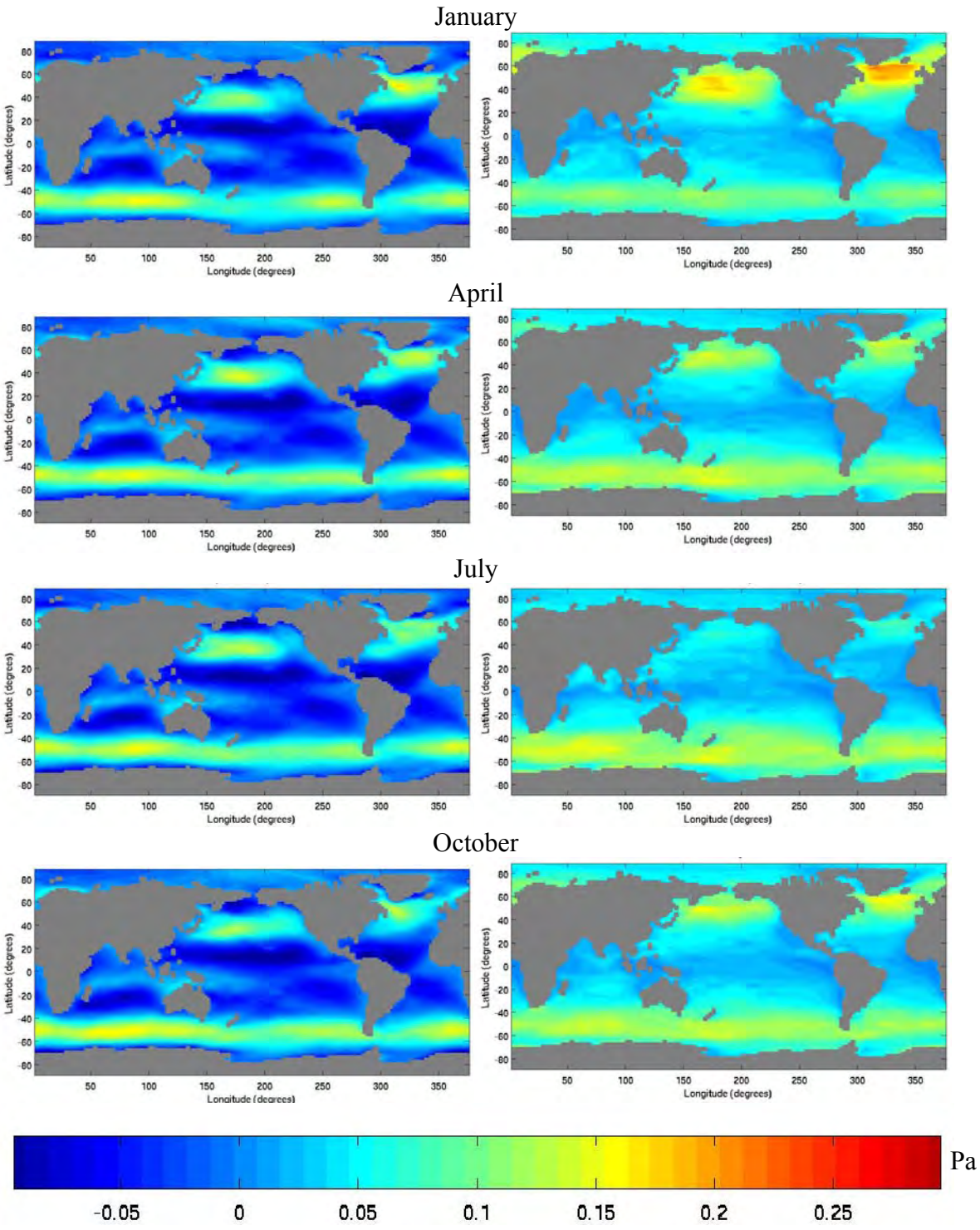


**Figure 9 - Four-hour NCEP dataset 1978-2007, 2°×2.5° box: Zonal component of wind stress (Pa). Left column is four monthly means from all 30 months of data, right column is standard deviation of all 30 months of data from each monthly mean.**

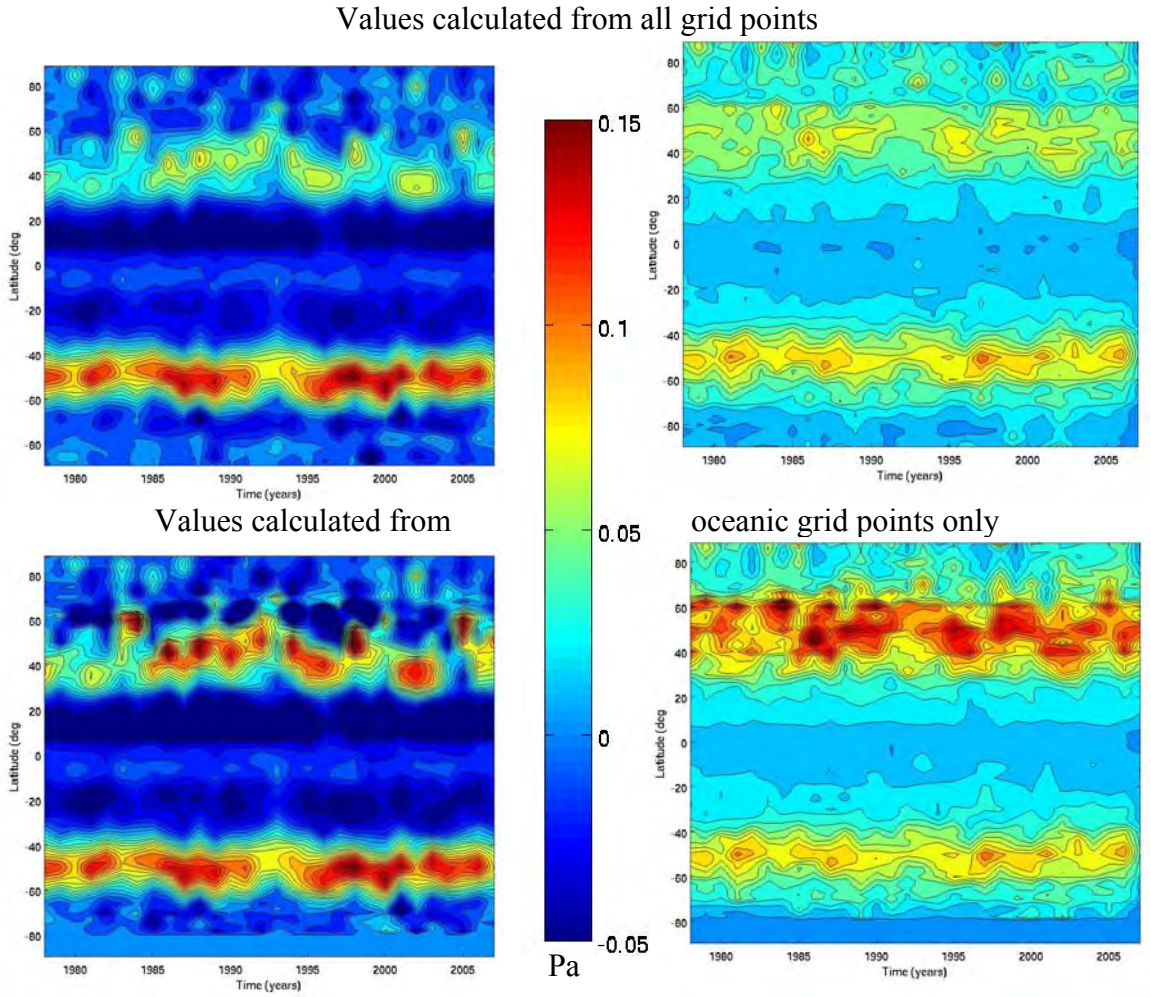


**Figure 10 – Four-hour NCEP dataset, Januarys 1978-2007, 2°×2.5° box: Zonal mean of the zonal component of wind stress (Pa). X-axis is year, ranging from 1978 to 2007. Y-axis is latitude, ranging from -90° to 90°. Left column is the zonal mean of each annual January mean, right column is zonal mean of standard deviation from each annual January mean.**

First we calculated the climatological monthly mean of the zonal component of the wind stress for January, April, July, and October averaged over years 1978-2007. This mean and the related monthly standard deviation are shown in Figure 9. The magnitudes of the means and standard deviations are similar. In general, the highest magnitudes of the standard deviation (and hence variable wind stress) are correlated with the highest magnitudes of mean wind stress, peaking at 40-60° in the winter hemisphere.

Next we looked for long term trends. For each month of years 1978-2007, we calculated the monthly mean and the standard deviation from that monthly mean. The zonal average of January values is shown in Figure 10. Although it appears some long term variations exist (see Introduction for discussion), there is no apparent overall trend in the wind stress data. Other months yield similar results.

Figure 10 also indicates that the wind stress over land masses is much smaller than the wind stress over the ocean. For our ocean heat uptake study, this difference in land and ocean wind stress values is very useful for periodic sanity checks.

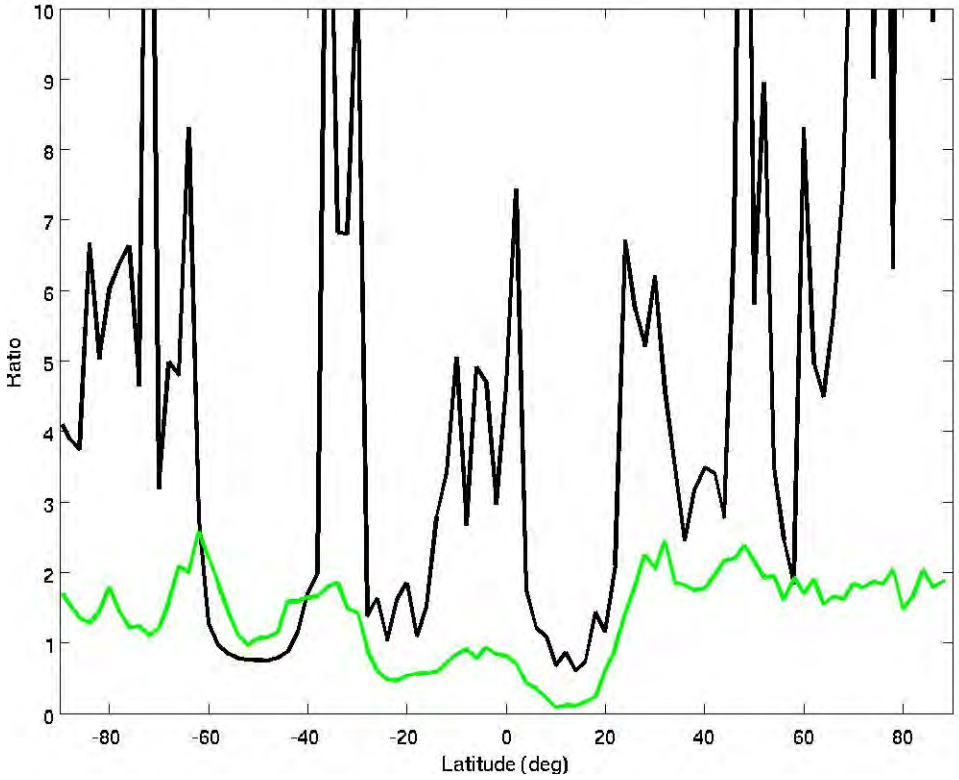


**Figure 11 - Four-hour NCEP dataset, 1978-2007, 2°×2.5° box: Global mean of the ratio of each January standard deviation to its January mean *u* wind stress. Black indicates using all values, green indicates only using values where the mean monthly wind stress was larger than 0.001 Pa.**

Finally, we formally examined whether areas of large mean wind stress magnitude and areas of large variable wind stress magnitude overlap. For each January of years 1978-2007, we calculated the global mean of the magnitude of the ratio of each January standard deviation to its January mean zonal wind stress. Small mean values yield large ratios; to remove division by zero errors, we removed data points with a zonal wind stress mean less than 0.0001 Pa. Figure 11 shows the original ratio (black) and the ratio with small means removed (green). All values were relatively time invariant (not shown). In general, mean wind stress magnitude is correlated with variable wind stress magnitude. At the equator, the mean wind stress is larger than variable wind stress, while elsewhere the variable wind stress is larger than the mean wind stress. These results indicate that it may be possible to parameterize variable wind stresses by correlating the mean and variable wind stresses. This is left to future work.

*2.2.2. Patterns and limitations in the NCEP Data*

After characterizing the NCEP dataset, we attempted to identify processes or limitations we should study further. Questions include:

- What are the predominant timescales?
- Is a change of the variable wind stress in one location correlated to a change of variable wind stress in another location?
- How are strong wind stress events (such as tropical cyclones) represented in the 2.5°×2.5° dataset?

Due to the introduction of satellite data in 1978 and the consequent step function in variable wind stress, this analysis was limited to years 1978 to 2007.

2.2.2.1. Timescales of the NCEP dataset

To identify timescales of the NCEP dataset, we computed a power spectral density decomposition (fast Fourier transform) on the unaltered six-hour NCEP wind magnitude dataset (combination of zonal and meridional components) from 1978 to 2007[2]. To have the best chance of identifying short timescales, we examined several different points randomly chosen from the high variable wind stress band of the Southern Ocean[3].

Results were qualitatively similar for all locations. Raw data (not pictured) was very noisy (red noise), and neither the annual nor the seasonal cycle could be identified. We did identify a spike at 12 hours, indicating that more energy rests in the 12 hour frequency than in surrounding times. Assuming the NCEP model responds quickly, we would expect to calculate a diurnal cycle from 0Z and 12Z data for some longitudes. However, this spike occurs at all longitudes examined (not shown), hence we believe the 12 hour spike to be an artifact of the NCEP data reanalysis process.

In an attempt to better identify timescales, we windowed the data. Figure 12 gives the geometrically windowed decomposition[4] at one point (52°S, 111.25°W). Values are white noise at low frequencies, and red noise at high frequencies. However, we still cannot identify an annual or seasonal cycle in the log-log domain. This finding agrees with Figure 19, which shows a weak seasonal cycle in the southern ocean for the NCEP dataset (not observable in a log-log domain). At a location where the seasonal cycle is high (eg 42°N), a seasonal cycle appears (not shown, a weak bump at high magnitudes in the log-log domain).

To avoid windowing the dataset in the frequency domain, we can instead reduce noise by using a zonally averaged dataset. We used the zonal mean wind magnitude at 52°S every six hours from 1978 to 2007. The (unwindowed) power spectral density decomposition is shown in Figure 13. The data is less noisy, and strongly resembles red noise. Due to zonal averaging we do not expect to see a diurnal timescale; however, we cannot identify the annual and seasonal timescales. Instead, we can identify a timescale of roughly half a month (and smaller aliased frequencies). Investigation of the physical mechanism causing this behavior is left to future studies.

In summary, we could not reliably identify NCEP wind magnitude timescales using a Fourier analysis on Southern Ocean data. Future research can focus on these timescales. In general, the addition of more data should better yield a timescale. Additionally, it is possible that examining data at more locations (including in the Northern Hemisphere) would yield a timescale. Also, perhaps a Fourier analysis on raw data (instead of on the NCEP reanalysis) may yield a timescale.

[2] Fft values are normalized by 1; time series with different timesteps result in the same fourier transform.
[3] We also examined several points in the north Atlantic Ocean. These points yielded a
[4] A geometrical windowed Fourier decomposition yields a similar number of points at both low and high frequencies. Code was supplied by Raffaele Ferrari.

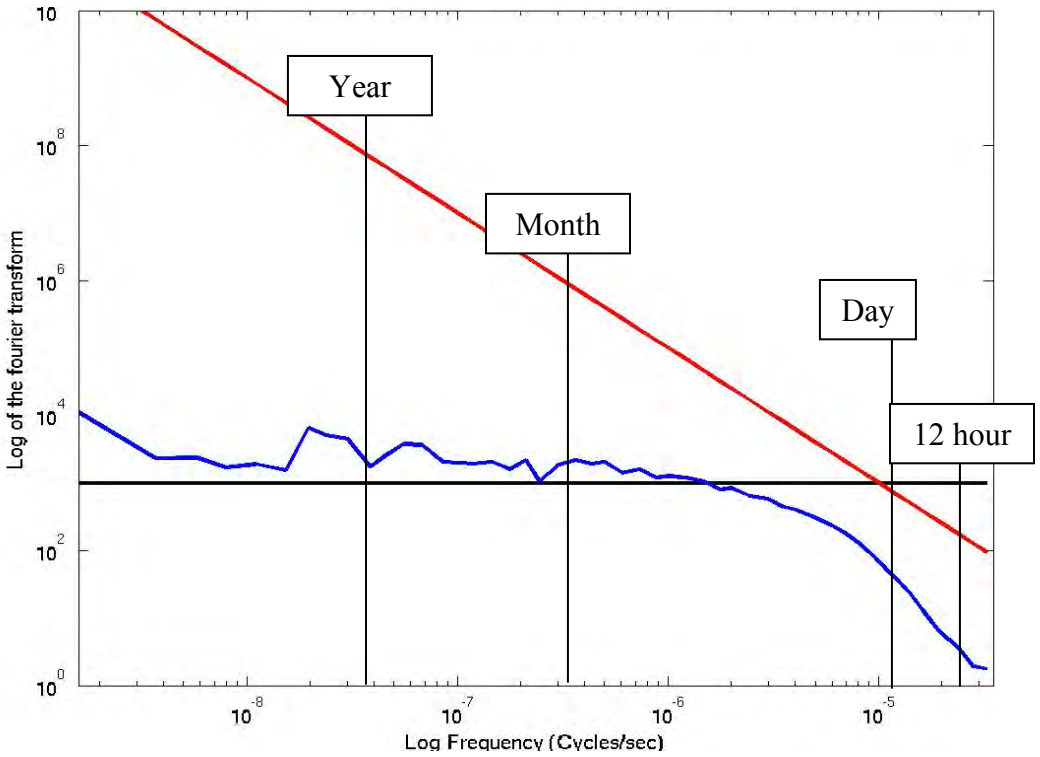


**Figure 12 - Six-hour NCEP dataset 1978-2007 at 52°S, 111.25°W. The power spectral density decomposition was windowed every 1024 points to reduce noise. Low frequency data appears pink due to the windowing process.**

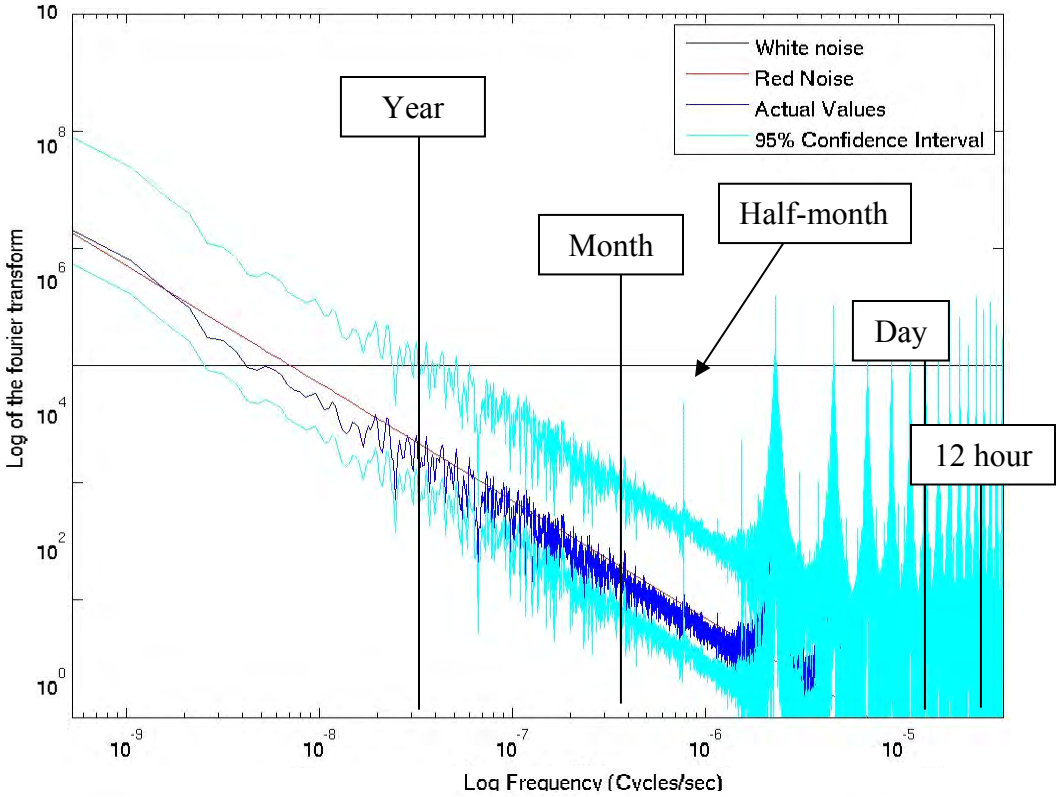


**Figure 13 - Six-hour NCEP dataset 1978-2007, zonally averaged at 52°S.**

2.2.2.2. Spatial patterns in the NCEP data

Next we examined whether a change of variable wind stress in one location is correlated with a change in variable wind stress at another location. To identify these spatial patterns, we used an empirical orthogonal function analysis (EOF). Due to memory limitations, we could not examine the entire dataset. Spatially, we tested the globe, individual oceans, and the 40°-60° band of the individual oceans (the band with high SD as given in Figure 10). Temporally, we tested seasons and months.

In most cases, the first eigenvalue was not well distinguished from subsequent eigenvalues. Therefore we could not identify a significant spatial pattern to the NCEP wind stress variability. In those very few cases where the first eigenvalue was strong compared to the second and third eigenvalue, we found dipoles similar to the North Atlantic Oscillation and the Southern Annular Mode. An autocorrelation analysis indicates a timescale of 2-5 days, that of an atmospheric synoptic system (i.e. eddies).

2.2.2.3. Tropical cyclones in the NCEP dataset

Finally we examined how strong wind stress events (such as tropical cyclones) are represented in the NCEP dataset. To obtain a clear signal (unbiased by nearby land), we picked two hurricanes that reached category 5 strength in open ocean. The NOAA Coastal Services Center Historical Hurricane Tracks tool supplied position, 1-minute maximum sustained wind velocity, and eye pressure data. Figure 14-Figure 15 characterize Isabel 2003 (Atlantic), while Figure 16-Figure 17 characterize Ioke 2006 (Pacific). Note as Isabel approaches North America the NCEP wind velocities increase; this is presumably due to the inclusion of more data in the reanalysis.

Generally we find that the six-hour average NCEP wind velocities are much less than the NOAA 1-minute maximum sustained wind velocity. This occurs because the NCEP values are averaged over time and space, while the NOAA values are instantaneous[5]. However, hurricanes are clearly visible as an elliptical area of increased wind velocity compared to the background noise. Figure 18 shows the maximum wind velocity in the vicinity of Isabel for the entire year of 2003. Tropical storm Fabio (2003, H5) and tropical storm Isabel (2003, H5) stand out at roughly 30-35 knots compared to the background noise of roughly 20-25 knots.

*2.2.3. Applying the NCEP dataset*

This section summarizes the characteristics of the NCEP dataset. Means and standard deviation peak at 40-60° in the winter hemisphere, similar to other datasets (i.e. ECMWF). We find that the NCEP resolution is sufficient to capture some variable wind stress. NCEP monthly means and monthly standard deviations are of the same magnitude. Strong wind stress events (tropical cyclones) are observed. Due to these magnitudes, it may be possible to force a model run with NCEP variable wind stress and observe an ocean response.

[5] The Atlantic Oceanographic and Meteorological Laboratory of the NASA Hurricane Research Division (http://www.aoml.noaa.gov/) compiles wind analyses of Atlantic tropical cyclones from the best available data (Powell et al., 1998). On September 13, 2003 at 0130 UTC, Isabel's eye was centered on 21.8°N, 59.3°W with a 1 minute maximum sustained surface wind velocity of 129 knots and an 1 minute sustained surface wind velocity of 70 knots at a one-degree radius. An average over this two degree box yields an average 1 minute sustained surface wind velocity of 90 knots.


**Figure 14 – Path of Isabel, 2003. Category is denoted by color: Red indicates H5-H3, pink indicates H2-H1, yellow indicates tropical storm, green indicates tropical disturbance, and a plus indicates extratropical. Courtesy of the NOAA Coastal Services Center Historical Hurricane Tracks (http://maps.csc.noaa.gov/hurricanes/viewer.html)**

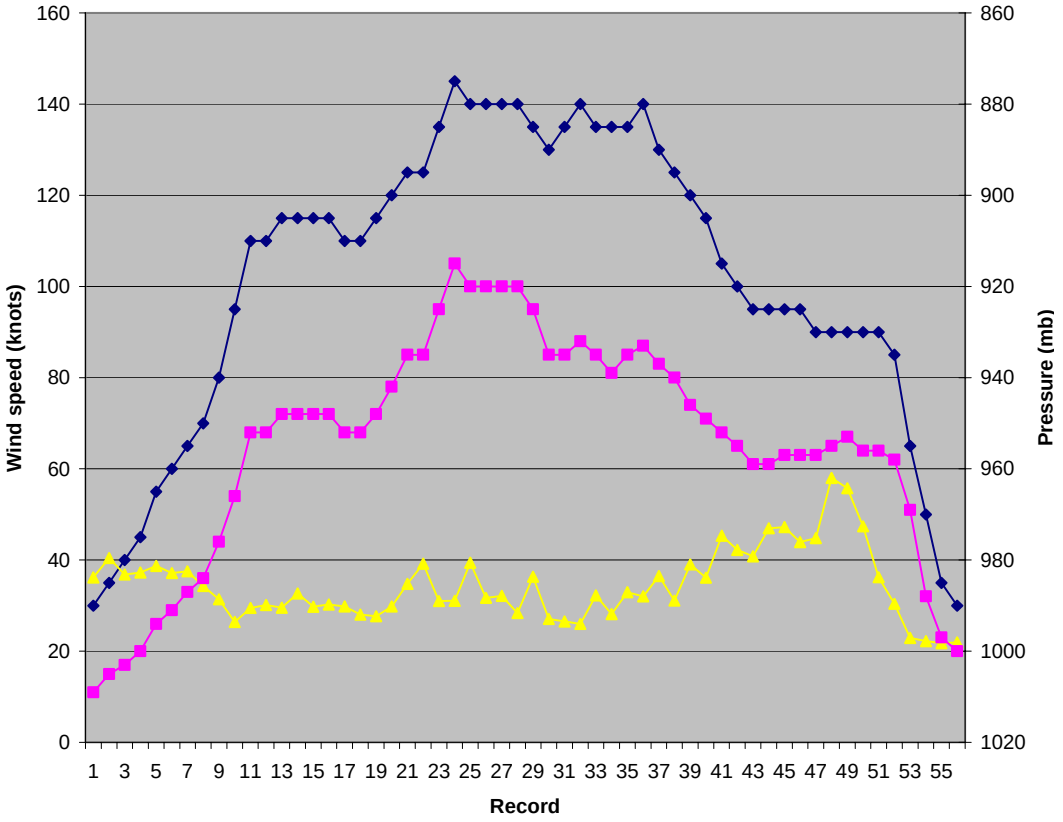


**Figure 15 – Evolution of Isabel, 2003 over time. The x-axis is the record number. Blue diamond is the NOAA recorded maximum sustained 1-minute wind velocity (knots, left y-axis). Pink square is the NOAA recorded pressure in the eye (mb, right y-axis). Yellow triangle is the temporally matching maximum wind velocity (knots, left y-axis) in the vicinity of Isabel (10°-40°N, 30°-85°W).**

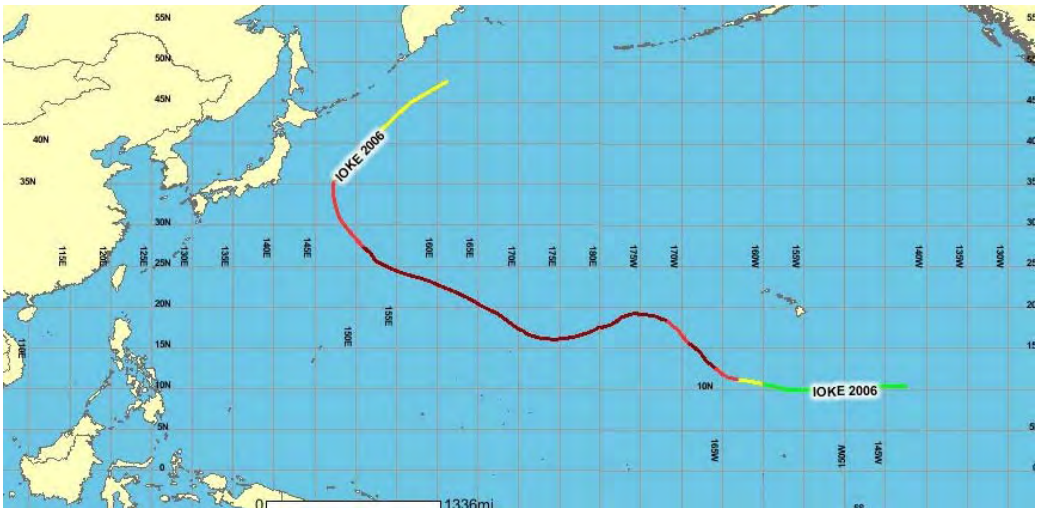


**Figure 16 - Path of Ioke, 2006. Category is denoted by color: Red indicates H5-H3, pink indicates H2-H1, yellow indicates tropical storm, and green indicates tropical disturbance. Courtesy of the NOAA Coastal Services Center Historical Hurricane Tracks (http://maps.csc.noaa.gov/hurricanes/viewer.html)**

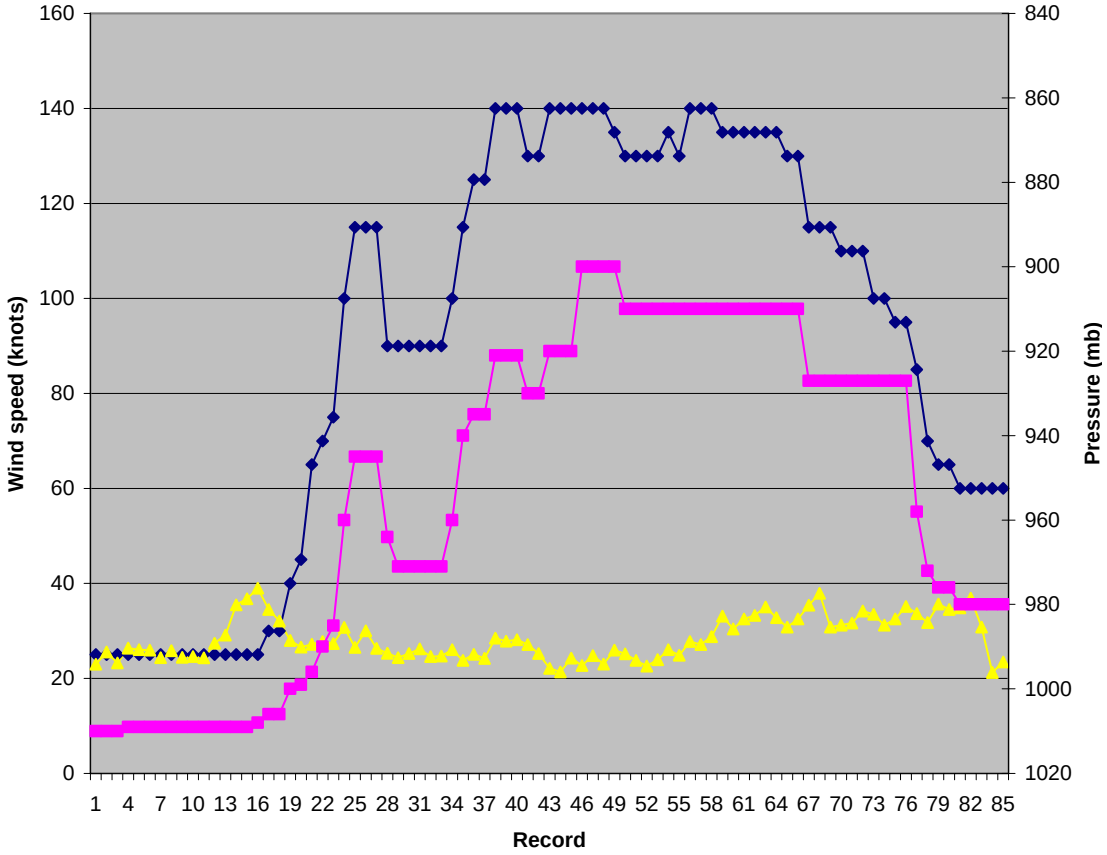


**Figure 17 - Evolution of Ioke, 2006 over time. The x-axis is the record number. Blue diamond is the NCAR recorded maximum sustained 1-minute wind velocity (knots, left y-axis). Pink square is the NCAR recorded pressure in the eye (mb, right y-axis). Yellow triangle is the temporally matching maximum wind velocity (knots, left y-axis) in the vicinity of Isabel (10°-40°N, 30°-85°W).**

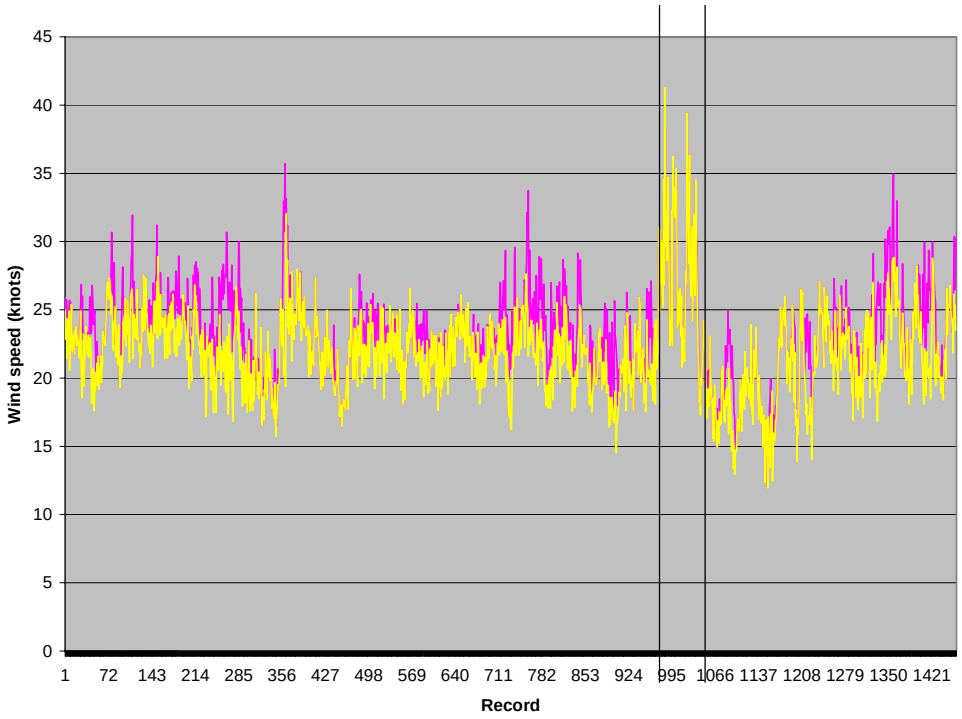


**Figure 18 - Maximum wind velocity (knots) in the vicinity of Isabel for the year 2003. Pink refers to measurements in (10°-25°N, 30°-85°W). Yellow describes measurements in (10°-25°N, 30°-67°W). The first vertical black line indicates Fabio 2003's entrance to this box (another category 5 hurricane), while the second black line indicates Isabel 2003's exit from this box.**

Since the addition of satellite data significantly altered the wind stress in the Southern Ocean, we limit the remainder of this study to thirty years of the NCEP dataset (1978 to 2007). However, due to the long timescale response of the ocean and model procedures, this dataset must be extended beyond thirty years. We could not identify significant timescales or spatial patterns of the variable wind stress. Therefore, since the mean wind stress and distribution of variable wind stresses appear invariant with time, we simply repeated the thirsty year dataset for as long as needed.

## 2.3. MODEL DESCRIPTION

Due to long timescales in the ocean and the importance of the mixed layer depth to ocean heat uptake (see Introduction), this study requires a computationally efficient ocean model with a good mixed layer depth parameterization. This study uses the MIT Integrated Global System Model (IGSM), a coupled 2D atmosphere 3D ocean model (Sokolov et al., 2005, Marshall et al 2004, Dutkiewicz et al. 2005). Here we briefly describe the atmosphere model, ocean model, and coupling procedure.

### *2.3.1. GISS 2D Atmospheric Model Data*

The Goddard Institute for Space Studies (GISS) 2D atmospheric model is adapted from the GISS GCM (Stone & Yao 1990, Hansen et al 1983, Sokolov & Stone 1995, Sokolov et al. 2005). It calculates the wind stress using the primitive equations and passes momentum, heat, and moisture fluxes to the ocean. The model has eleven layers in vertical: four in the planetary boundary layer, five in the troposphere, and two in the

stratosphere. Spatial coverage is 4° in latitude. The temporal timestep for dynamics is 20 minutes, for physics is hourly.

The model's numerics and parameterizations of physical processes closely parallel those of the GISS GCM. This code includes all significant greenhouse gases, such as $H_2O$, $CO_2$, $CH_4$, $N_2O$, CFCs, etc., and twelve types of aerosols (Hansen et al., 1983). Parameterized clouds include convective clouds (associated with moist convection) and large-scale or supersaturated clouds (formed due to large-scale condensation.). Other components include a linked set of coupled land models, the Terrestrial Ecosystem Model (TEM), and a now more fully integrated Natural Emissions Model (NEM), and the Community Land Model (CLM). Feedbacks in the surface heat and freshwater fluxes are allowed. Extensive tests of the capability of this 2D atmospheric model when coupled to an ocean GCM indicate that the models' performance is similar to but computationally more efficient than 3D atmospheric models (Kamenkovich et al., 2002; Huang et al., 2003; Dalan et al., 2005; Sokolov et al., 2005).

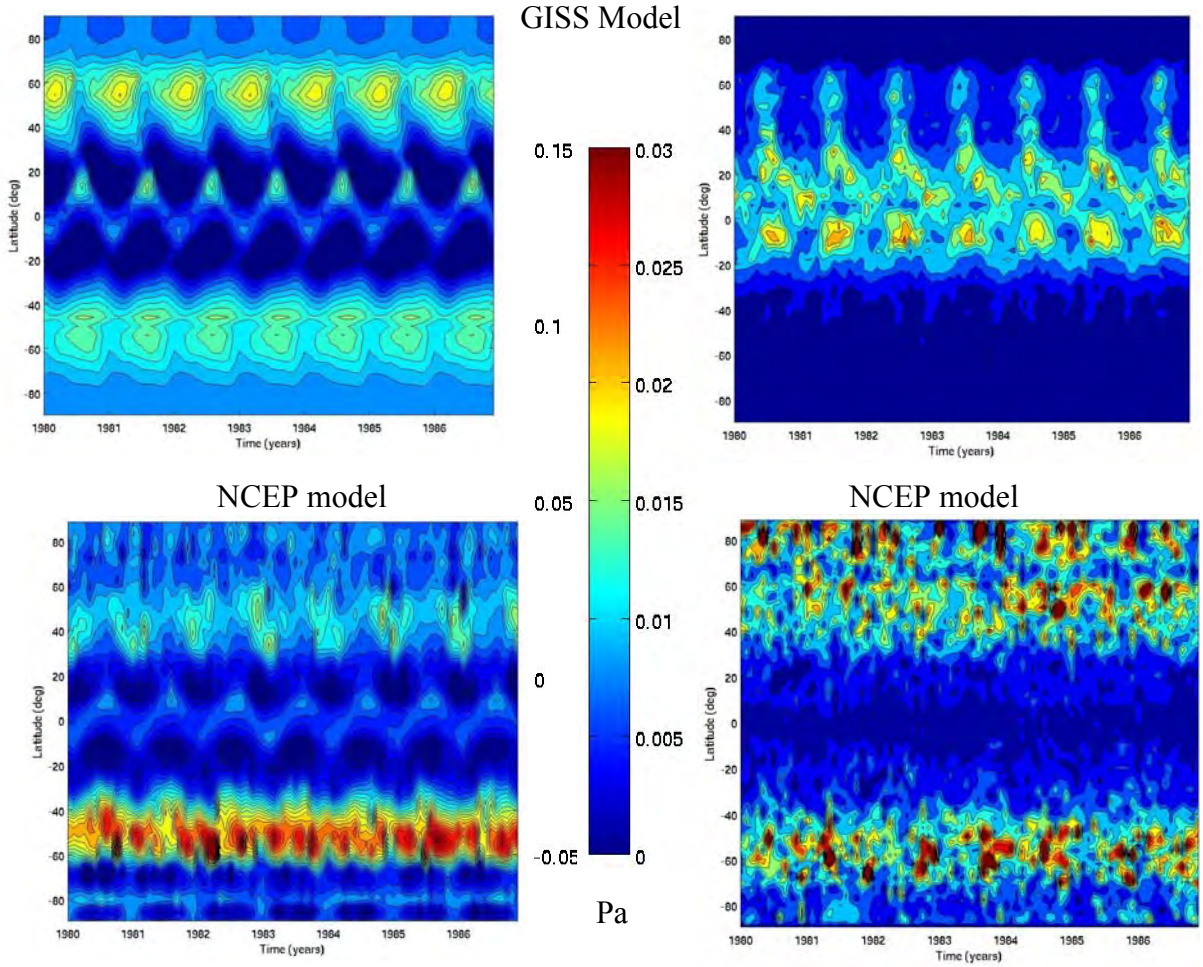


**Figure 19 – Four-hour GISS and NCEP dataset, 1980 to 1986, 2°×2.5° box: Zonal mean zonal wind stress (Pa). X-axis is time in months, ranging from January 1980 to December 1986. Y-axis is latitude, ranging from -90° to 90°. Left column (and left label on contour bar) is monthly zonal mean, right column (and right label on contour bar) is standard deviation from each monthly zonal mean.**

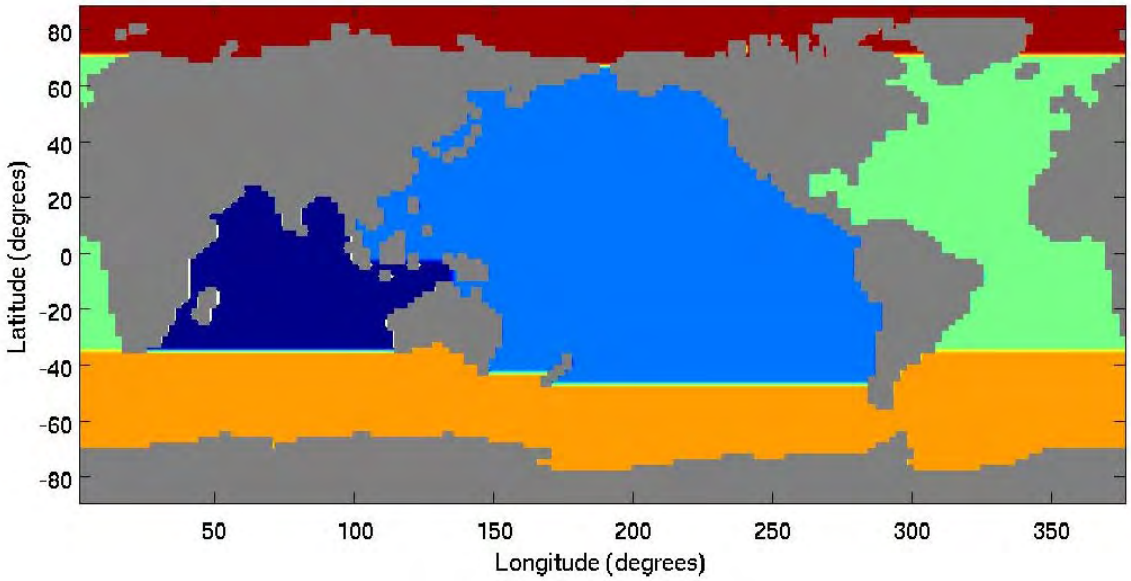


**Figure 20 – Oceans defined in the MIT Ocean General Circulation Model. Grey is land, red is the Arctic Ocean, orange is the Southern Ocean, green is the Atlantic Ocean, royal blue is the Pacific Ocean, and dark blue is the Indian Ocean.**

Figure 19 shows the evolution of the GISS zonal mean zonal wind stress values for 1978-2007. The standard deviation of the zonal NCEP mean was calculated for comparison[6]. Magnitudes and patterns differ between the datasets. Spatially, the GISS mean wind stress dataset lacks the very strong 40°-60°S band, but has a strong equatorial and 40°-60°N band. Temporally, the 40°-60°N mean wind stress band peaks in the summer instead of the winter. Due to the zonal averaging, the standard deviations are an order of magnitude less than the means. Standard deviations are smaller in the GISS set, but are still correlated with areas of high mean wind stress. The seasonal cycle appears strong in both the mean and standard deviation of the GISS model, weak in the mean of the NCEP data, and nonexistent in the standard deviation of the NCEP.

*2.3.2. 3D Ocean*

This study requires an ocean model with an appropriate parameterization for mixed layer depth and oceanic boundary layer mixing. We will employ the MIT Ocean General Circulation Model with a suitable mixing scheme (K profile parameterization, or KPP, Large et al.1994) and sufficient resolution to resolve mixed layer processes (specifically, 2º×2.5º horizontal resolution with 22 vertical levels). Temporal coverage is every four hours. Parameterizations include the Gent-McWilliams-Redi parameterization (GMR, Gent and McWilliams 1990, Redi 1982) with a surface tapering scheme, a thermodynamic sea-ice model, and a biogeochemical component.

For small wind stresses (below the sea spray drag regime) and on scales comparable to the model's resolution, this ocean model is suitable to examine the sensitivity of ocean heat uptake to transient wind stress. Note the sensitivity of ocean heat uptake to transient wind stress will be a function of how KPP mixes heat down and

[6] Note, a comparison of the standard deviation of the NCEP mean, Figure 10, and the standard deviation of the zonal NCEP mean, Figure 19, indicates that the NCEP data has large variability along a latitude band.

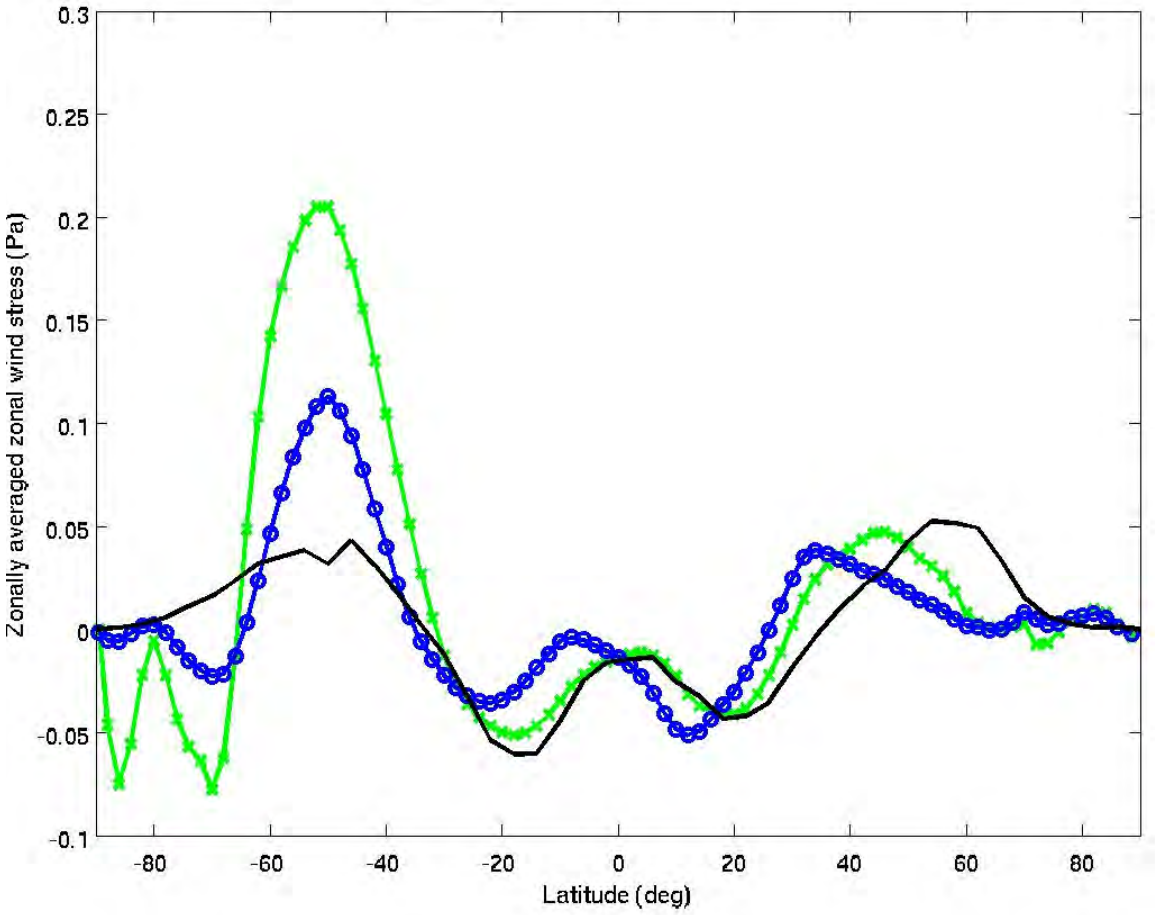


**Figure 21 - Annual globally averaged zonal wind stress for one randomly chosen year (PW). Data sets include the NCEP wind velocity data (o-blue line), Trenberth climatological wind stress data (x-green line), and GISS 2D atmospheric model data (solid black line).**

alters the mixed layer depth; future work will examine other mixing schemes. Jeff Scott has finalized an improved model with tidal mixing, improved river mouth mixing (employing a simplistic representation of Ferrari 2006), and parallelization (decreased computation time).

For reference, the MIT Ocean General Circulation model oceans are defined in Figure 20.

### *2.3.3. Coupling*

Coupling is done at every ocean timestep (four hours); the hourly atmospheric fluxes of surface heat, freshwater, and momentum are averaged over this period. Unfortunately, sub-gridscale parameterizations, differing resolutions, construction of 2D fields from 1D fields, and other problems cause the present-day simulation to drift away from the current climate. Three types of flux adjustments are used to prevent model drift.

The surface heat flux is "fixed flux adjusted". First the model is spun up for 1000 years with restoring boundary conditions in the top 10m grid cell (during which the 2D atmosphere's heat flux is exchanged with the ocean). At the end of this period, we diagnose these restoring fluxes, which henceforth are added to the surface heat flux equation.

Freshwater forcing is flux adjusted from "observed" values. First the model is spun up for 1000 years with observed freshwater forcing (evaporation minus precipitation minus runoff; the 2D atmosphere's fluxes are not passed to the ocean). At the end of this period, we diagnose the difference between the observed value and the atmospheric model value. Then a new damping term (as a function of the diagnosed difference) is added to the freshwater flux equation.

Since the GISS dataset lacks a strong southern wind stress (see Figure 21), the momentum forcing (wind stress) is anomaly coupled. In this process, first the model is spun up for 1000 years. At year 1000, we diagnose the monthly mean atmospheric winds. For each subsequent coupling timestep, the monthly mean atmospheric winds are subtracted from the model values to yield the anomaly from the monthly mean. A climatological mean field (smoothed over time) is added to the anomaly values. This new value is passed to the ocean.

The anomaly coupling process requires a mean wind field. Since this study examines NCEP variable wind stresses, ideally the mean wind field should come from the NCEP dataset. However, the NCEP wind stress field is rather weak; and cannot sustain a reasonable overturning circulation. The stronger Trenberth mean wind stress field (see Figure 21)[7] yielded a much more realistic and efficient spinup. Therefore, to remain consistent with previous models, this study uses the Trenberth mean wind stress[8].

The Trenberth average monthly mean wind stresses were calculated from twice daily 1000 mb winds (0Z, 12Z), years 1980 to 1986 of the European Center for Medium Range Weather Forecasts (ECMWF) wind velocity dataset (Trenberth et al., 1990). Spatial coverage was converted to 2°×2.5° for inclusion in the MITgcm. Monthly mean wind stresses for January, April, July, and October are shown in Figure 22. In general, means peak at 40-60° in the winter hemisphere. These spatial and temporal patterns are similar to the NCEP monthly mean wind stress (Figure 9), but larger than the GISS magnitudes, mainly from 40°S to 60°S. The Trenberth variable wind stress was not available for examination.

[7] This occurs because the NCEP drag coefficient ($C_D$) is constant with velocity, while the Trenberth $C_D$ is very large at high wind velocity. The Trenberth $C_D$ was calculated using climatological sea surface temperature of surface fluxes (Trenberth et al., 1990). A lower limit of $v$=1m/s was used on the drag coefficient. Further discussion of drag coefficients is given in Köhl & Heimbach (2008).

[8] A full explanation is much more complicated and beyond the scope of this thesis.

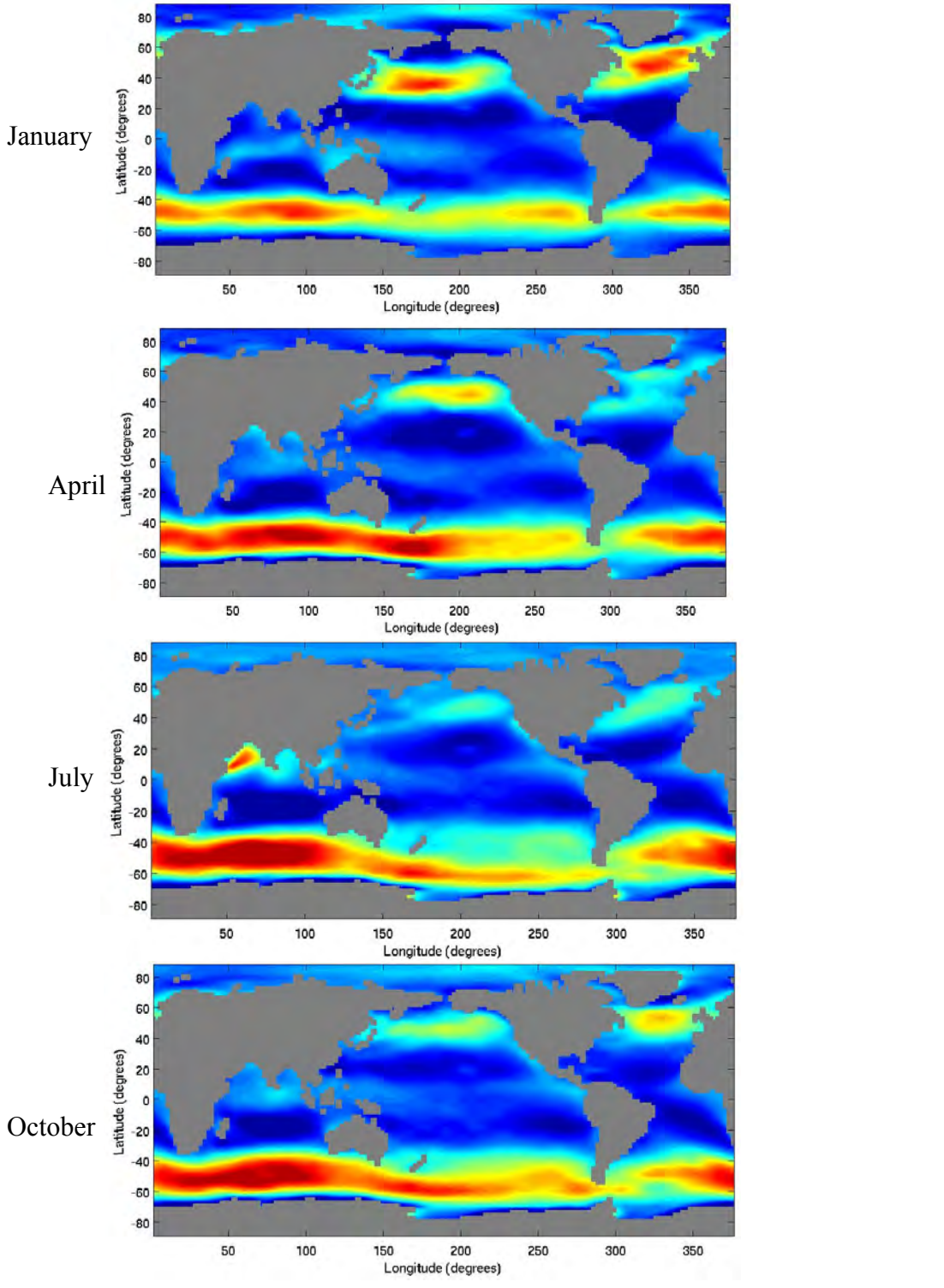


**Figure 22 - Twelve-hour Trenberth dataset 1980-1986, 2°×2.5° box: U January mean wind stress (Pa).**

# CHAPTER 3: OCEAN SENSITIVITY TO VARIABLE WIND STRESS

This thesis seeks to characterize the effects of variable wind stress on ocean properties in a coarse resolution model. On the near-instantaneous timescale, we already know how the model ocean will react to variable wind stress. Recall Large et al 1994 concluded that, given the correct surface forcings and advective transports, KPP will distribute properties properly in the vertical over timescales from hours[9] to years. Hence in our model, we already have a good understanding of how the instantaneous mixed layer depths (and other associated ocean values) are sensitive to variable wind stress.

However, the literature review of Chapter 1 indicates that we do not know whether/how variable wind stress may affect longer timescale model ocean properties. Hence this thesis will use a variety of model runs to answer the remaining questions posed in CHAPTER 1:

- Are ocean properties (i.e. ocean heat content) sensitive to changes in the variable wind stress? If yes, is correct wind stress variability important for predictions of the ocean mean state?
- In a coarse resolution model, can variable wind stress be the major source of variability of the MOC (and other ocean metrics)?

First we examined whether variable wind stress would change the mean state of the ocean in our coarse resolution model. Section 3.1 demonstrates that our coarse resolution model is sensitive to variable wind stress on long timescales. We then construct and characterize Model A (GISS wind stress anomalies) and Model B (NCEP variable wind stresses).

Next we tested our models' responses to a forcing scenario. In Section 3.2 we force Model A and Model B with a current climate scenario (including carbon dioxide, volcanic eruptions, and solar forcing). Model output is compared to observations.

Given the response to the current climate scenario, we would also like to know if changes in the control state have an effect on global warming scenarios (our probable future). Section 3.3 examines the sensitivity of ocean metrics to variable wind stress in two global warming scenarios. Scenario 1 is forced with a 1% $CO_2$ increase per year for 130 years. Scenario 2 is forced with observed forcing from 1860-1990 from Section 3.2, and then a business as usual emissions scenario from 1990-2100.

## 3.1. NO FORCING SCENARIO: CONTROL STATE

As a simple test, first we verified that an arbitrary change in the magnitude of the GISS wind stress anomaly would change the annual mean ocean heat content in our coarse resolution model in a no forcing scenario (control state). Recalling that the global NCEP variable wind stress fluctuations along a latitude band (Figure 10) were an order of magnitude higher than the GISS zonal wind stress anomaly at each latitude (Figure 19),

[9] For the hourly testing, they tested their parameterization versus data from the Ocean Storms experiment of D'Asaro 1985. Seven storms whose peak wind stresses all surpass 0.4 Pa were examined. Table 3 in Large et al gives the response of KPP to the wind stress events; KPP predictions show pretty good agreement to observations.

we created scenarios where we multiplied the GISS wind stress anomaly by a certain factor up to 10 (0×, 1×, 5×, 10×). The IGSM was spun-up to equilibrium with the 1× scenario, then run for an additional 80 years for each scenario.

The 0× scenario reached equilibration, and was very similar to the 1× response. Therefore we conclude the zonal GISS wind stress anomaly is too small to have any meaningful effect on ocean heat uptake. For the remainder of this study, we assume the 1× and 0× scenario are essentially equivalent. Future studies would use a 0× scenario.

Although a much longer integration was needed to isolate the equilibrated response, we observed regional differences in ocean heat content between the 5× and 10× scenarios and the 1× scenario (Figure 23). Differences are on the order of 0.01-0.1% of the total heat content, and are a result of an abundance of interesting but non-obvious behaviors; magnitudes and patterns nonlinearly vary horizontally and vertically.

Given that the annual mean ocean heat content of our coarse resolution model responded to altered wind stress anomaly scenarios, a study of equilibrated differences would be appropriate.

5× wind stress anomaly run minus 1× wind stress anomaly run

10× wind stress anomaly run minus 1× wind stress anomaly run

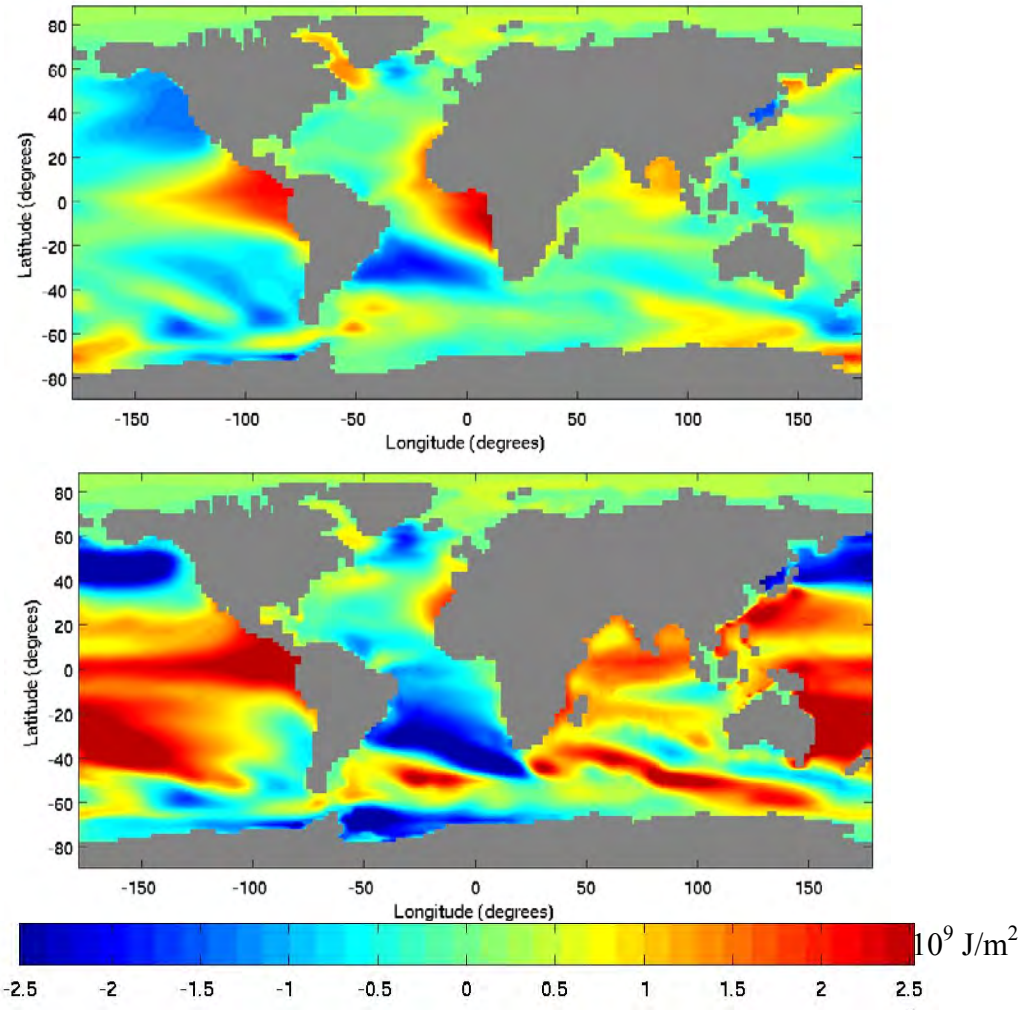


**Figure 23 – Differences in model ocean heat content over depths 0-3000m for an 80 year run, $10^9$ J/m$^2$. Depths 0-700m (thermocline only) yield similar spatial patterns to depths 0-3000m (but smaller magnitudes).**

*3.1.1. Spinups*

To examine the effects of variable wind stress on ocean properties, we used the IGSM described in Section 2.3. Two spinup procedures where used[10]:

Model A. : The no variable wind stress spinup. Here we ran the model with GISS wind stress anomalies for 1000 years at 1980 forcings, then diagnosed the flux adjustments. The flux adjusted model was run for another 2000 years with the GISS wind stress anomalies at 1860 forcings, and during the last 100 years, TEM was turned on. The final value is considered the fully spun-up 1860 value.

Model B. : The NCEP variable wind stress spinup. Here we ran the model with NCEP variable wind stresses for 1000 years, then diagnosed the flux adjustments. The flux adjusted model was run for another 1000 years with the NCEP variable wind stresses and the1860 forcing of $CO_2$. The last 100 years TEM was turned on. The final value is considered the fully spun-up 1860 value.

The "control state" of each model begins in 1860, and has been run for an additional 240 years (for comparison with remainder of the study) with no change in forcing.

Note, a comparison between Model A and Model B would, strictly speaking, study the effects of a large change in the Southern Ocean with small changes elsewhere. However, our previous conclusion that the 0× and 1× variable wind stress scenarios are equivalent indicates that Model A can be considered a "no variable wind stress" scenario.

*3.1.2. Mixed Layer Depths*

Recall that we already have a good understanding of how the instantaneous mixed layer depths (and other associated ocean values) are sensitive to variable wind stress. Here we will compare Model A and Model B to determine whether mean mixed layer depths are also sensitive to variable wind stress[11].

Figure 24 shows the mixed layer depths averaged over 1860 to 1865. Model B has a deeper Southern Ocean mixed layer depth than Model A. This occurs because in the Southern Ocean, NCEP contains very high variable wind stress capable of permanently deepening the mixed layer depth below the convective mixed layer depth (see Introduction for discussion). Outside of the Southern Ocean, Model B has slightly more uniform mixed layer depths than Model A; low (high) latitudes have shallower (deeper) mixed layer depths. It is unclear whether this difference is a direct result of variable wind stress, or an indirect result of the variable wind stress's effect on ocean heat content, temperature, and/or salinity.

We also examined monthly mixed layer depths (not shown). Both Model A and Model B display seasonal variability. Model B monthly mixed layer depths also display

[10] We also examined an intermediate model, the GISS/NCEP spinup. First we took the fully spun-up 1860 state of Model A. Then the model was run for another 200 years with the NCEP variable wind stresses, followed by another 100 years where TEM was turned on. The final value was considered the fully spun-up 1860 value. The only difference between this model and Model B was the flux adjustments (and the fact that this model was not as well equilibrated as Model A or Model B; some modest drift remained).

There appeared to be little difference between this model and Model B; models yield very similar states, and show similar patterns throughout the rest of this study. Future researchers should note that if time is limited, to reduce computational time one could use the standard GISS wind stress anomaly spinup and apply the new wind stresses in 1860 as desired.

[11] Note instead of instantaneous values, we examined an annual average over a five year interval. This is consistent with the remainder of this study, where 5 year ranges are needed to compare to observations.

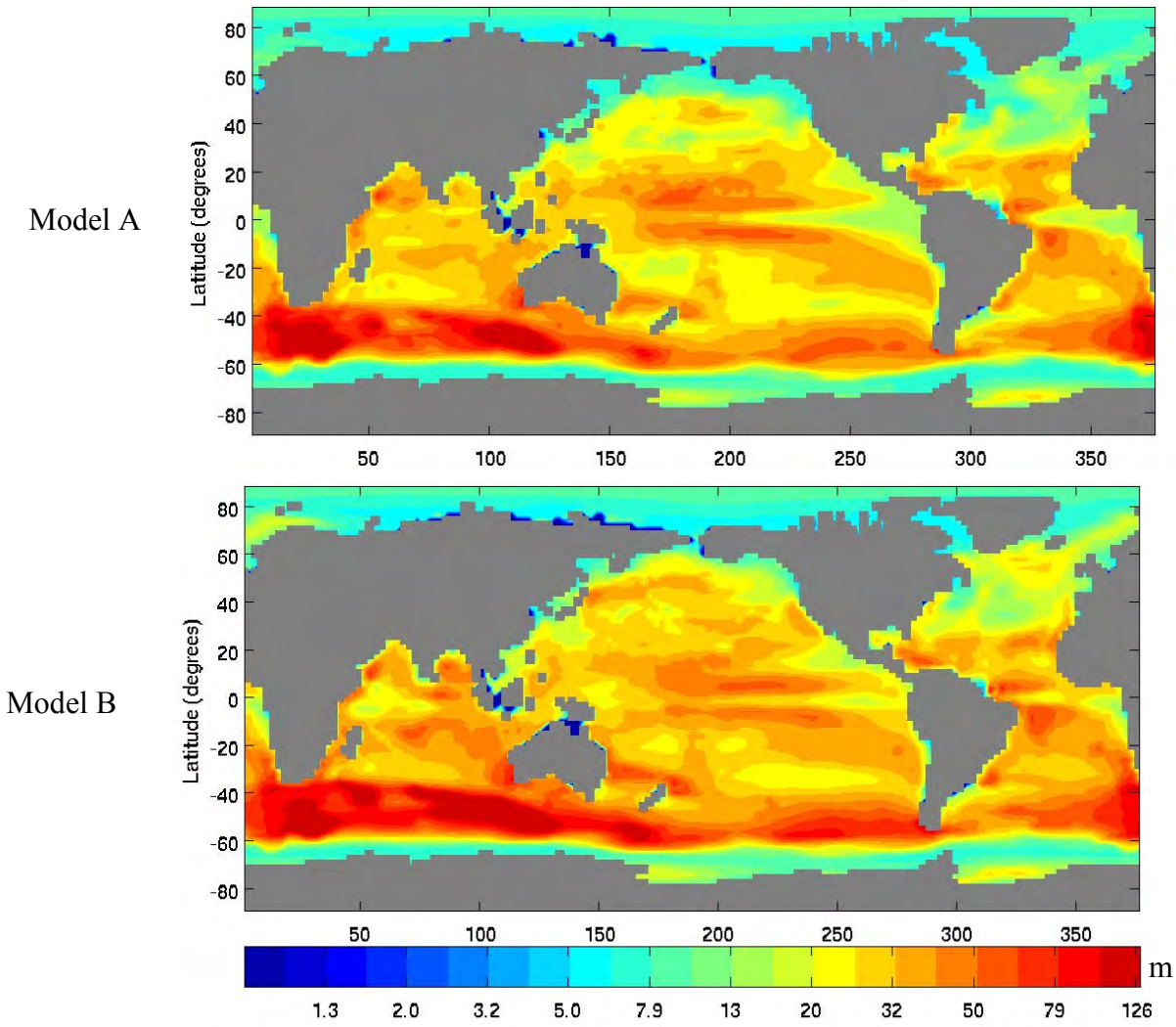


**Figure 24 – Mixed layer depth (m), control run, average 1860 to 1865.**

interannual variability (while Model A values do not). Depth variations are of roughly 1-2m with a periodicity of 30 years, reflecting the 30 year variable wind stress dataset.

### *3.1.3. Ocean Heat Content*

We examined the ocean heat content averaged over 1860 to 1865. Both models contain $3.5\times10^{26}$J in an average year, but spatial patterns differ.

Figure 25 shows a latitude/longitude plot of the annual average ocean heat content ($J/m^2$) summed over depths 0-3000m for an average of years 1860 to 1865. Along a latitude circle, both models have more heat per unit area in the Atlantic Ocean than in the Indian and Pacific Oceans (generally paralleling ocean temperature at depth).

Figure 26 shows the latitude/longitude ocean heat content difference image (Model B minus Model A). In general, the ocean heat content differences between Model B and Model A are 1-2 orders of magnitude smaller than ocean heat content values. In the Atlantic and Pacific, the deeper (shallower) mixed layer depths of Figure 24 match areas of increased (decreased) ocean heat content. In the Southern Ocean, the deeper mixed layer curiously results in less ocean heat content. Additionally, Model B has a strange heating event going on in the Pacific corner, which we cannot explain.

Model A

Model B

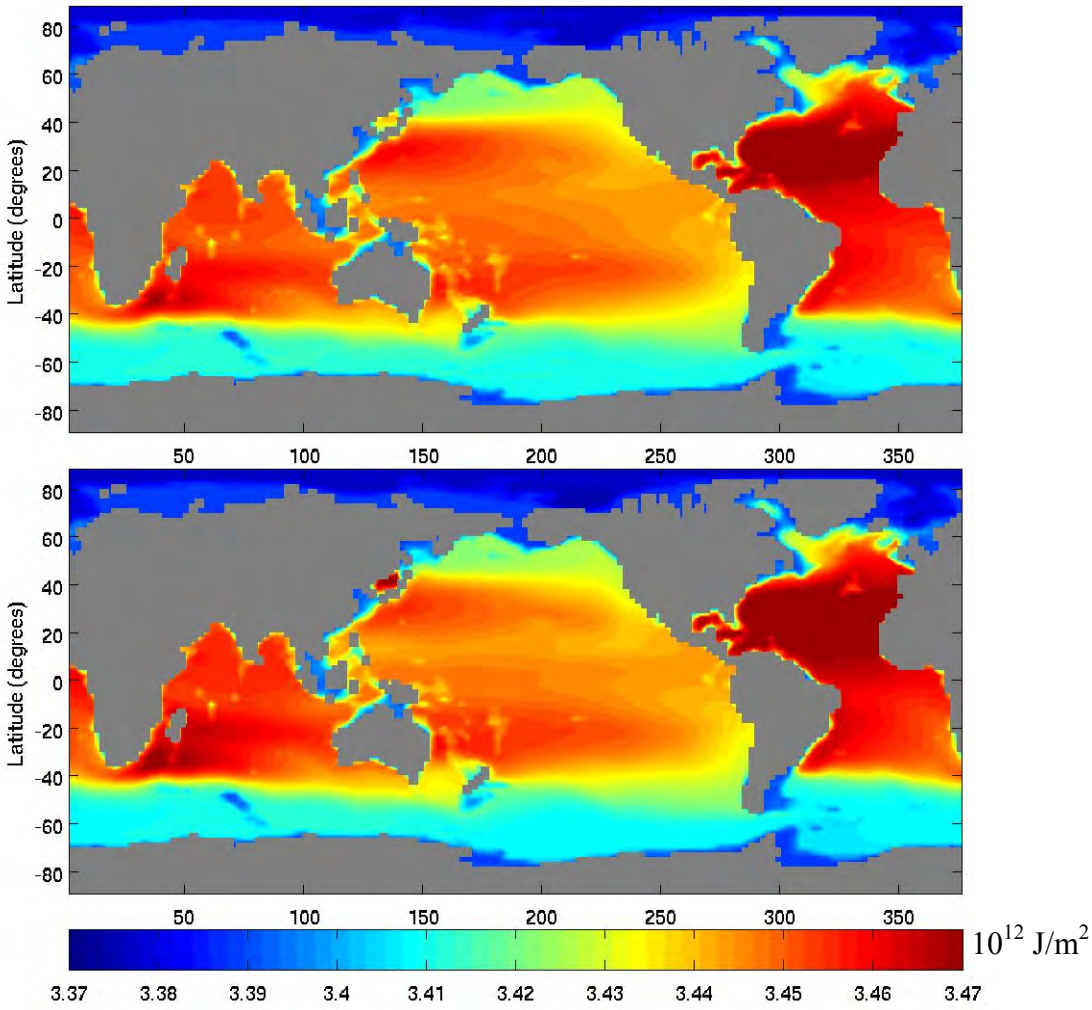


**Figure 25 –Ocean Heat Content, control run. Averaged over 1860-1865, over depths 0-3000m ($10^{12}$ J/m$^2$). Depths 0-700m (thermocline only) yield similar spatial patterns, but smaller magnitudes.**

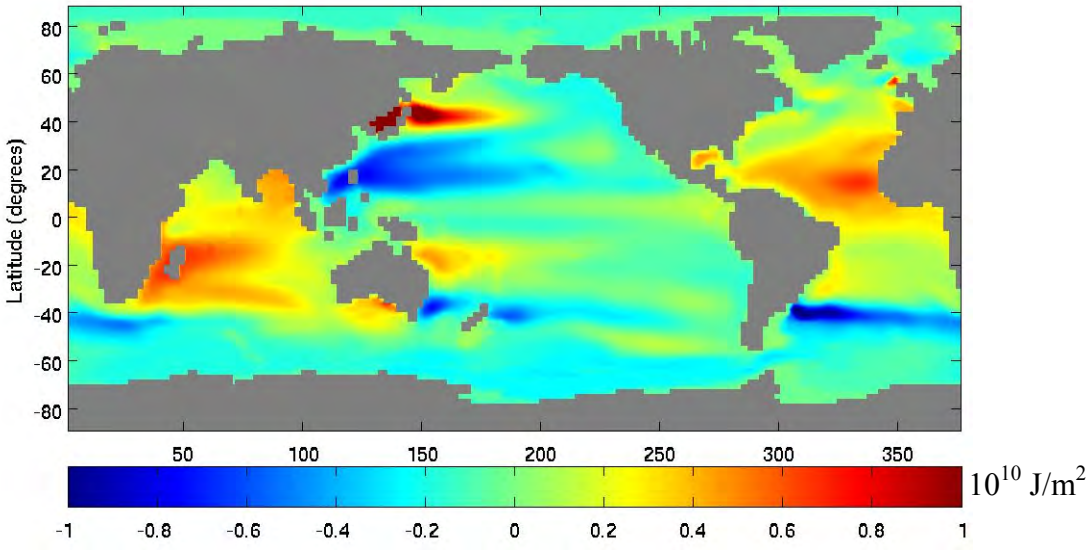


**Figure 26 –Figure 24's Model B minus Model A. Ocean Heat Content units are ($10^{10}$ J/m$^2$).**

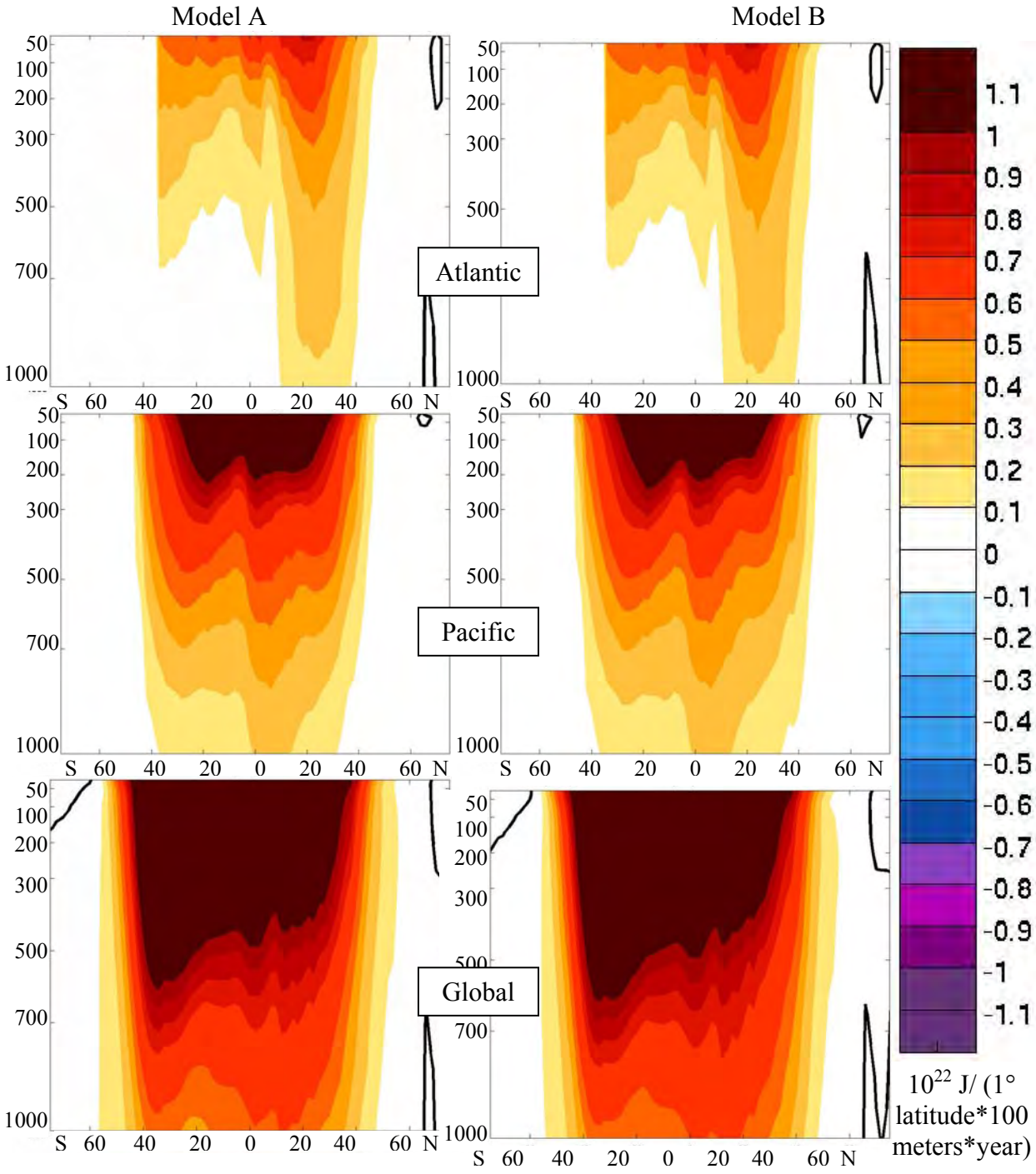


**Figure 27 – Zonally integrated ocean heat content in 1° latitude belts for 100m thick layers, annually averaged for years 1860 to 1865 ($10^{22}$ J/(1° latitude*100 meters*year) ). X-axis is latitude (80°S to 80°N), Y axis is depth (0-1000m). Values are NOT weighted by the different ocean belt lengths. Heat content values are plotted at the midpoint of each 100-m layer.**

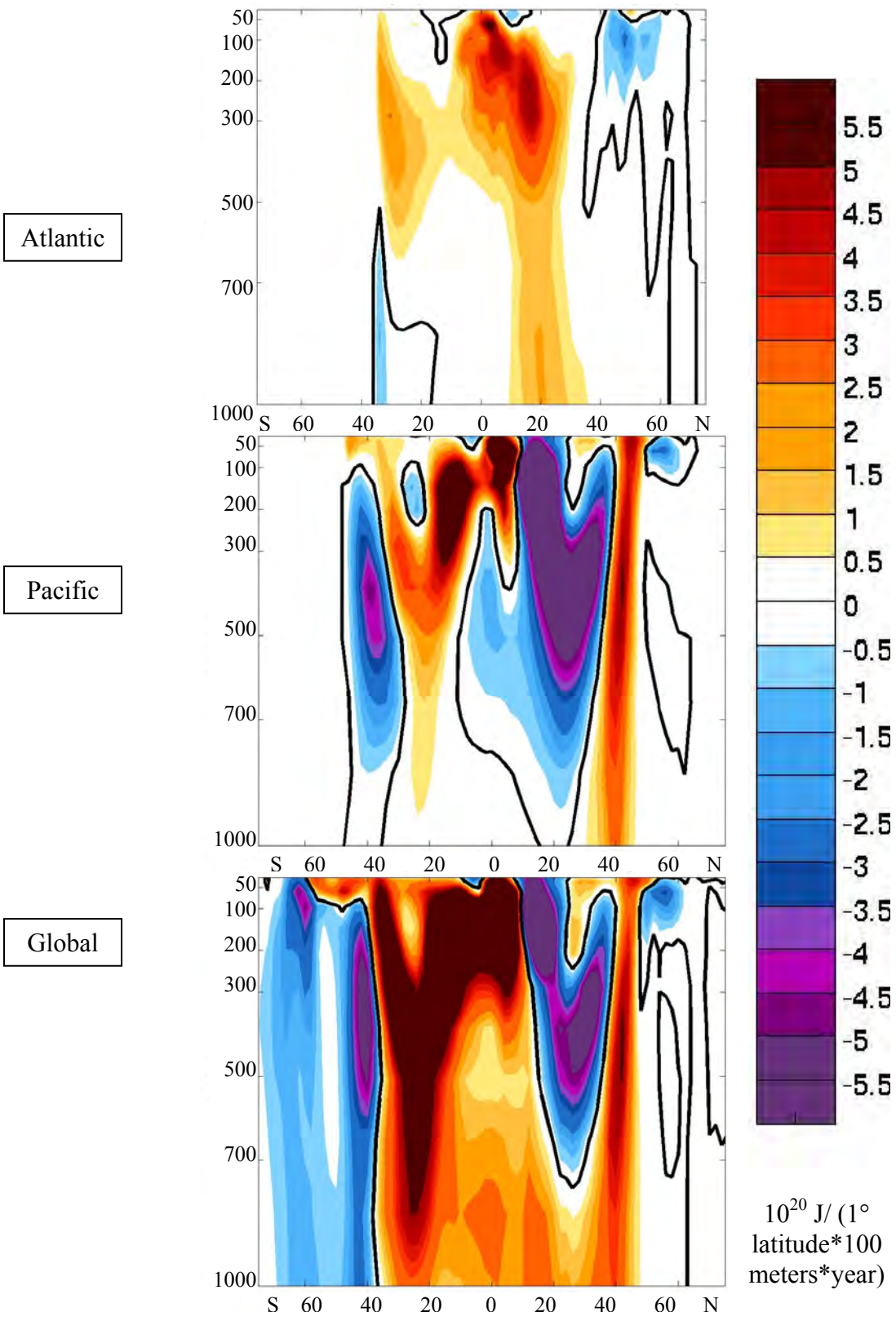


**Figure 28 -Figure 27's Model B minus Model A. Ocean Heat Content units are ($10^{20}$ J/(1° latitude*100 meters*year) ). X-axis is latitude (80°S to 80°N), Y axis is depth (0-1000m).**

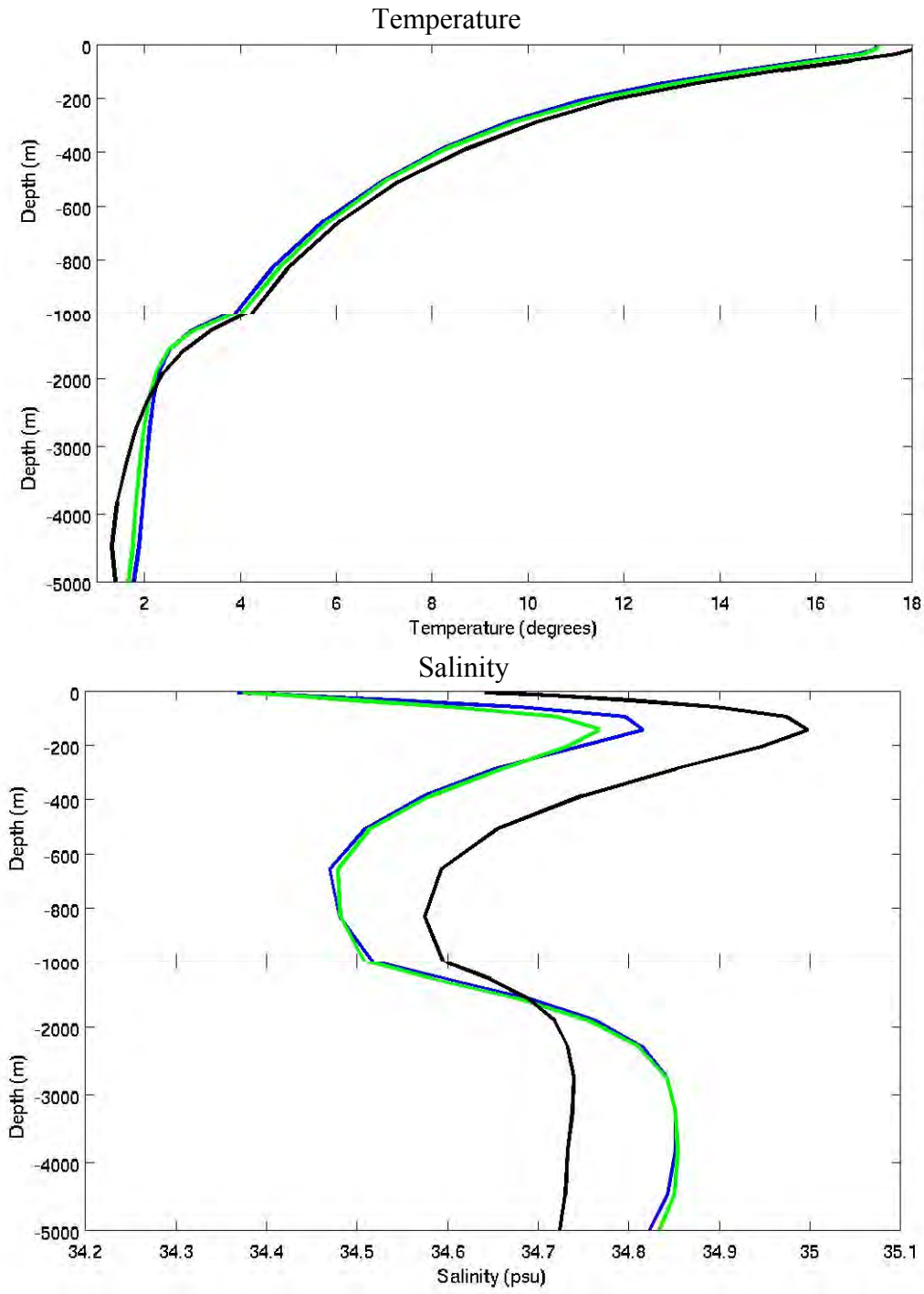


**Figure 29 –Globally averaged ocean temperature (°C) and salinity (psu) at depth. Model A is in blue, Model B is in green, Levitus observations are in black.**

Figure 27 shows the zonally integrated ocean heat content (J) of the Pacific, Atlantic, and global oceans in 1° latitude belts for 100m thick layers, annually averaged for years 1860 to 1865 (n.b., values are not strictly comparable to Figure 25). Model A and Model B have nearly identical ocean heat content structure, with warm waters clustered near the surface at the equator. Heat penetrates deeply in the northern Atlantic and in the Southern Ocean.

Figure 28 shows the latitude/depth ocean heat content difference image (Model B minus Model A). Again, the ocean heat content differences between Model B and Model A are 1-2 orders of magnitude smaller than ocean heat content values. Model B has larger energy content in the northern hemisphere Atlantic Ocean and the southern hemisphere Pacific Ocean, while Model A has larger energy content in the northern hemisphere Pacific Ocean. Due to its relative size, the Pacific dominates the global pattern.

Finally, Figure 29 shows the globally average ocean temperature and salinity at depth for Model A and Model B. For reference, Levitus observations are denoted in black. We find that both models have very similar temperature structure, with Model B having cooler deep water. In general both models exaggerate salinity profiles, although Model B has a less exaggerated surface salinity structure.

*3.1.4. Meridional Overturning Circulation and Meridional Heat Flux*

Next we explored whether the ocean heat content differences between Model and Model B were transient or permanent. Figure 30 shows the maximum in the annually averaged Atlantic meridional overturning circulation (assumed to be in 28-74°N). Model A demonstrated a sinusoid-like variability with some apparent decadal variability (roughly 30 years) and with magnitude of 0.5PW. Model B demonstrated the same basic sinusoidal variability, but with non-sinusoidal annual deviations of an additional 1-2PW. In Model B, the full behavior repeats every 30 years, likely due to a combination of the base year 30 period and the choice of the 30 years of the NCEP variable wind stresses. The Model variability of Model A (which looks like a 30 year cycle) is coincidentally similar to that of Model B (with a more variable imposed 30 year cycle).

Then we examined the effect of variable wind stress on the meridional heat flux. Figure 31 shows the annual average meridional heat flux averaged from years 1860 to 1865. We find that Model B shifts the position and increases the magnitude of the meridional heat flux, most notably on the peak values. Monthly values (not shown) show similar shift. Since it can be difficult to alter the meridional heat flux, even this small shift is significant (at least in climate models).

*3.1.5. Other Fields*

After identifying the periodicity in the maximum of the meridional overturning circulation over time, we chose to examine changes over time in the sea surface temperature (Figure 32), the sea surface salinity (Figure 33), and the surface air temperature (Figure 34). Surface temperature plots are very noisy, but Model B is discernibly warmer than Model A. Model B has larger sea surface salinity than Model A, but the explanation is likely complicated by different mixed layer salinity structure in various ocean basins.

However, the sea surface salinity also shows a distinct 30 year periodic behavior in Model B and no periodic behavior in Model A. We believe this occurs due to the repetition of the 30 years of NCEP variable wind stress (1978-2007). Given more time, we could attempt to remove this periodicity by either randomly picking NCEP variable wind stress from year to year, or doing a correlation between mean wind stress and variable wind stress and applying a parameterization.

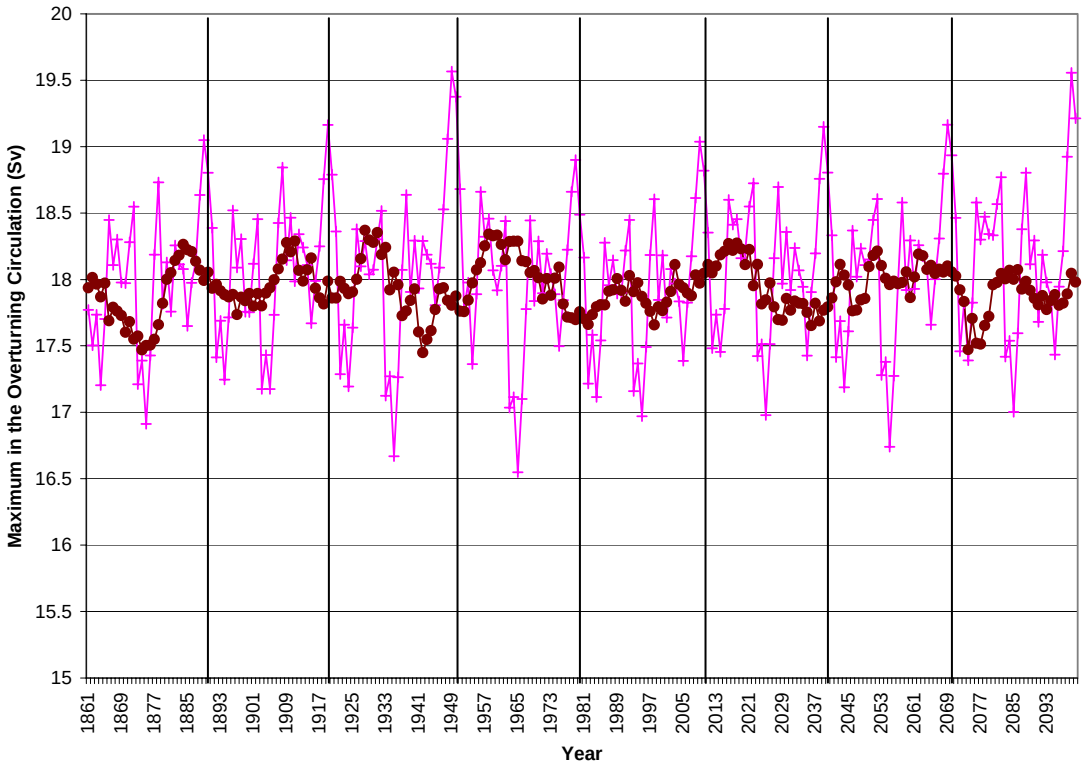


**Figure 30 –Maximum in the Atlantic Meridional Overturning Circulation (28-74°N). Model A is in magenta circles, Model B is in pink pluses. Vertical Lines indicate 30 year intervals.**

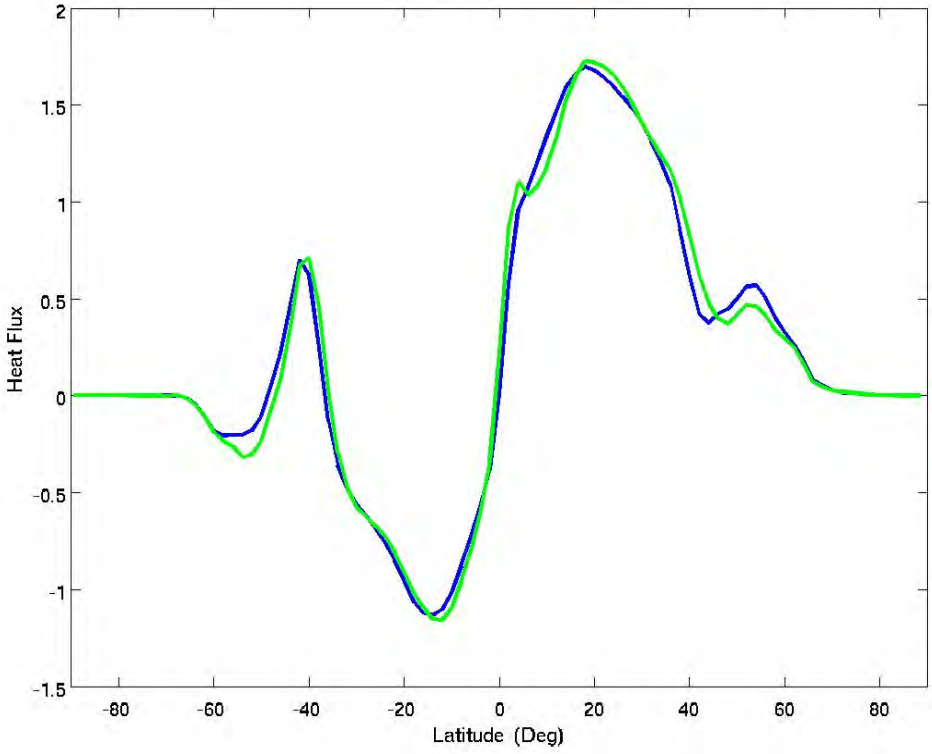


**Figure 31 –Meridional Heat Flux (PW) control run, averaged over 1860 to 1865. Model A is in blue, Model B is in green.**

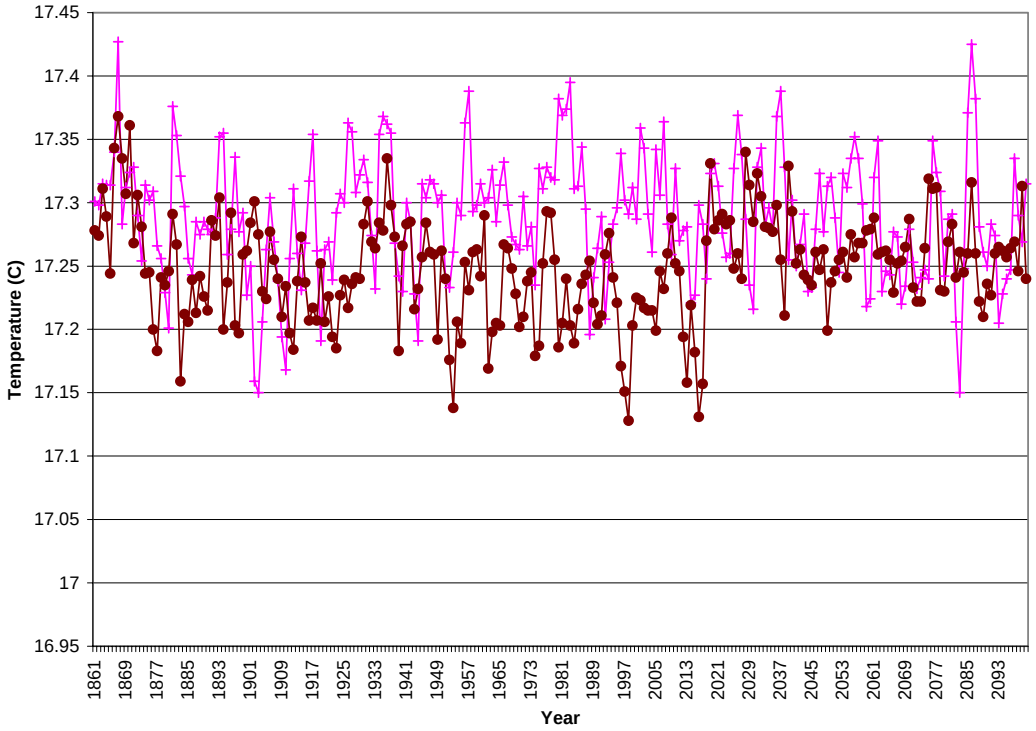


**Figure 32 – Globally averaged annually averaged sea surface temperature (C), 1860 to 2100. Model A is in magenta circles, Model B is in pink pluses.**

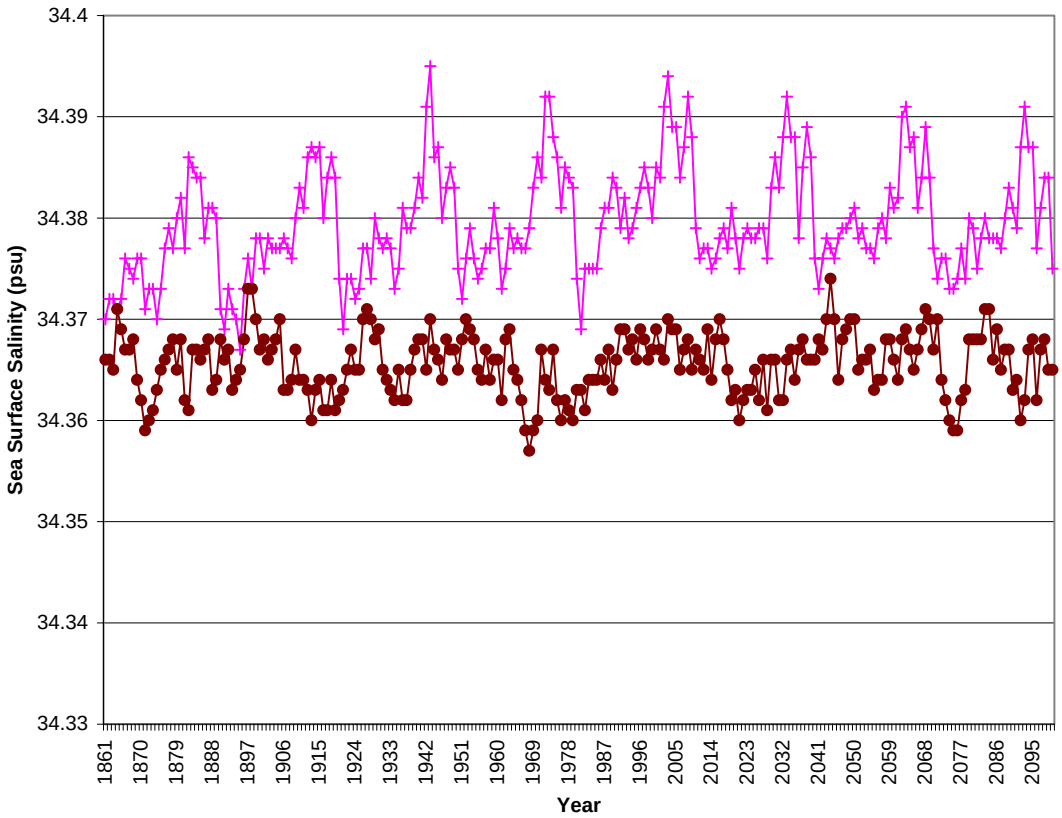


**Figure 33 – Globally averaged annually averaged sea surface salinity (psu), 1860 to 2100. Model A is in magenta circles, Model B is in pink pluses.**

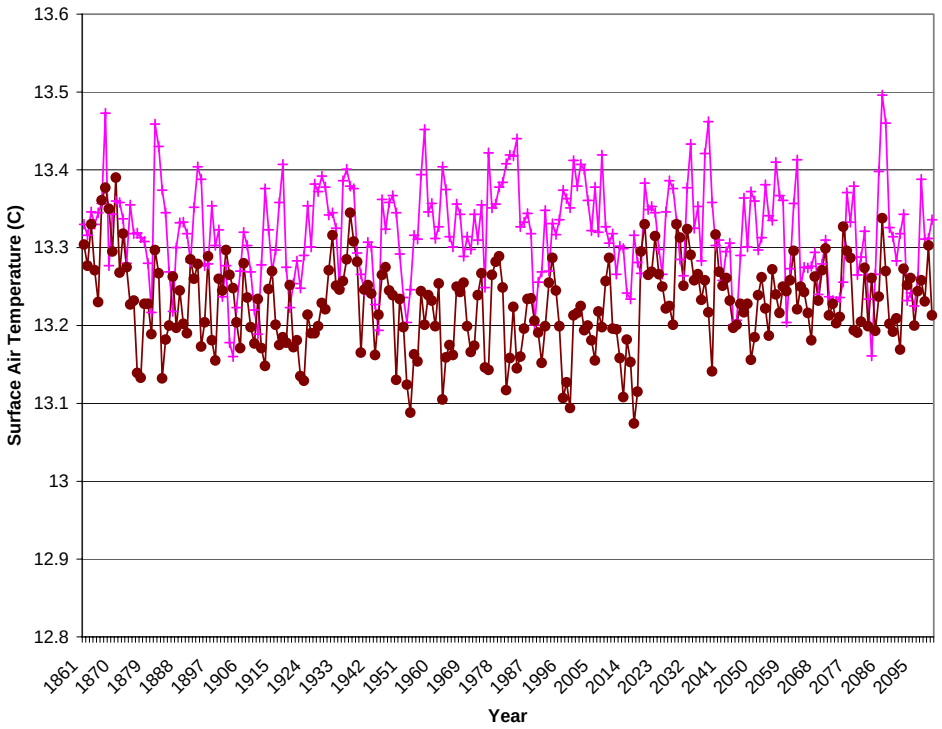


**Figure 34 – Globally averaged annually averaged surface air temperature (C), 1860 to 2100. Model A is in magenta circles, Model B is in pink pluses.**

### *3.1.6. Frequency Response of the Ocean*

We have demonstrated that variable wind stress alters mean ocean properties. Some suggested this occurs because the variable wind stress may excite an inertial response in the ocean, observed as an enhanced energy in ocean response at high frequencies. We tested this hypothesis by calculating the Fourier analysis of the ocean velocity magnitude at four locations where the variable wind stress was high and the mixed layer depth changed greatly between Model A and Model B.

Results were similar regardless of location (Southern or Atlantic Ocean). Figure 35 shows the geometrical windowed results for two depths (4m, 142.5m) at (73.75°E, 52°S). Slopes are similar between models; values are red, and a bump appears at approximately 10 days. A spike (only visible in un-windowed data) appears at the 24 hour frequency. Values decreased as depth decreased, but bumps remained.

Differences between the model responses were mainly limited to magnitude of the response. At all frequencies, Model A yields lower values than Model B. Un-windowed values (not shown) were much smoother for Model A. These differences probably occur because the stronger variable wind stress forcing of Model B excites a stronger ocean response. However, it is unclear why Model A sometimes shows a strong bump at frequencies near a day, while Model B only shows a small spike in un-windowed data.

We conclude that the addition of variable wind stress causes a nearly uniform increase in ocean response over all frequencies less than a month, but it is unclear whether some frequencies are more important than others. Future studies should examine this conclusion further, perhaps by forcing a model of finer spatial resolution with different temporal resolution of variable wind stress.

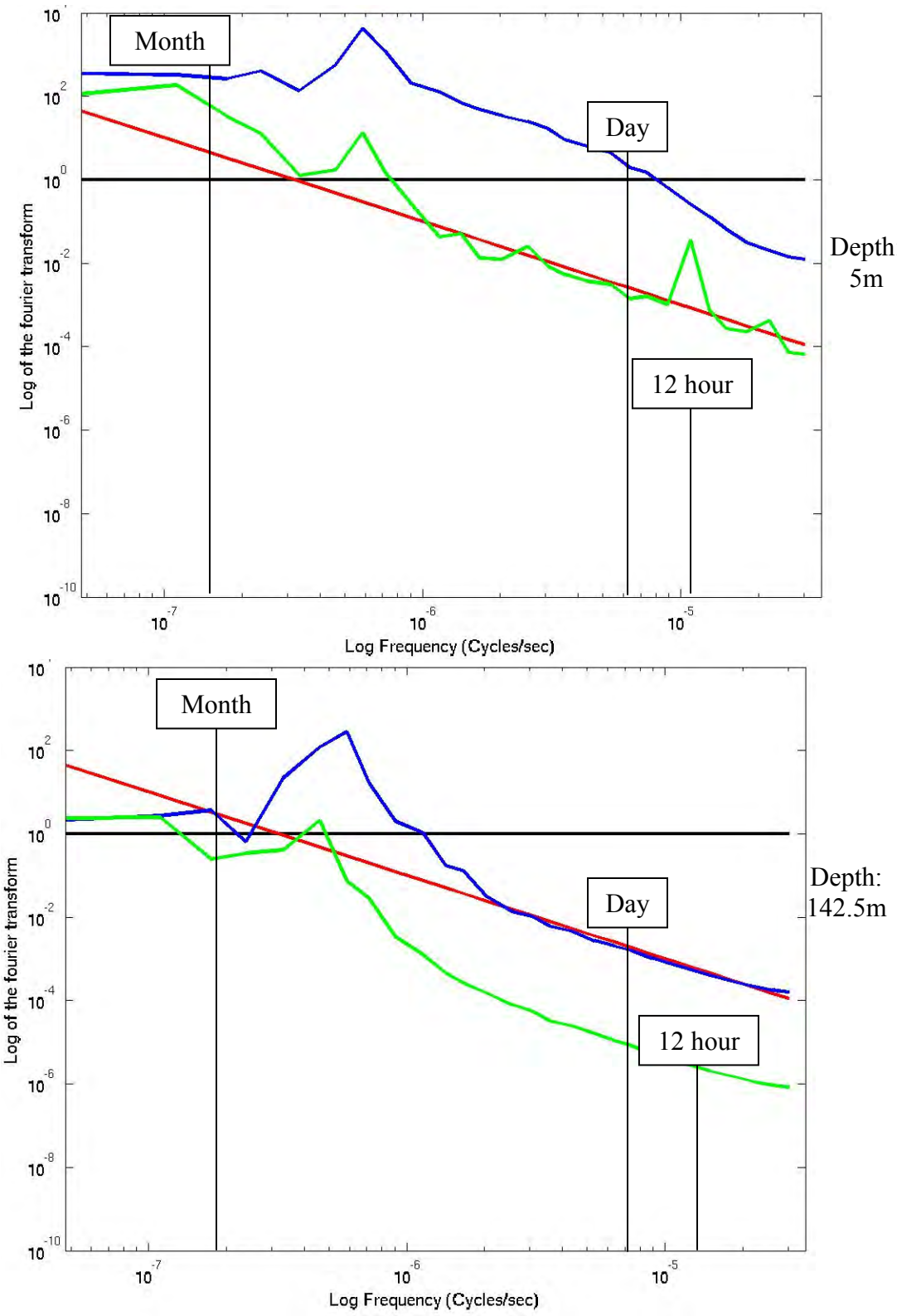


**Figure 35 - Ocean velocity magnitude at depth at (73.75°E, 52°S). Values are geometrically windowed (larger windowing at higher frequencies), code courtesy of Raffaele Ferrari. Model A is green line, Model B is blue line, White noise (black) and red noise (red) are provided for reference.**

## 3.2. WEAK FORCING SCENARIO: RECENT CLIMATE CHANGES, 1860-2005

Next we examine whether the model response to observed climate forcing over the period 1860-2005 is affected by variable wind stress. Presumably, either the different mean state or inclusion of variable wind stress could lead to different responses in the climate.

We chose a recent climate change scenario observed forcings (e.g. $CO_2$, volcano eruptions, solar forcing, etc) from 1860 to 2005. All changes are fairly weak, but changes have been dominated by $CO_2$ in the last 30 years. Where possible, model output was compared with observations or published results.

### *3.2.1. Mixed Layer Depth*

First we examined whether the use of NCEP variable wind stresses instead of the GISS wind stress anomaly might alter the mixed layer depths. The average mixed layer depths of Model A and Model B for years 1955-2003 are almost identical to the mixed layer depths of the control state (Figure 24). In all areas, Model B values are closer to but do not surpass the Levitus climatology (Figure 6).

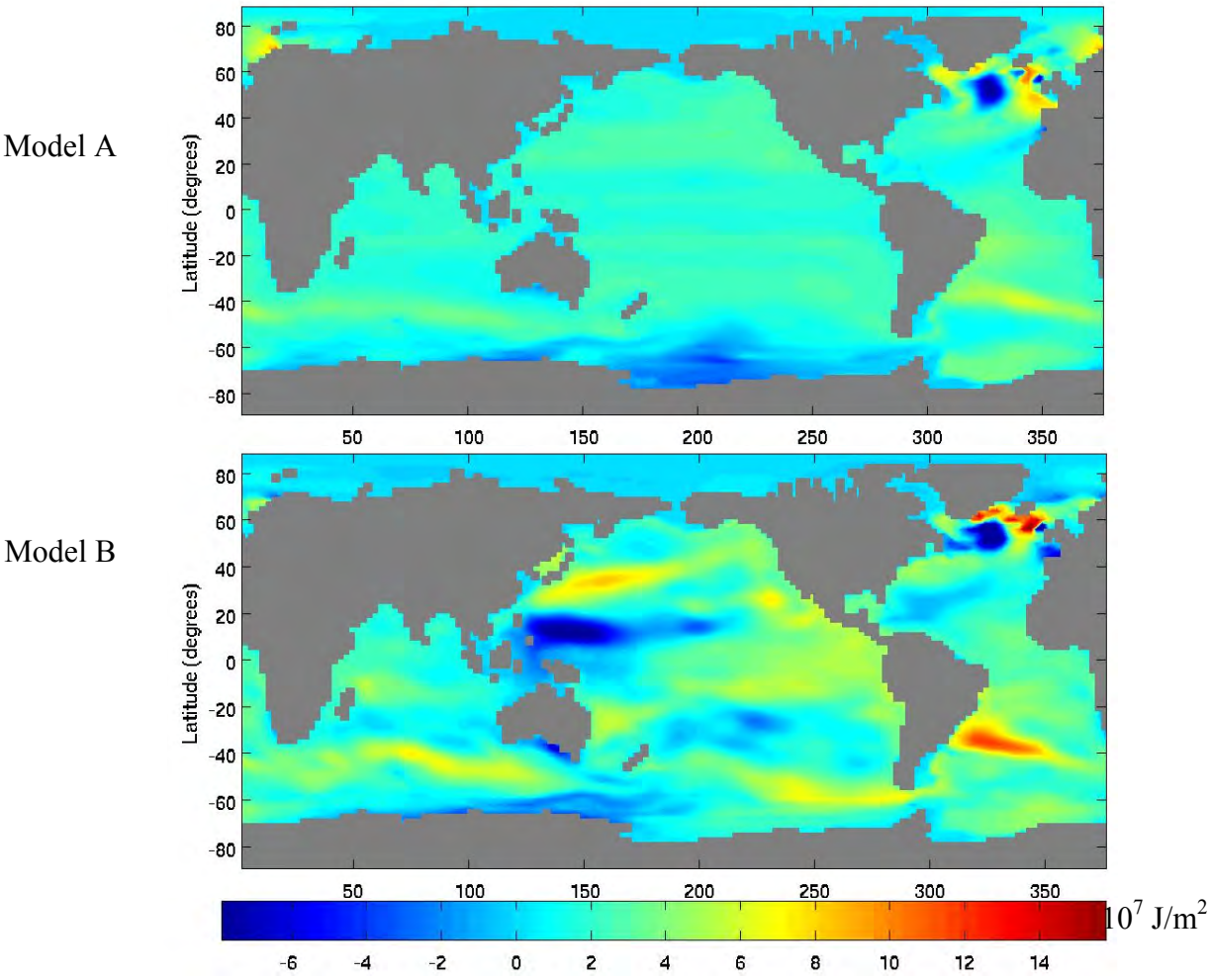


**Figure 36 - Ocean Heat Uptake, recent climate change minus control run. Values are from an average of years 1955-1959 to an average of year 1994-1998, units of annual average $10^7$ J/m$^2$. Depth range is 0-3000m. Depths 0-700m (thermocline only) yield similar spatial patterns to depths 0-3000m (but smaller magnitudes). Levitus values are given in Figure 5.**

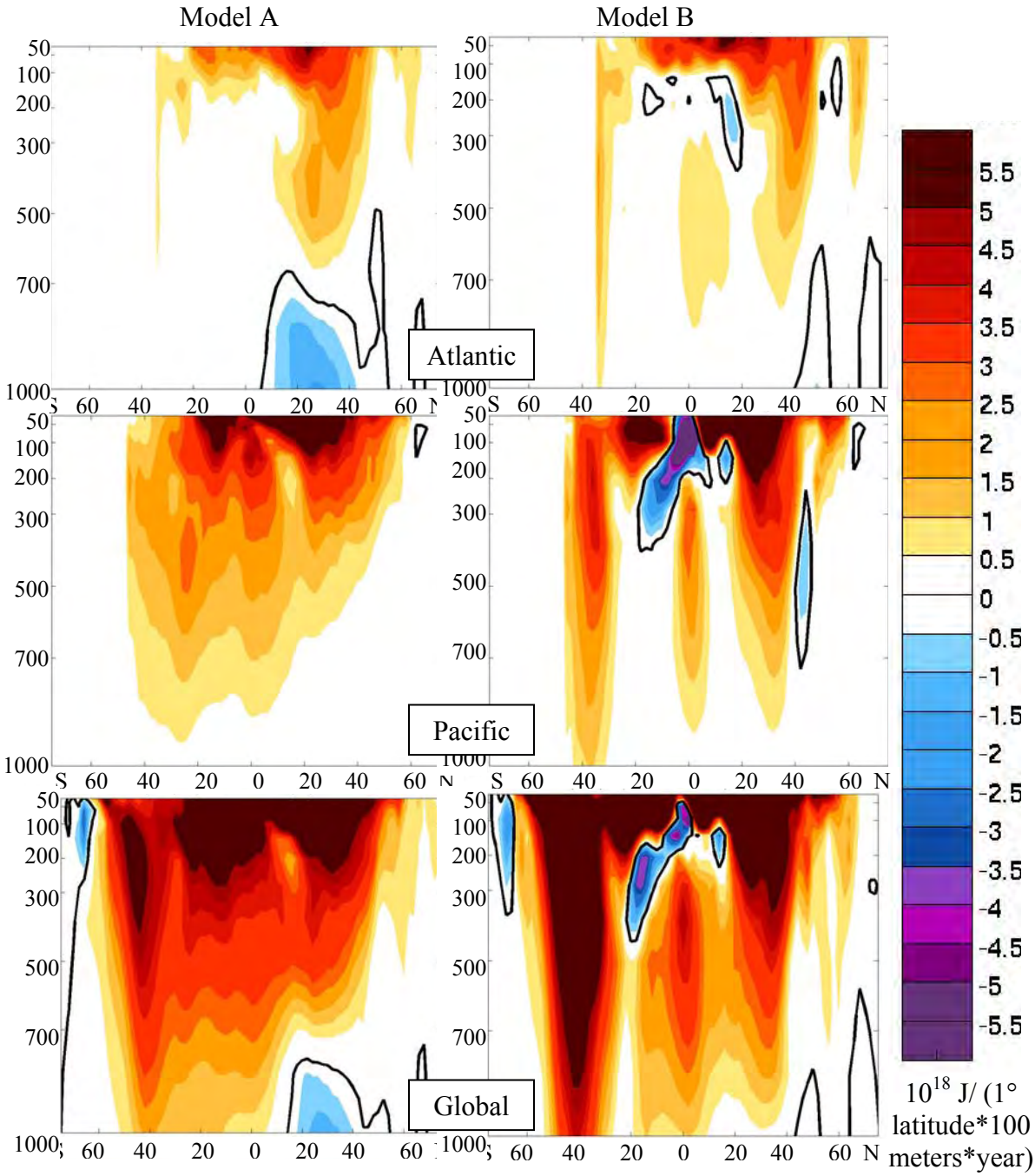


**Figure 37 - Zonally integrated ocean heat uptake in 1° latitude belts for 100m thick layers, annually averaged for years 1955 to 2003 ($10^{18}$ J/(1° latitude*100 meters*year) ). X-axis is latitude (80°S to 80°N), Y axis is depth (0-1000m). Heat uptake values are plotted at the midpoint of each 100-m layer.**

### *3.2.2. Ocean Heat Uptake*

Next we calculated the global ocean heat uptake over depths 0-3000m for average of years 1955-1959 to average of years 1994-1998 (range chosen for comparison to published data). Model A had an average annual ocean heat uptake of $17.8\times10^{22}$J.

Model B had an average annual ocean heat up take of $19.4\times10^{22}$J. Both values are overestimated compared to the Levitus value of $14.2\times10^{22}$J (Table 1).

Figure 36 shows a latitude/longitude plot of the annual average ocean heat uptake ($J/m^2$) summed over depths 0-3000m for an average of years 1955-1959 to an average of years 1994-1998 (range chosen for comparison to published data, Figure 5). The regional ocean heat uptake in Model A shows little spatial variation, probably due to its zonal nature. Conversely, Model B shows a strong regional pattern. The ocean heat uptake in the Pacific Ocean is of the same magnitude and spatial pattern as Levitus observations (Figure 5). The ocean heat uptake in the Atlantic Ocean is increased in magnitude, and rearranged slightly. This does not capture the Levitus spatial pattern; Lozier et al. (2008) confirms that without correct surface buoyancy and a fine resolution model, we will not capture the NAO. A significant spatial pattern also appears in the Southern Ocean; these enhanced values are not present in the observations, perhaps due to the dearth of observations in the Levitus dataset.

Figure 37 shows the zonally integrated ocean heat uptake (J) of the Pacific, Atlantic, and global oceans in 1° latitude belts for 100m thick layers, annually averaged for years 1955-2003 (range chosen for comparison to published data Figure 3 and Figure 4)[12]. Model A has a large ocean heat uptake spike at depth in the Southern Ocean, but otherwise has relatively uniform ocean heat uptake. Model B has significantly altered ocean heat uptake at depth. Globally, the Pacific and Southern oceans dominate. In these two oceans, ocean heat uptake is increased and penetrates more deeply, adopting a spatial pattern very similar to observed ocean heat uptake. However, there is little change in the Atlantic toward observations; the warm/cold pole in the North Atlantic is less pronounced than in observations.

One interesting phenomenon is the appearance of a dipole in the Pacific equatorial region. Pierce et al (2005) suggests this strong cooling event may be part of a natural mode of climate variability in the Pacific Ocean. We investigated this hypothesis by examining several consecutive year periods, shown in Figure 38. In our model, the cooling/warming event does appear to be periodic in nature with a timescale of roughly 5 years. This natural variability is consistent with various linear trends (Forest et al. 2008, Ishii et al 2006, and IPCC). Note, it is interesting that we observe a long term oscillatory response in the ocean when we could not find any timescales of this sort in the NCEP variable wind stress data.

### *3.2.3. Meridional Overturning Circulation and Meridional Heat Flux*

Next let us examine the effect of variable wind stress on the meridional meridional heat flux. Figure 39 shows the meridional heat flux mean over 1955-2003. We find that the maximum in the Atlantic meridional overturning circulation (not shown) decreases slightly in both cases, and once again Model B varies more greatly in time. Additionally, Model B shifts the position and increases the magnitude of the meridional heat flux a small amount.

[12] Note, ocean heat content values of Figure 37 are not strictly comparable to Figure 36. The former is a measure of $J/m^2$, while the latter is a measure of J/(1°band of ocean × 100m) .

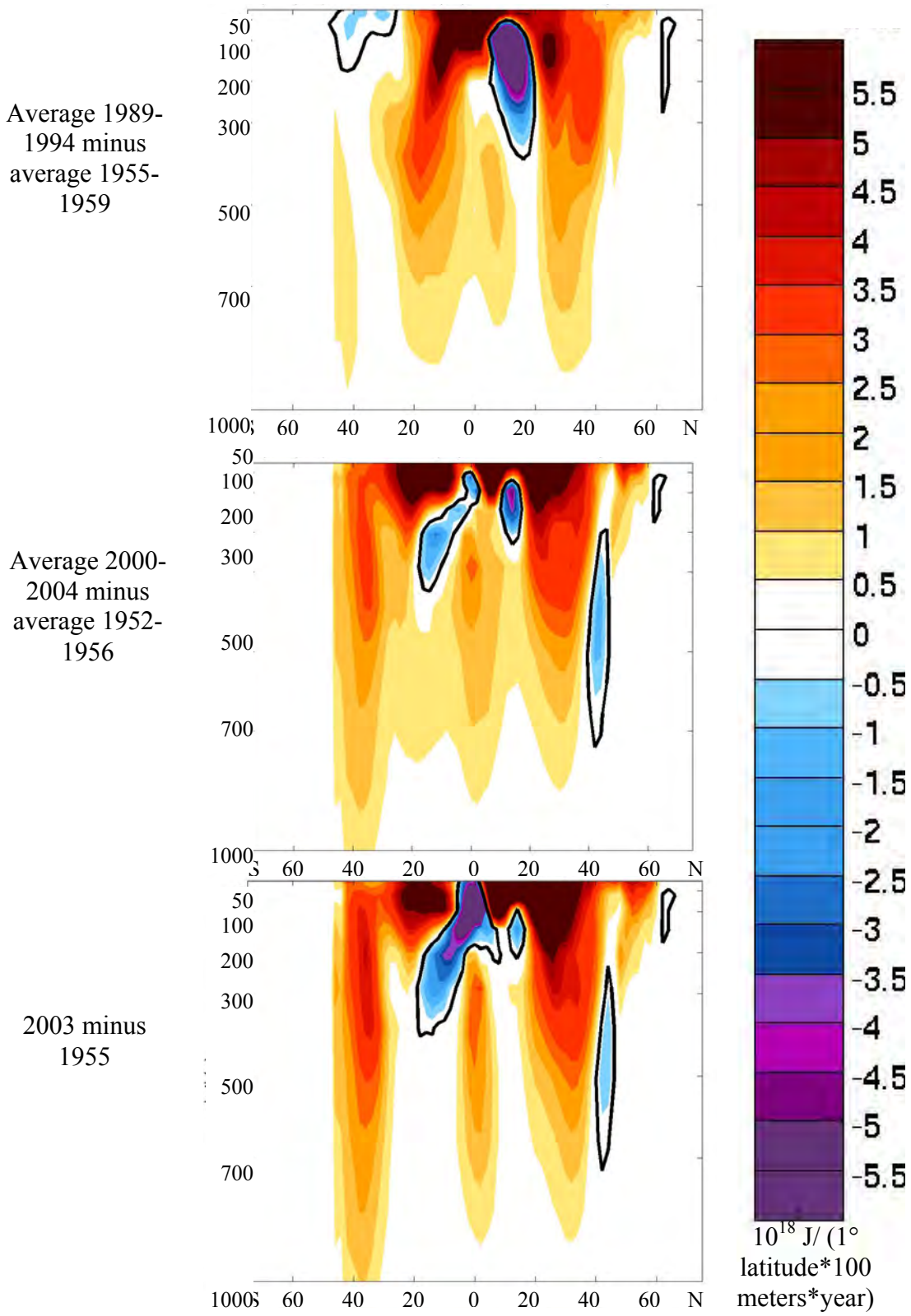


**Figure 38 - Zonally integrated Pacific Ocean heat uptake in 1° latitude belts for 100m thick layers, annually averaged ($10^{18}$ J/(1° latitude*100 meters*year) ). Evolution of Pacific Dipole over time. X-axis is latitude (80°S to 80°N), Y axis is depth (0-1000m). Heat uptake values are plotted at the midpoint of each 100-m layer.**

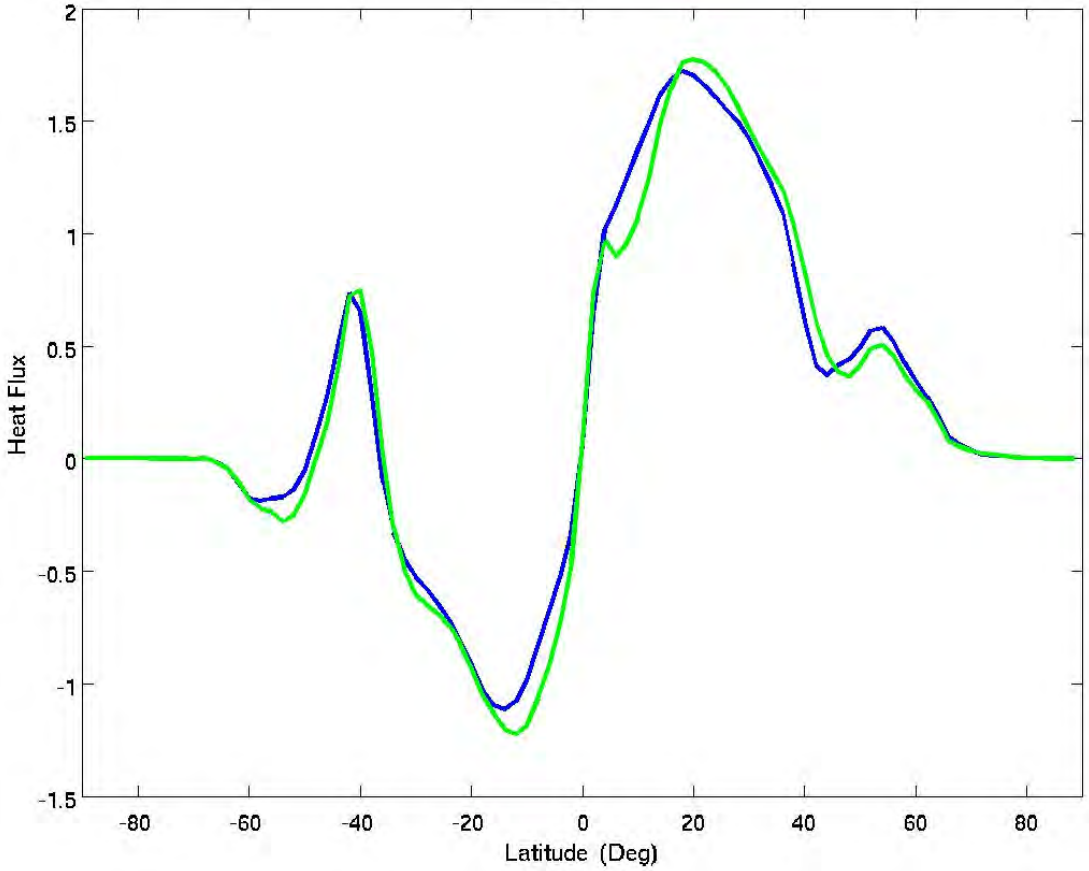


**Figure 39 –Meridional Heat Flux (PW) calculated annually, then averaged over 1955 to 2003. Model A is in blue, Model B is in green.**

*3.2.4. Other Fields*

Next we examined globally averaged values from 1860 to 2003. For brevity, only four fields are given in this paper; sea surface temperature (C, Figure 40), sea surface salinity (psu, Figure 41), surface air temperature (C, Figure 42), and sea level rise (temperature expansion only, m, Figure 43).

Both Model A and Model B are consistent with a slight warming scenario. We find that the sea surface temperature, surface air temperature, and sea level rise are increased compared to the control run. The meridional heat flux and seasonal values of sea ice decrease slightly compared to the control run. The freshwater flux and sea surface salinity do not appear to change compared to the control run.

Differences between Model A and Model B reflect earlier findings of increased ocean heat uptake in Model B. Although the final sea surface temperature and surface air temperature are similar between models, the sea level rise (similar to a metric of integrated temperature change) is larger in Model B.

Observations of the surface air temperature anomaly were available, and graphed as a solid black line with an appropriate offset in Figure 42. Variability is greater in Model B, and roughly would seem to give a better visual match to variability in observations than Model A.

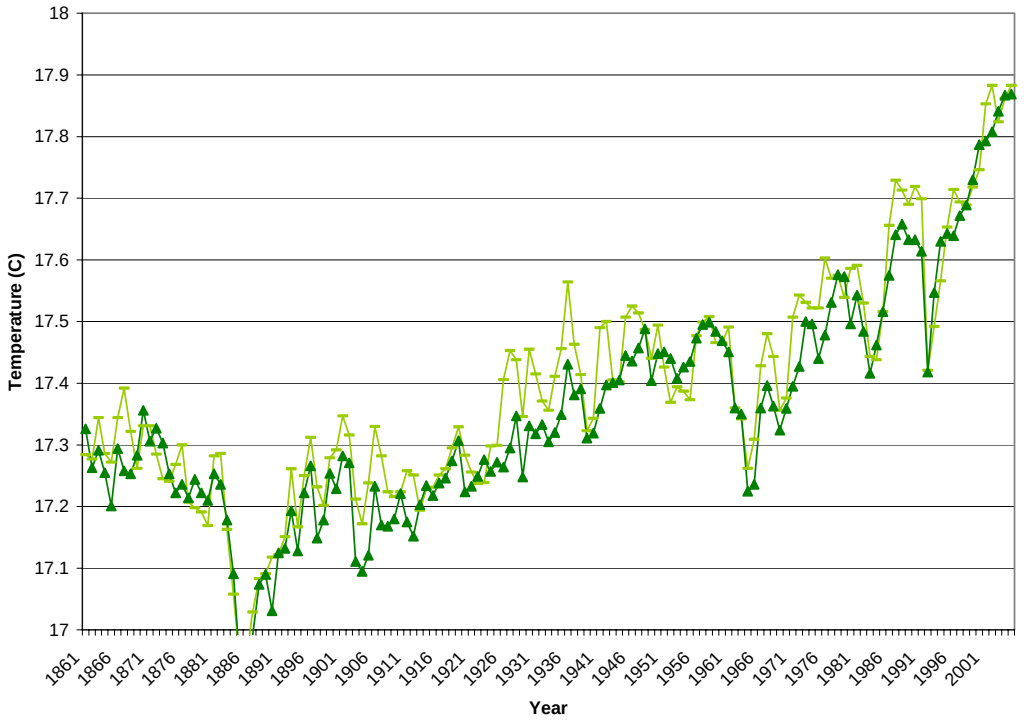


**Figure 40 – Globally averaged annually averaged sea surface temperature (C), 1860 to 2003. Model A is in green triangles, Model B is in lime dashes.**

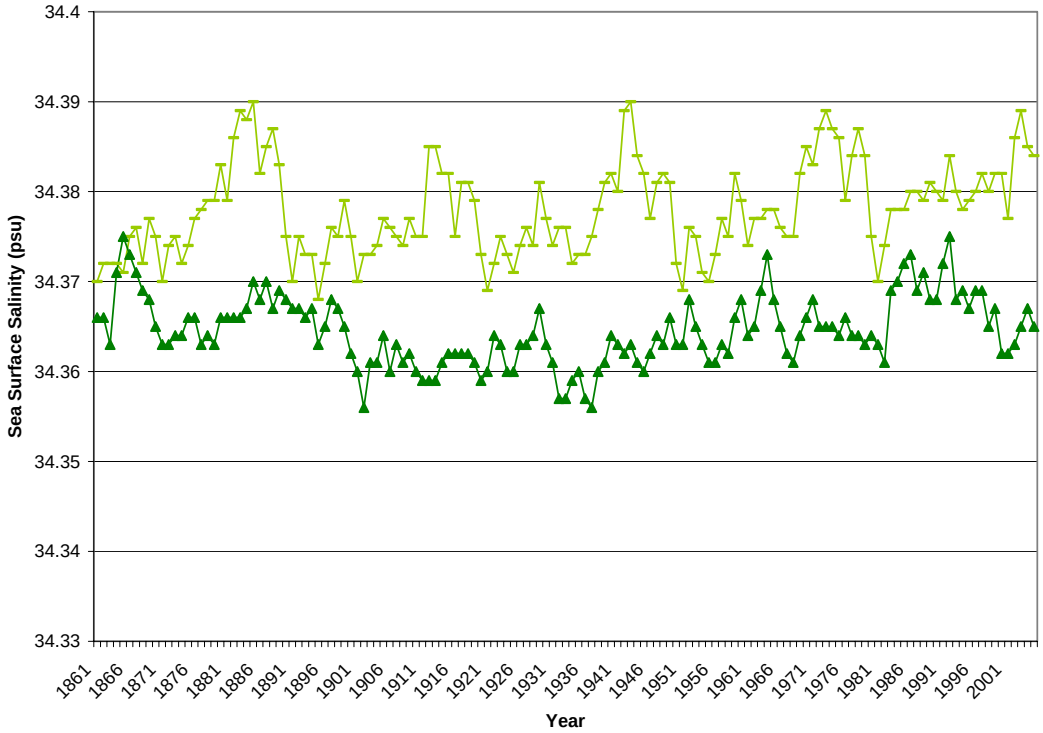


**Figure 41 – Globally averaged annually averaged sea surface salinity (psu), 1860 to 2003. Model A is in green triangles, Model B is in lime dashes.**

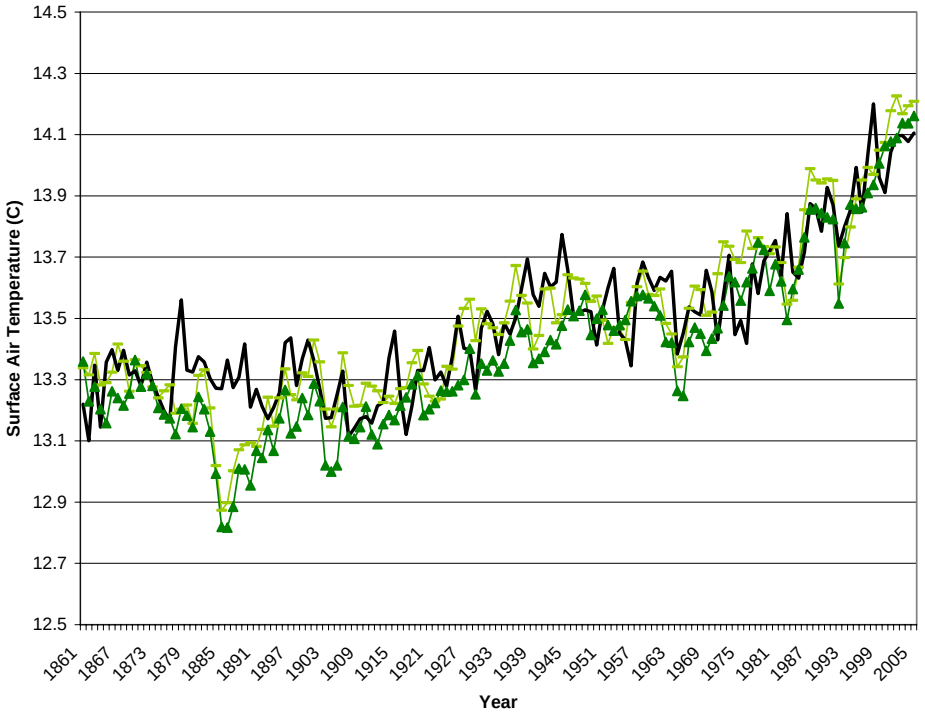


**Figure 42 – Globally averaged annually averaged surface air temperature (C), 1860 to 2003. Model A is in green triangles, Model B is in lime dashes. Black solid line is observed temperature anomaly with appropriate offset to match mean model surface air temperature.**

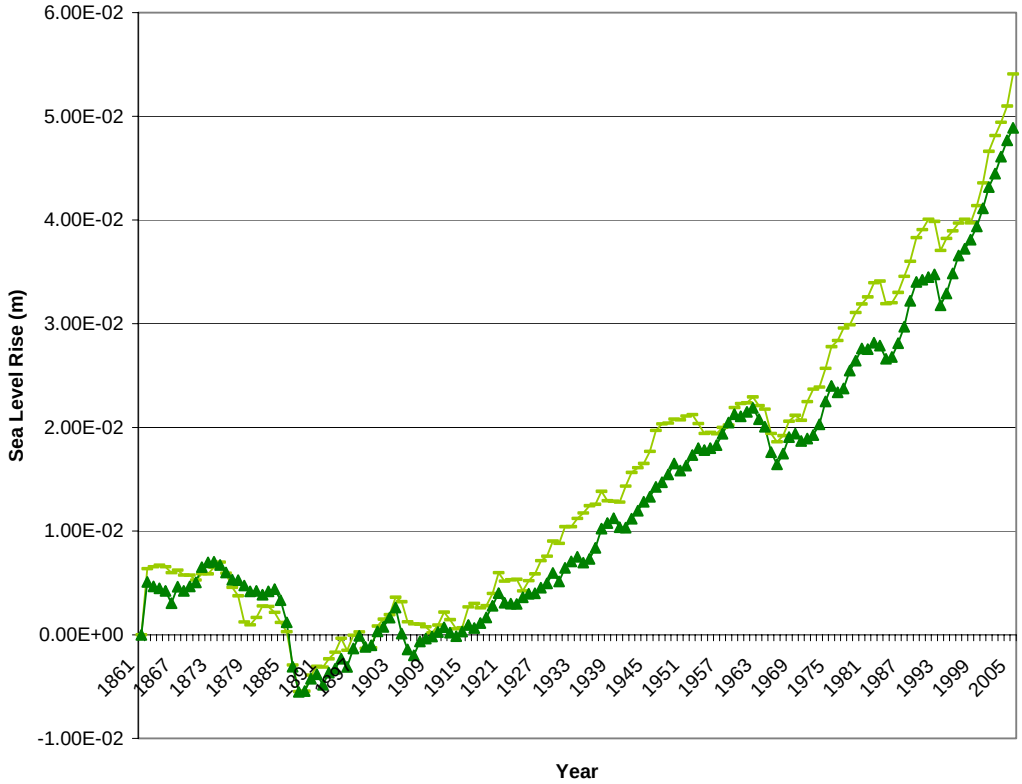


**Figure 43 – Globally averaged annually averaged sea level rise (m), 1860 to 2003. Model A is in green triangles, Model B is in lime dashes.**

## 3.3. STRONG FORCING SCENARIO: GLOBAL WARMING SCENARIO

Next we will examine whether either changes to the mean ocean state or the changes to the variable wind stress (i.e. Model B instead of Model A) will affect a strong forcing scenario (a global forcing scenario). We examined two global warming scenarios:

Scenario 1. This global warming scenario begins at the end of the spinup, or Year 1, with an initial $CO_2$ level of 286ppm. $CO_2$ levels were increased 1% per year until Year 130 (1043ppm, all other forcings held at 1860 level).

Scenario 2. This global warming scenario began at year 1991 of the recent climate change run (Section 3.2). For years 1991 to 2100, forcings were obtained from the "business as usual" emissions scenario from the MIT Emissions Prediction and Policy Analysis (EPPA) model (Mayer et al 2000, Babiker et al 2001, and Webster et al 2002). This scenario included many different types of emissions (e.g. $CO_2$, sulfates, aerosols, methane, etc).

We then forced Model A and Model B with the two scenarios. $CO_2$ forcing values (Scenario 1) and equivalent $CO_2$ forcing values (Scenario 2, Model A & Model B) are shown in Figure 44 (with IPCC scenarios given for reference). Results (including ocean carbon uptake) were qualitatively similar between the two scenarios, so this section will only present the Scenario 2 figures. Scenario 1 figures are available in the appendix.

Note, Model A allows feedback to mean state by anomalous "additions" to Trenberth. Figure 45 shows that the global average magnitude of Model A's mean wind stress decreases with increased forcing. Model A's variability (on top of the mean variability) can also vary. Model B does not allow feedbacks to the wind stress; future studies should allow this feedback.

**Figure 44 – $CO_2$ or Equivalent $CO_2$ of Forcing Scenarios (ppm). Scenario 1 $CO_2$ values are given as the solid blue line. Equivalent $CO_2$ values were provided by Andrei Sokolov for Model A Scenario 2 (solid pink line) and Model B Scenario 2 (solid brown line). Standard IPCC scenarios run in a complex GCM, though not strictly comparable, are provided for reference. A2 is the light blue squares, B2 is the purple circles, and IS92a is the yellow triangles (courtesy of the Canadian Centre for Climate Modeling and Analysis.)**

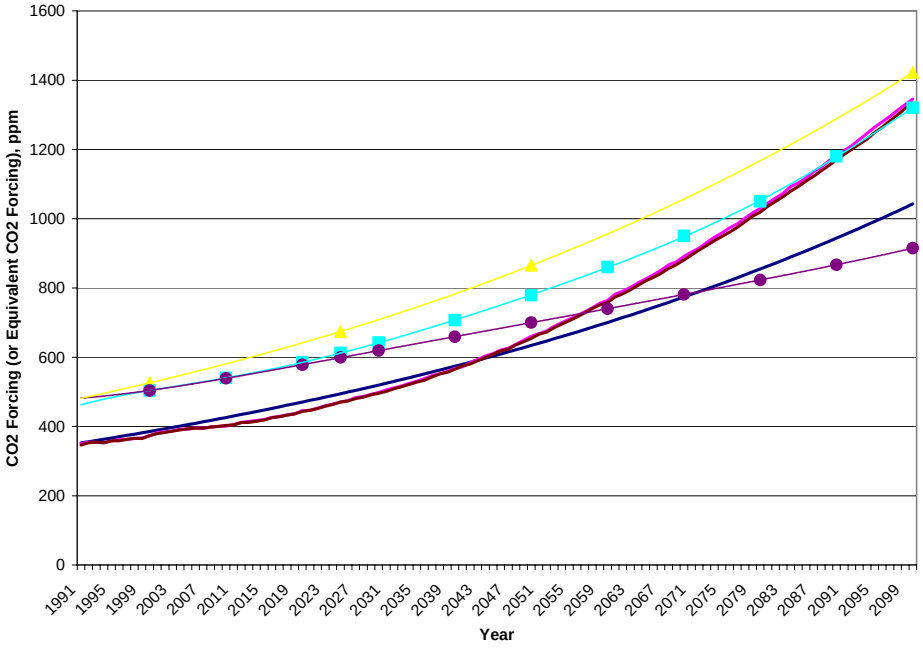

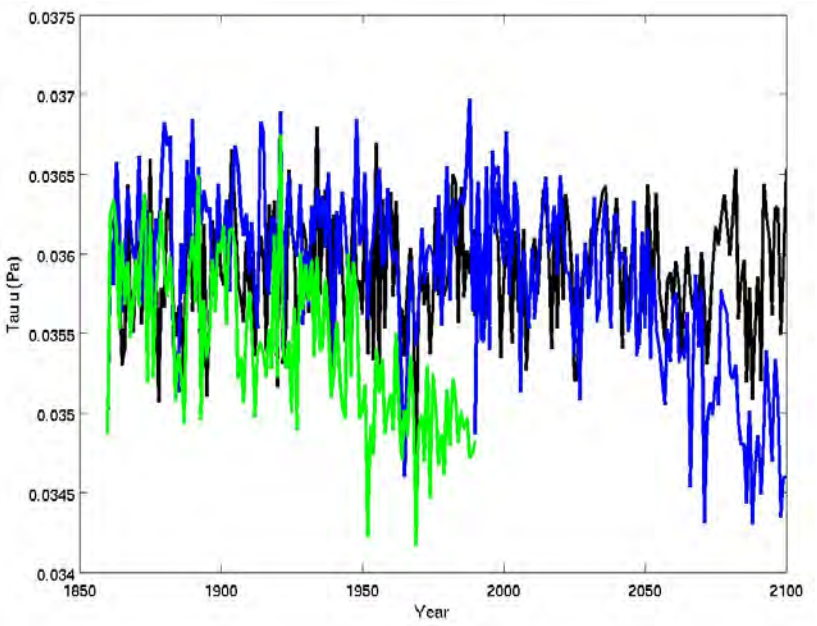


**Figure 45 - Average Magnitude of $\tau_u$ in Model A runs. Green is Scenario 1, blue is Scenario 2, and black is control.**

Model A

Model B

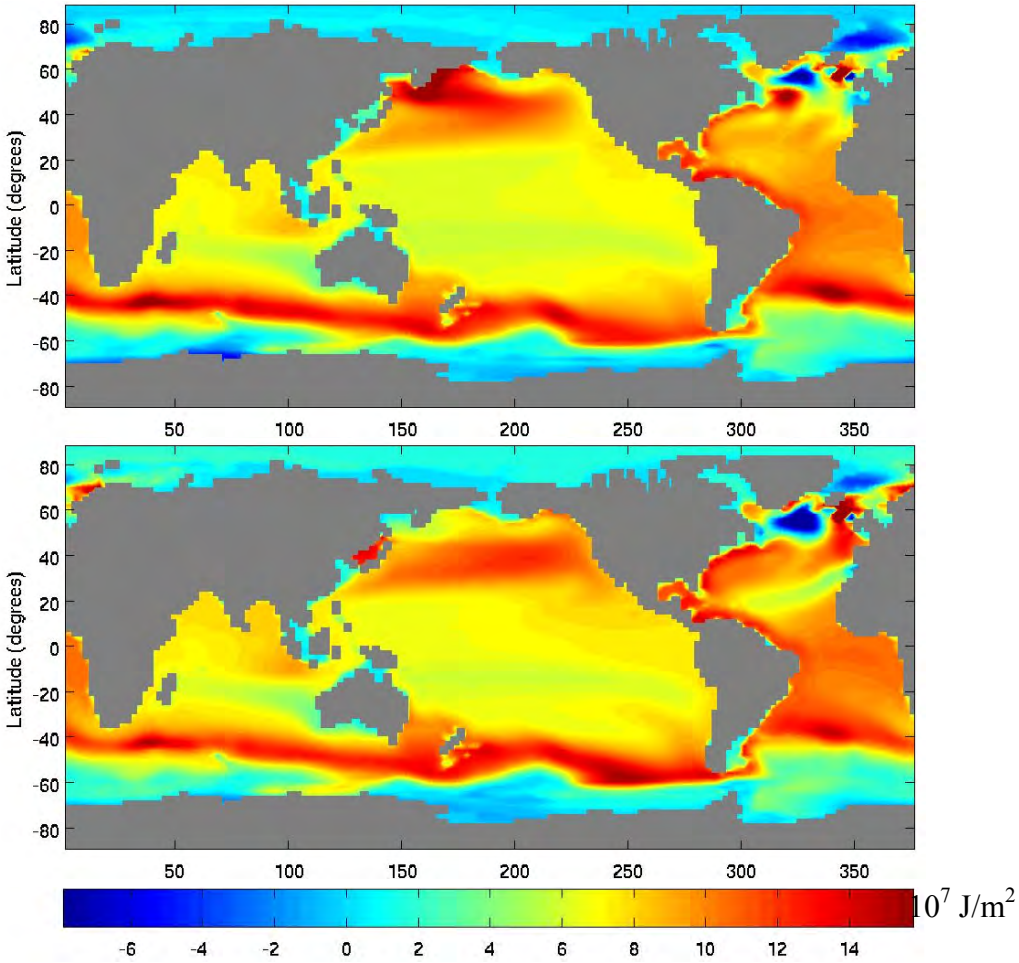


**Figure 46 - Ocean Heat Uptake, Scenario 2 minus the control run. Values are from an average of years 1991-1996 to an average of year 2040-2045, units of annual average $10^7$ J/m$^2$. Depth range is 0-3000m. Depths 0-700m (thermocline only) yield similar spatial patterns to depths 0-3000m (but smaller magnitudes).**

Model A

Model B

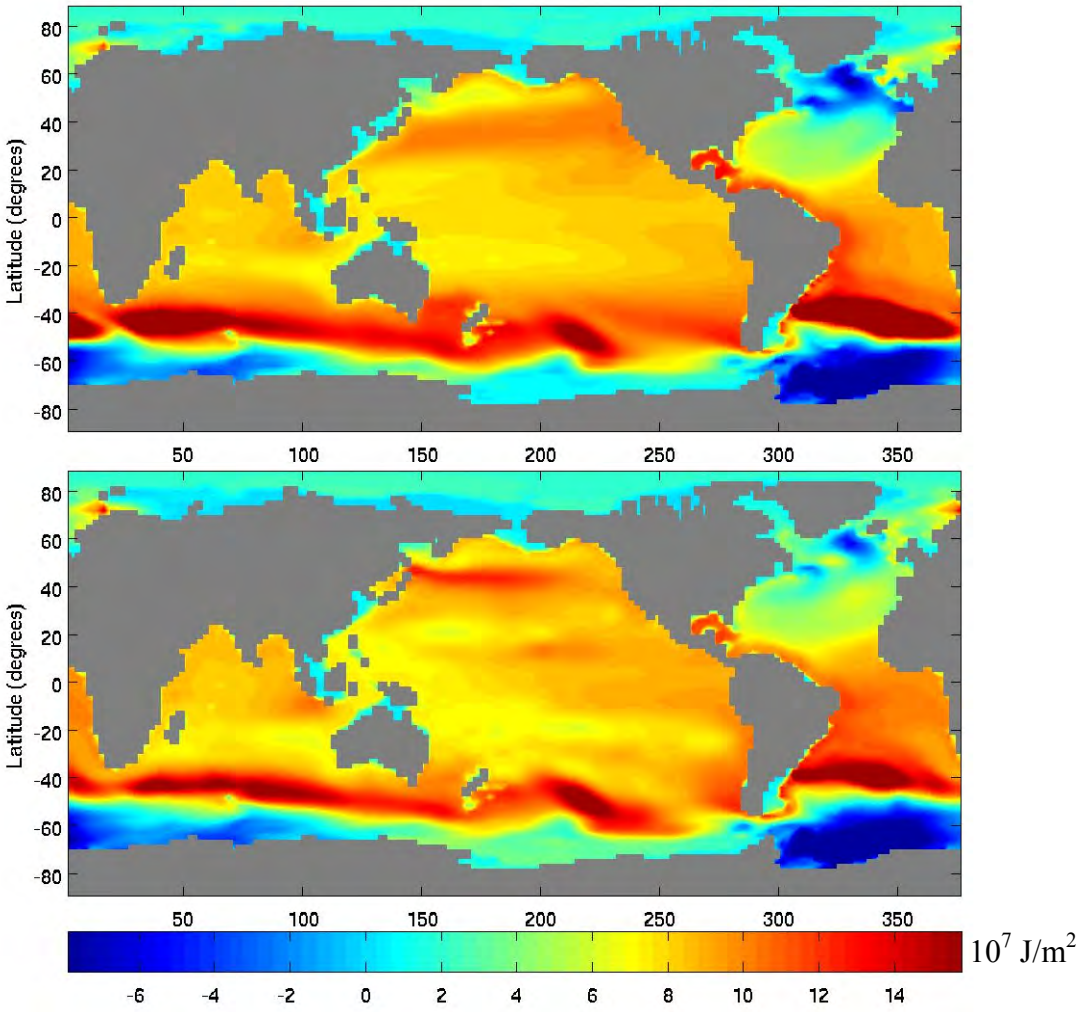


**Figure 47 - Ocean Heat Uptake, Scenario 2 minus the control run. Values are from an average of years 2045-2050 to an average of year 2095-2100. Depth range is 0-3000m, units of annual average $10^7$ J/m$^2$. Depths 0-700m (thermocline only) yield similar spatial patterns to depths 0-3000m (but smaller magnitudes).**

Examining magnitudes, it appears that both scenarios uniformly shallow the mixed layer depth (by about 1-2m) for both model runs. This is consistent with a global warming forcing. For spatial patterns, refer to Figure 38.

*3.3.1. Ocean Heat Uptake*

Inspection of the model results indicates nonlinear increase in ocean heat uptake with time. Therefore, to best discuss ocean heat uptake, we examined averaged results between the first and second half of the run separately. Both runs uptake a much larger value of heat than the 20$^{th}$ century forcing run.

Figure 46 (Figure 47) shows a latitude/longitude plot of the annual average ocean heat uptake summed over depths 0-3000m for an average of years 1991-1996 (2045-2050) to an average of years 2040-2045 (2095-2100). Model A and B results are very similar, especially over 2050-2100. In the first half of the run, the strongest heat uptake occurs in the Southern Ocean high wind stress band and the North Atlantic ocean. Global

Model A

Model B

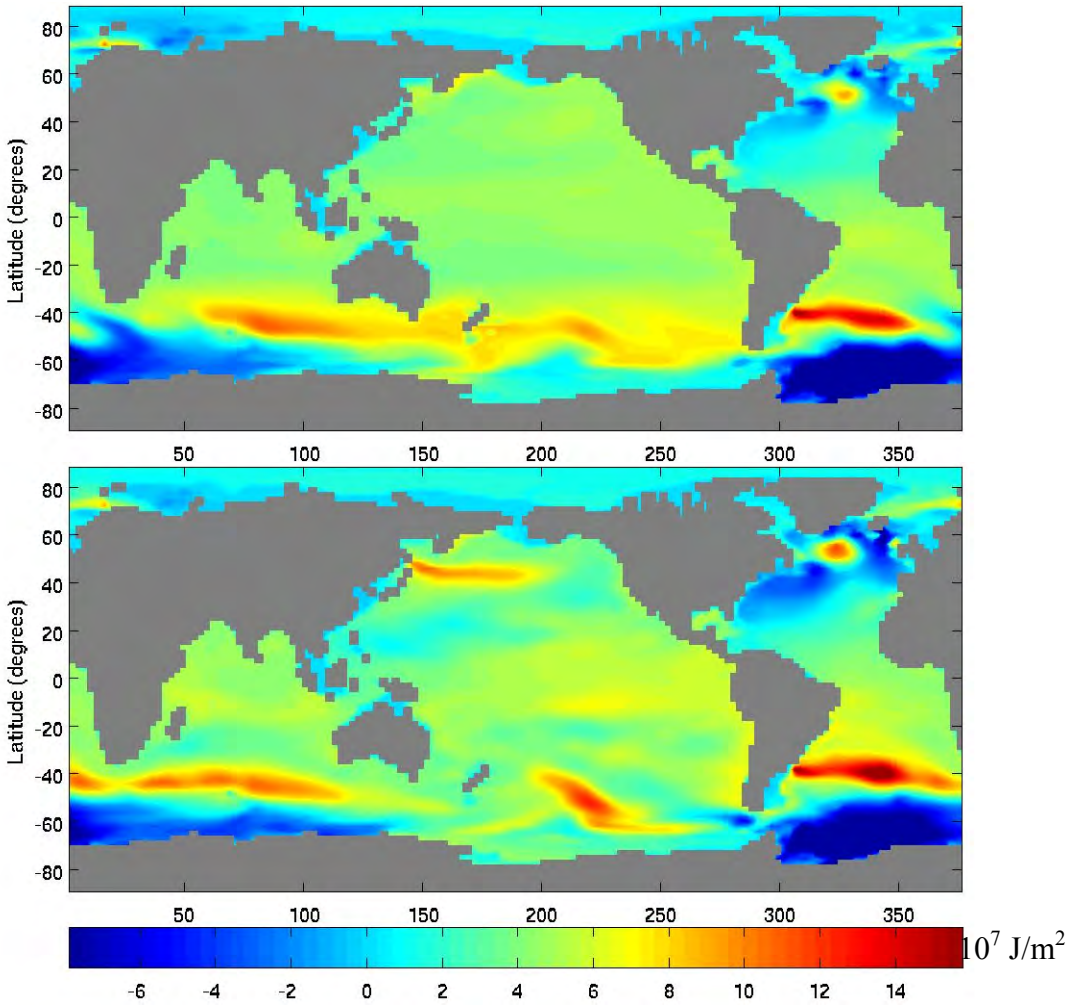


**Figure 48 – Difference image; Figure 47 minus Figure 46, (annual average $10^7$ J/m$^2$). Depth range is 0-3000m, units of annual average $10^7$ J/m$^2$. Depths 0-700m (thermocline only) yield similar spatial patterns to depths 0-3000m (but smaller magnitudes).**

ocean heat uptake increases. The slight North Atlantic dipole vanishes, and a strong Southern Ocean dipole south of the Atlantic appears (possibly a strengthening of the southern annular mode, SAM).

Patterns and magnitudes of ocean heat uptake are similar whether using Model A or Model B. Figure 48 shows the difference image of Figure 46 and Figure 47. Over time, Model B begins to uptake more heat at the equator, and less in the Southern Ocean. Additionally, the dipole of the southern Atlantic appears to strengthen more in Model B.

Figure 49 (Figure 50) shows the average ocean heat uptake (J) in a 1° latitude band, 100m deep box at depth of the Pacific, Atlantic, and global oceans for an average of years 1991-1996 (2045-2050) to an average of years 2040-2045 (2095-2100). Ocean heat uptake in the upper ocean layers is much larger than that associated over the period 1860-2005. Heat uptake occurs in mid-latitude Atlantic, in the equatorial Pacific, and in the Southern Ocean.

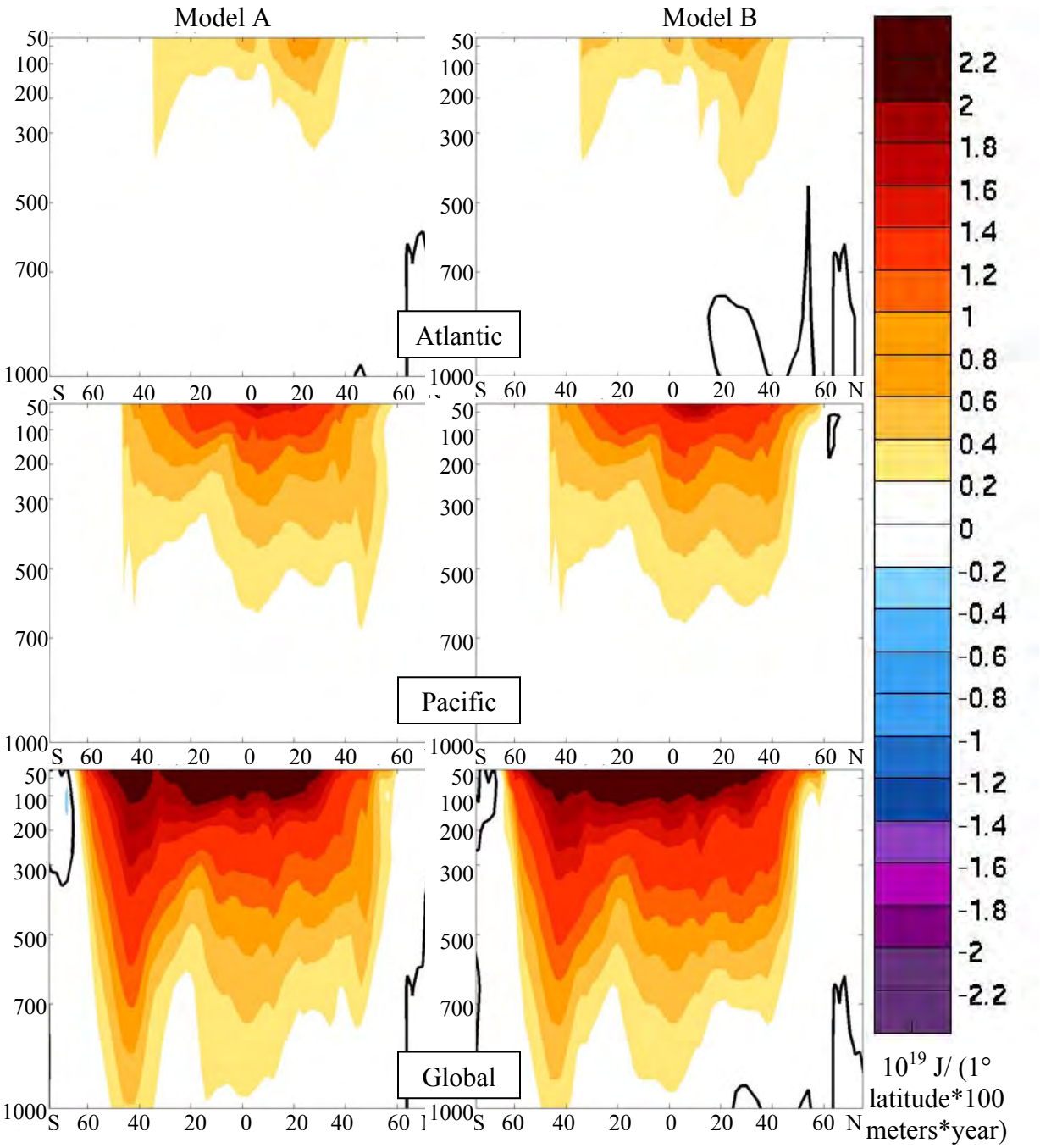


**Figure 49 - Zonally integrated ocean heat uptake in 1° latitude belts for 100m thick layers, average of years 1991-1996 to average of years 2040-2045 ($10^{19}$ J/(1° latitude*100 meters*year) ), Scenario 2 minus the control run. X-axis is latitude (80°S to 80°N), Y axis is depth (0-1000m). Note the contour range is quadruple of Figure 37. Heat uptake values are plotted at the midpoint of each 100-m layer.**

Figure 51 shows Figure 50 values minus Figure 49 values (the change in ocean heat uptake over time). The location of heat uptake at depth varies slightly between the two models. In this view, we find that ocean heat uptake magnitude at depth is slightly different between models. Model B appears to distribute heat uptake more evenly with latitude than Model A, and has a shallower heat spike into the Southern Ocean. Slightly more of Model B's heat uptake occurs in the upper layers.

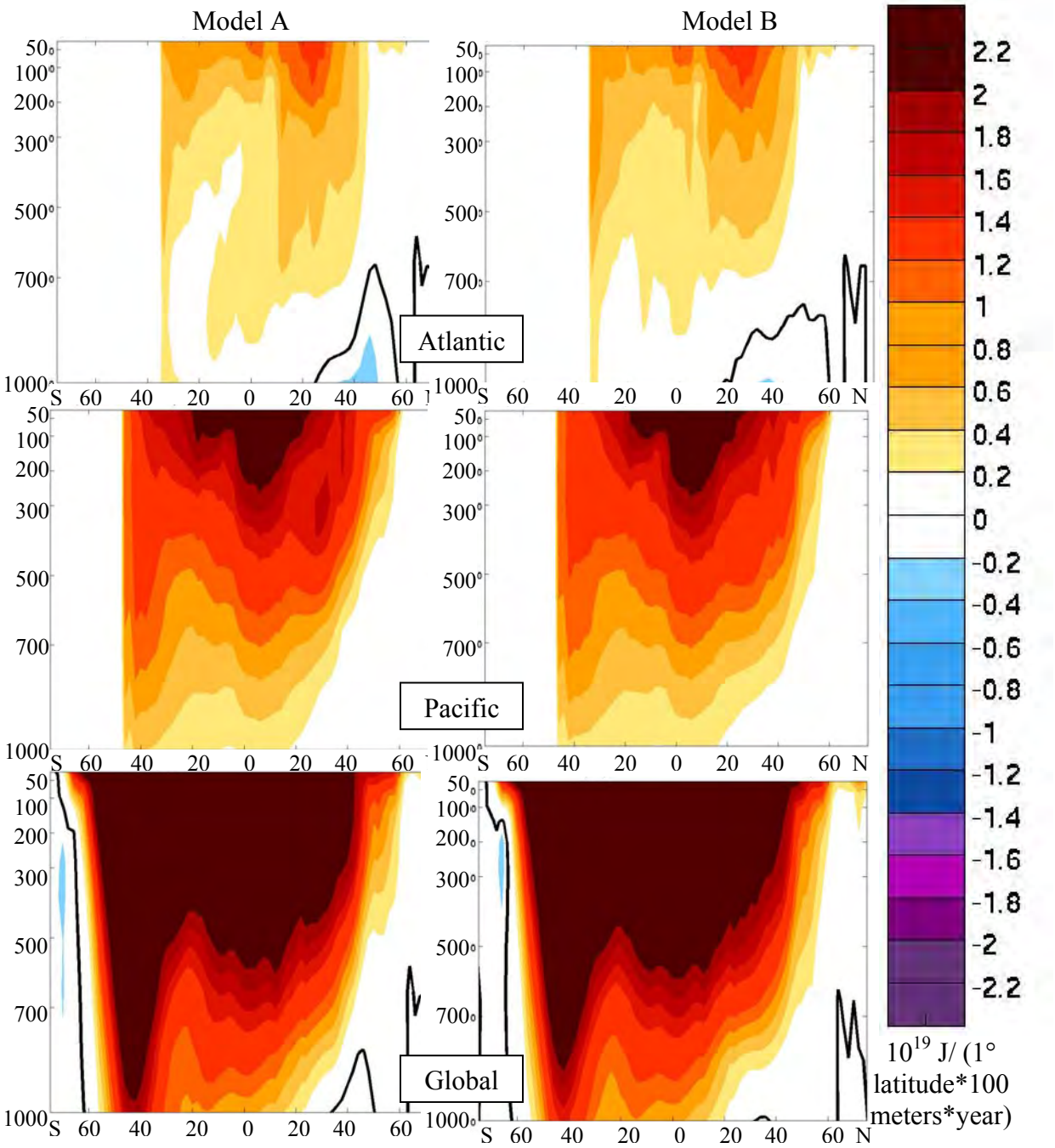


**Figure 50 - Zonally integrated ocean heat uptake in 1° latitude belts for 100m thick layers, average of years 2045-2050 to average of years 2095-2100 ($10^{19}$ J/(1° latitude*100 meters*year) ), Scenario 2 minus the control run. X-axis is latitude (80°S to 80°N), Y axis is depth (0-1000m). Note the contour range is quadruple of Figure 37. Heat uptake values are plotted at the midpoint of each 100-m layer.**

### *3.3.2. Meridional Overturning Circulation and Meridional Heat Flux*

Given our knowledge of variability in the control run, we expected to find that the maximum in the meridional overturning circulation have more variability in Model B than in Model A. Figure 52 shows the maximum in the Atlantic meridional overturning circulation (as diagnosed between 28-74°N) for all model runs. All runs indicate there is little variability in Model A outputs, but significant variability in Model B outputs. We

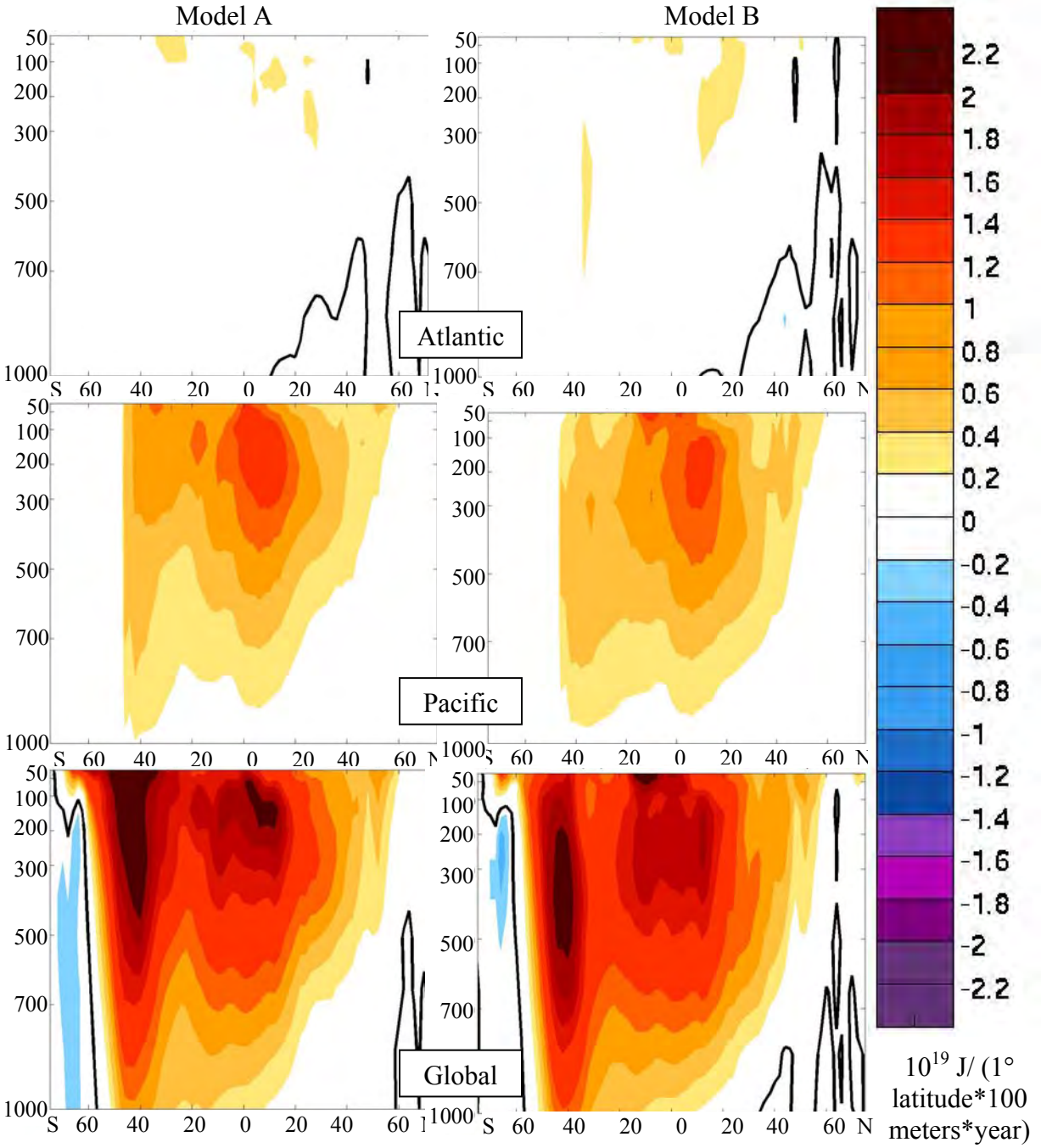


**Figure 51 – Difference image; Figure 50 minus Figure 49, ($10^{19}$ J/(1° latitude*100 meters*year) ). X-axis is latitude (80°S to 80°N), Y axis is depth (0-1000m). Note the contour range is quadruple of Figure 37. Heat uptake values are plotted at the midpoint of each 100-m layer.**

conclude that in this coarse resolution model, the major source of annual variability of the MOC, regardless of forcing, is surface wind variability (as opposed to internal model variability).

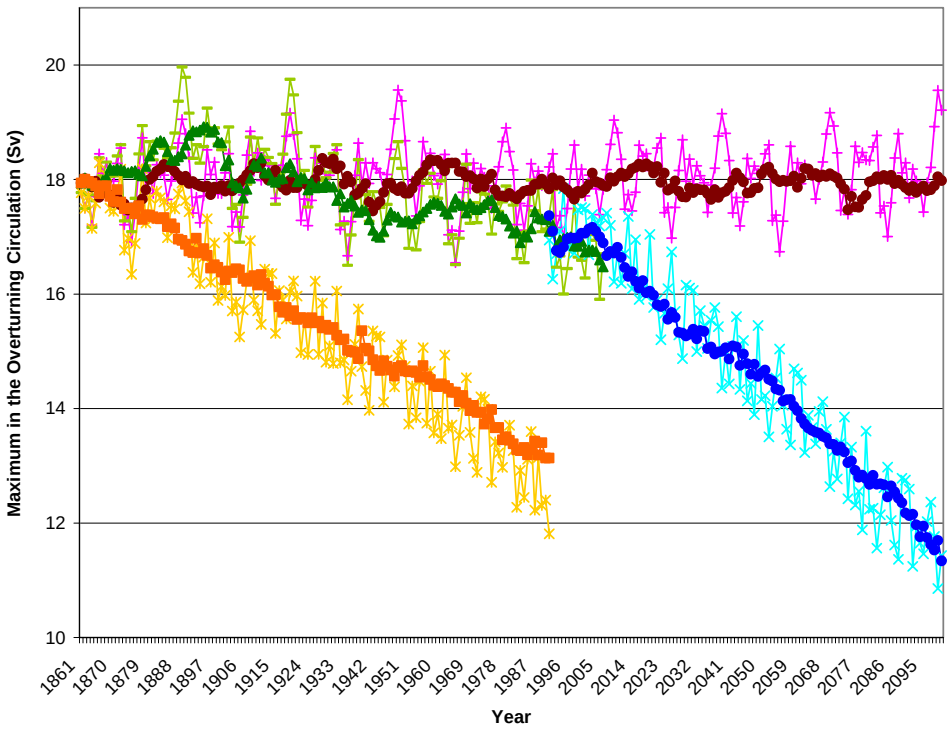


**Figure 52 –Maximum in the Atlantic Meridional Overturning Circulation (28-74°N). Model A control run is in magenta circles, Model B control run is in pink pluses, Model A recent climate change run is in green triangles, Model B recent climate change run is in lime dashes, Model A Scenario 1 is in orange squares, Model B Scenario 1 is in yellow stars, Model A Scenario 2 is in blue diamonds, Model B Scenario 2 is in light blue crosses.**

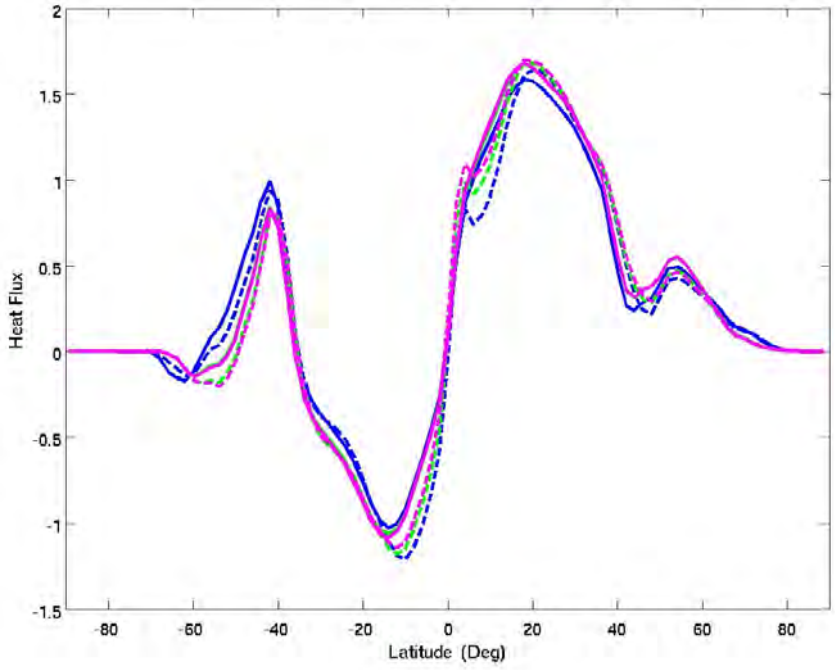


**Figure 53 - Meridional Heat Flux (PW), Scenario 2 forcing minus the control run. Model A is in solid lines, Model B is in dashed lines. Average of Years 1991-1996 is pink, average of Years 2045-2050 is green, average of Years 2095-2100 is blue.**

In addition to the variability, we find the maximum in the meridional overturning circulation decreases with increased forcing. In Scenario 1, the MOC Model B weakens more than the MOC of Model A; in Scenario 2, both model MOCs weaken similarly. More experiments are needed to test whether the MOCs of Model A and Model B will diverge.

Figure 53 shows the meridional heat flux of Scenario 2 at the beginning of the run (1991-1996), midway through the run (2040-2045), and at the end of the run (2095-2100). In both models, the northern peak remains near 20°N but decreases in magnitude, and the southern peak strengthens near 50°S.

*3.3.3. Other Fields*

Finally we examined globally averaged values from 1991 to 2100. Sea surface temperature is shown in Figure 54 (C), sea surface salinity is shown in Figure 55 (psu), surface air temperature is shown in Figure 56 (C), and sea level rise is shown in Figure 57 (m). Since this run is a global warming scenario, then sea surface temperature, sea surface air temperature, and sea level rise increase with time. The meridional heat flux and seasonal values of sea ice decrease with time, possibly collapsing near the end of the run. Model B has larger sea surface salinity than Model A, but the explanation is likely complicated by different mixed layer salinity structure in various ocean basins and the possible evaporation due to the warming atmosphere.

Differences between Model A and Model B reflect earlier findings of increased ocean heat uptake in Model B. Although the final sea surface temperature and surface air temperature are similar between models, the sea level rise (similar to a metric of integrated temperature change) is larger in Model B.

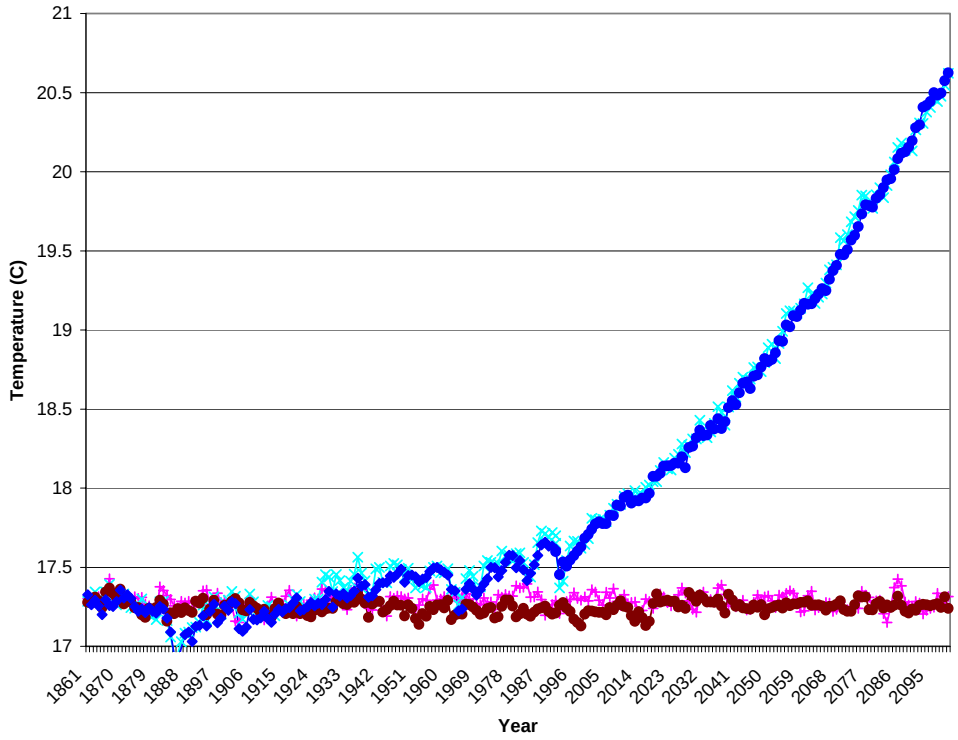


**Figure 54 – Globally averaged annually averaged sea surface temperature (C) , 1860 to 2100. Model A control run is in magenta circles, Model B control run is in pink pluses, Model A Scenario 2 is in blue diamonds, Model B Scenario 2 is in light blue crosses.**

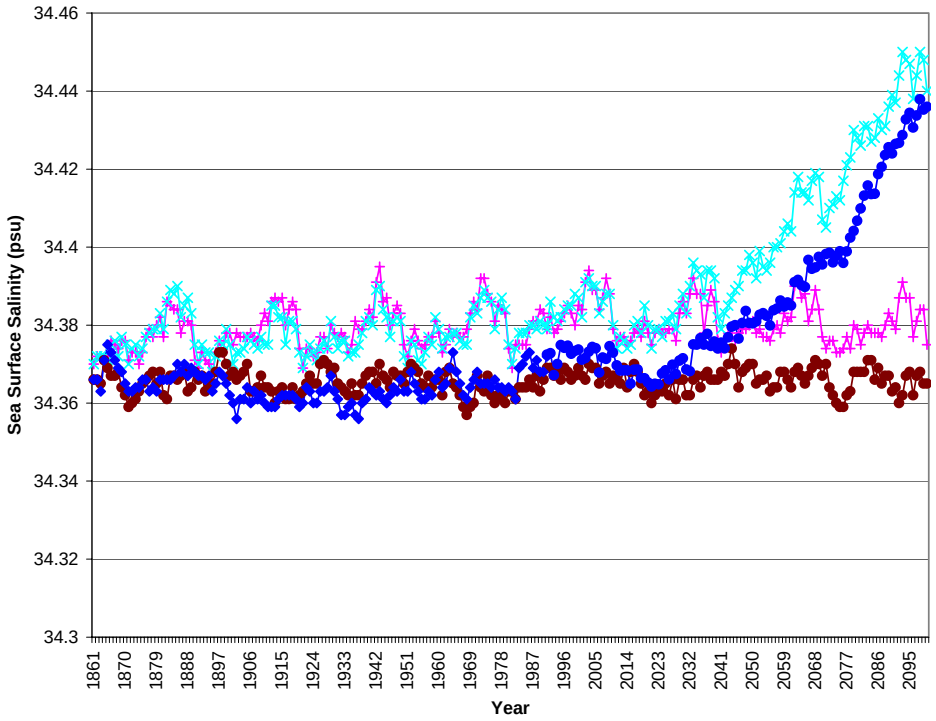


**Figure 55 – Globally averaged annually averaged sea surface salinity (pcu), 1860 to 2100. Model A control run is in magenta circles, Model B control run is in pink pluses, Model A Scenario 2 is in blue diamonds, Model B Scenario 2 is in light blue crosses.**

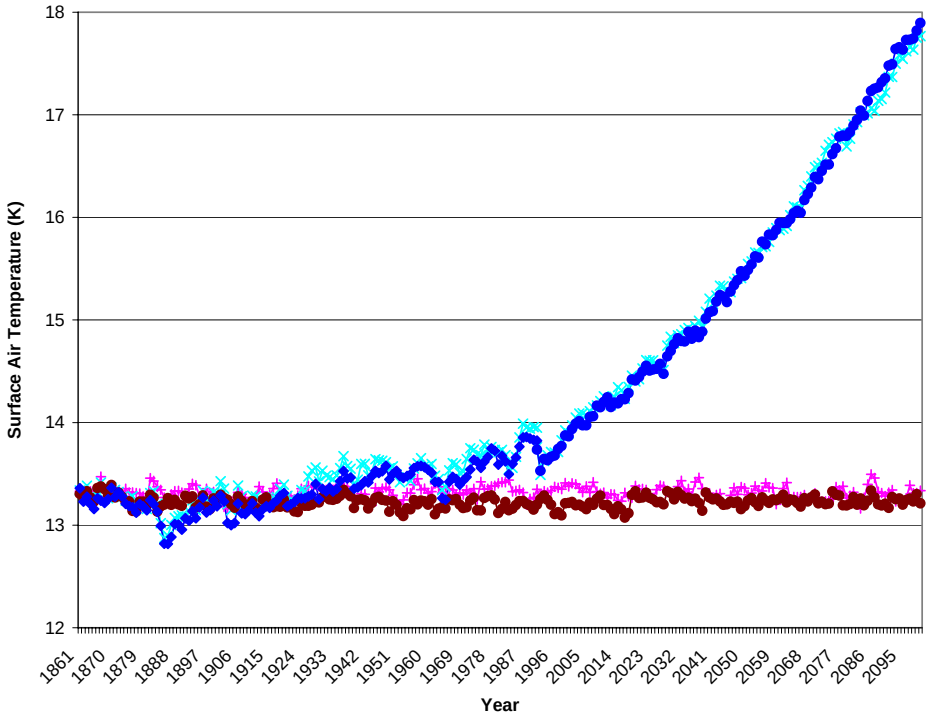


**Figure 56 – Globally averaged annually averaged surface air temperature (C), 1860 to 2100. Model A control run is in magenta circles, Model B control run is in pink pluses, Model A Scenario 2 is in blue diamonds, Model B Scenario 2 is in light blue crosses.**

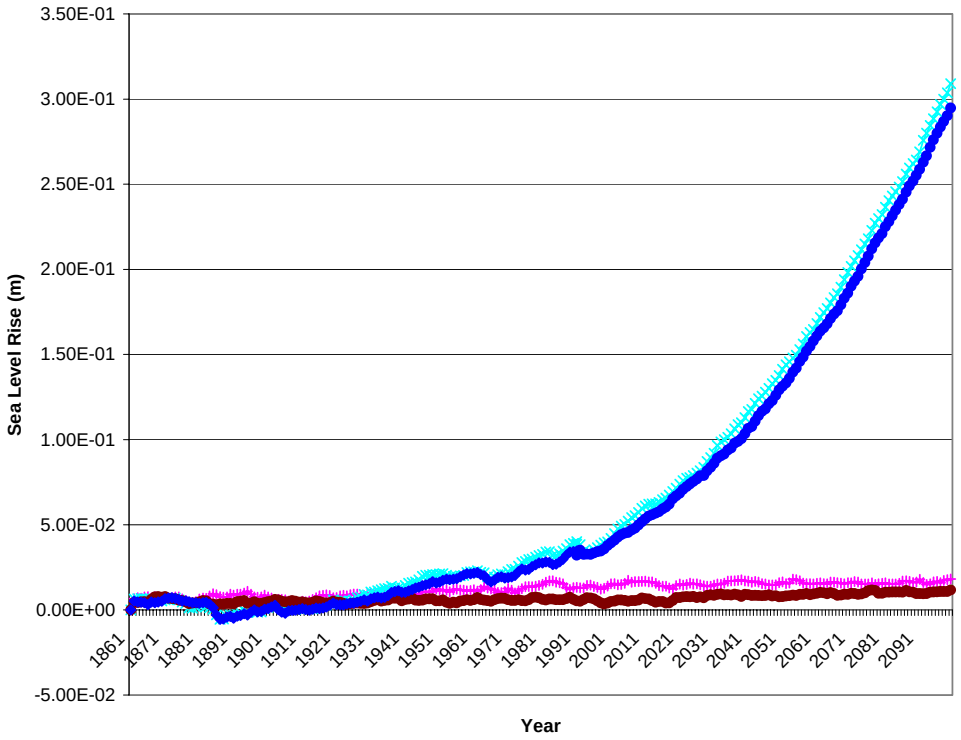


**Figure 57 – Globally averaged annually averaged sea level rise (m), 1860 to 2100. Model A control run is in magenta circles, Model B control run is in pink pluses, Model A Scenario 2 is in blue diamonds, Model B Scenario 2 is in light blue crosses.**

# CHAPTER 4: CONCLUSIONS & FUTURE WORK

## 4.1. SUMMARY

This study for the first time examines global variable wind stress datasets for short timescale spatial and temporal patterns. First we summarized the characteristics of the datasets and model used. Then we examined whether variable wind stress would change the mean state of the ocean or the model response to a forcing scenario. The following conclusions were obtained:

First, we find that the NCEP resolution is sufficient to capture some variable wind stress. NCEP monthly means and monthly standard deviations are of the same magnitude. Strong wind stress events (tropical cyclones) are observed. However, we could not reliably identify significant timescales or spatial patterns of the variable wind stress. An autocorrelation analysis on some few scattered points indicates a timescale of 2-5 days, that of an atmospheric synoptic system (i.e. eddies).

Second, we find that replacing no variable wind stress (Model A) with NCEP variable wind stress (Model B) significantly alters the mean ocean properties. Model B has a deeper Southern Ocean mixed layer depth than Model A, but shallower mixed layer depths elsewhere. These deeper (shallower) mixed layer depths match areas of decreased (increased) ocean heat content. Additionally, Model B shifts the position and increases the magnitude of the meridional heat flux, most notably on the peak values. Finally, the globally averaged surface temperatures indicate Model B is discernibly warmer than Model A (in agreement with increased sea surface salinity). Therefore variable wind stress can alter mean ocean properties.

Third, we have found that in a weak forcing scenario (observed forcing over the last century), ocean properties are sensitive to variable wind stress. All metrics indicate the global magnitude of ocean heat uptake increases in Model B compared to Model A. Spatially, most heat goes into upper layers and values appear to improve toward Levitus climatology or other observations. Internal modes of variability (such as an equatorial Pacific oscillation) are observed. Mixed layer depths improve toward the Levitus climatology, with the largest improvement in the Southern Ocean. The meridional overturning circulation is altered, a small but significant amount.

Fourth, we examined the response to two strong forcings scenarios: a 1% CO2 increase per year scenario, and a "business as usual" emissions scenario to 2100 from the MIT EPPA model. We find that Model A and Model B ocean metrics are very similar between scenarios. We believe this occurs because these global warming scenarios force the system very strongly, overwhelming any more subtle responses due to the differences in variable wind stress forcing.

Finally, we found that Model A demonstrated large periodic, non-sinusoidal annual deviations while Model B had much smaller deviation magnitudes. These results indicate that the high frequency variable wind stress (monthly or less) variable wind stresses can force a low frequency response regardless of forcing scenario. Fourier analysis indicates that the change in ocean metrics is due to a nearly uniform response over all frequencies less than a month, but it is unclear whether some frequencies are more important than others. Due to the lack of a strong excitation at inertial frequencies, we conclude the major source of annual variability of the MOC in this coarse resolution model, regardless of forcing, is surface wind variability (not internal model variability).

## 4.2. RECOMMENDATIONS FOR FUTURE WORK

This thesis has raised several more questions and recommendations for future work:

- Theoretical avenues
  - We observed a thirty year pattern in both Model A and Model B, which may be enhanced by our repetition of the 30 year NCEP variable wind stress dataset. What is the source? As a first step, we could randomly choose the NCEP winds each year to examine whether the response is an unidentified mode of variability in the data or a model response to representative wind stress fields.
  - Some studies have indicated that model behavior is very different between coupled and uncoupled models (Bugnion 2006). We should attempt to correlate the NCEP means to standard deviations and create a parameterization for variable wind stress as a function of the mean wind stress. The coupled model response to this parameterization may be very different from the uncoupled model response to the supplied variable wind stress.
  - A Fourier analysis indicates that in our coarse model, the ocean response to variable wind stress is a uniform increase at all frequencies. Future studies can examine the generality of this conclusion by forcing a model of finer spatial resolution with different temporal resolution of variable wind stress. If we could improve resolution of the shorter timescales, KPP will presumably better capture the oceanic inertial response.
- Model improvements
  - The observed pacific oscillation in the weak forcing scenario indicates that modes may exist in the model. Given sufficient computing resources, future studies should examine behavior from an ensemble of runs to remove any initial condition biases.
  - Recall we likened the GISS wind stress anomaly model to a no variability wind stress model. Future studies should employ a true no variable wind stress model.

# APPENDIX

Scenario 1 figures

Model A

Model B

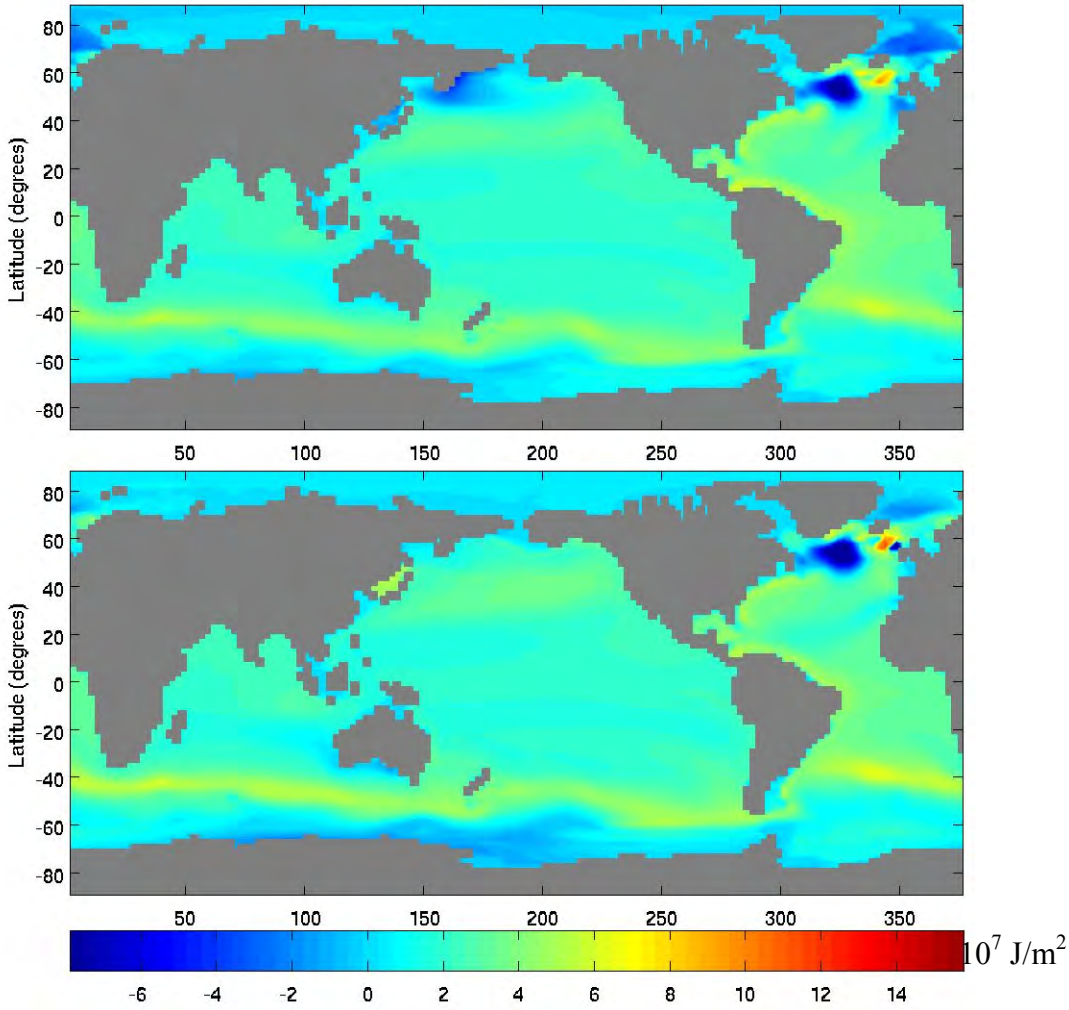


**Figure 58 - Ocean Heat Uptake, Scenario 1 minus the control run. Values are from an average of years 1-5 to an average of year 60-65. Depth range is 0-3000m, units of annual average $10^7$ J/m$^2$. Depths 0-700m (thermocline only) yield similar spatial patterns to depths 0-3000m (but smaller magnitudes).**

Model A

Model B

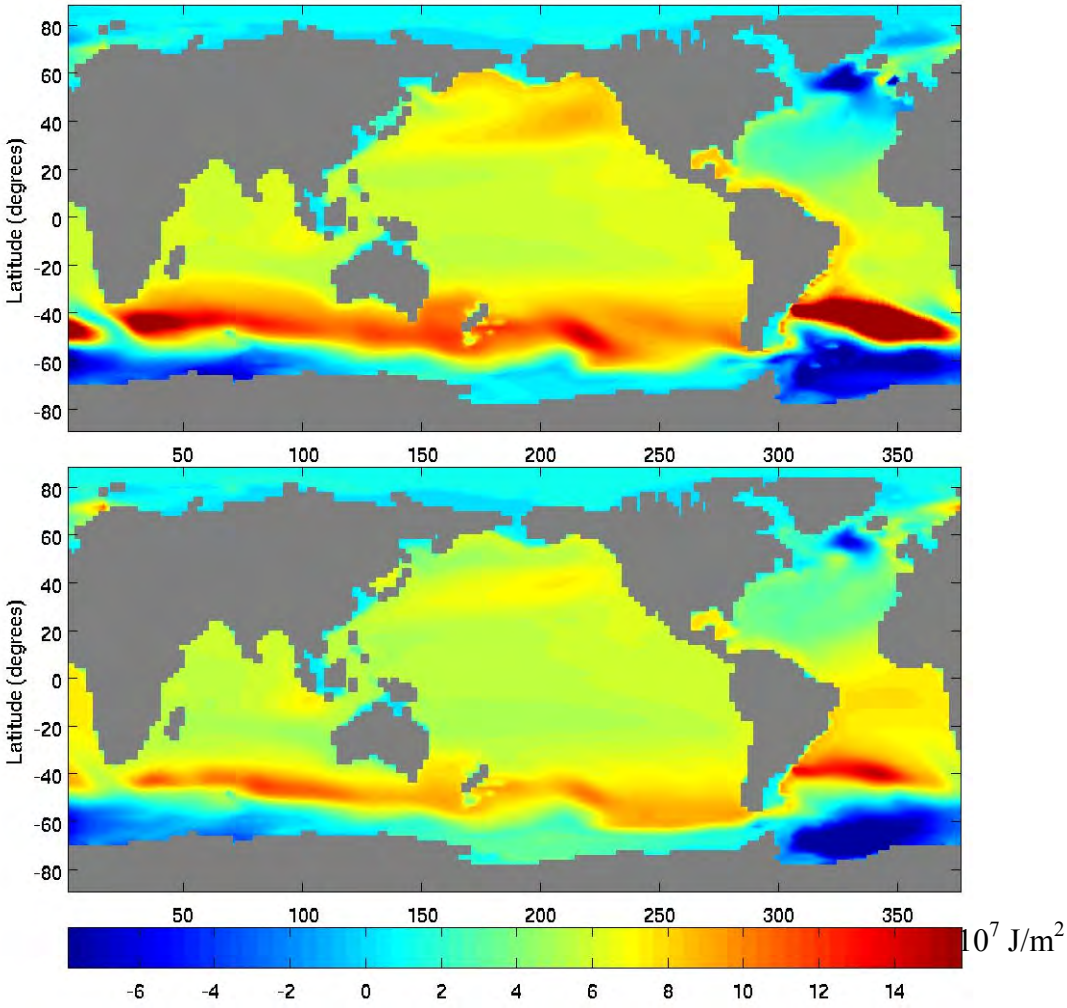


**Figure 59 - Ocean Heat Uptake, Scenario 1 minus the control run. Values are from an average of years 65-70 to an average of year 125-130. Depth range is 0-3000m, units of annual average $10^7$ J/m$^2$. Depths 0-700m (thermocline only) yield similar spatial patterns to depths 0-3000m (but smaller magnitudes).**

Model A

Model B

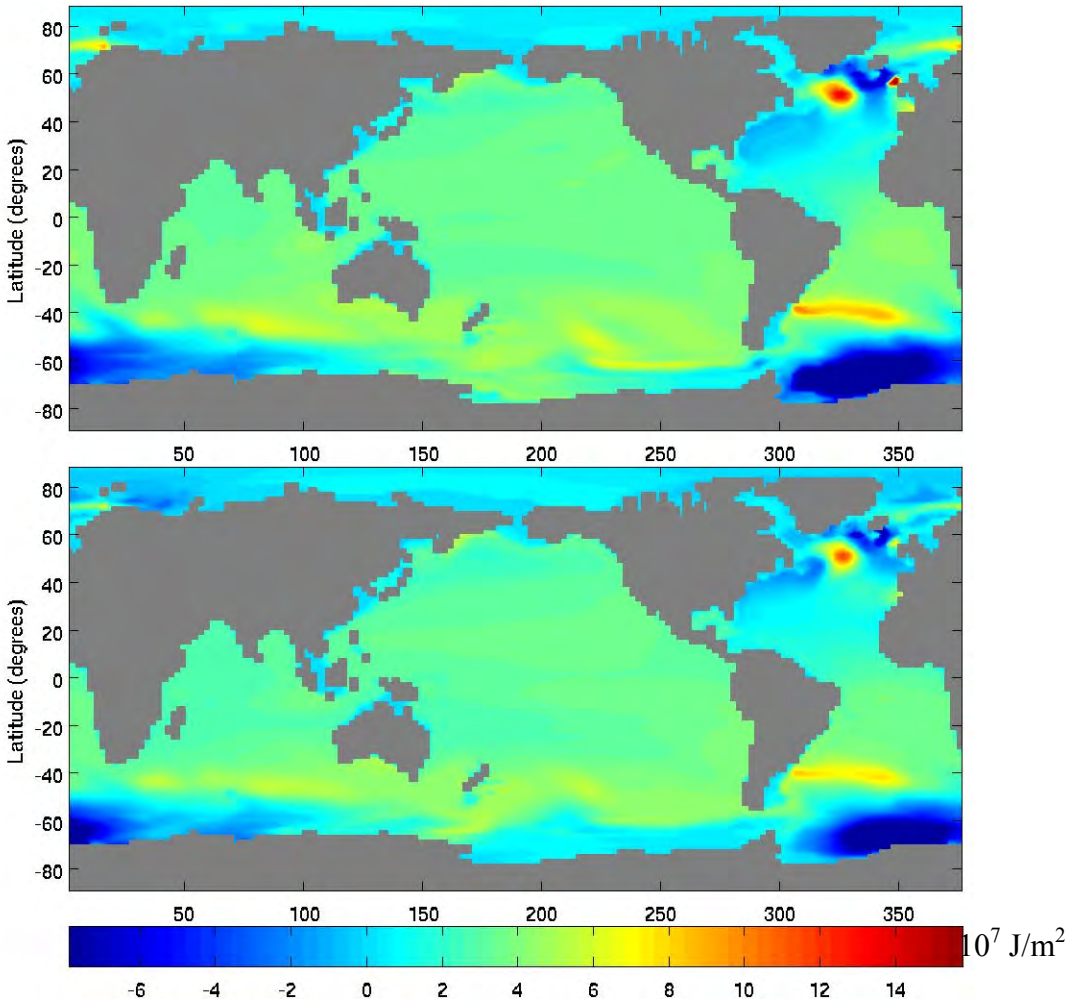


**Figure 60 – Difference image; Figure 59 minus Figure 58, (annual average $10^7$ J/m$^2$). Depth range is 0-3000m, units of annual average $10^7$ J/m$^2$. Depths 0-700m (thermocline only) yield similar spatial patterns to depths 0-3000m (but smaller magnitudes).**

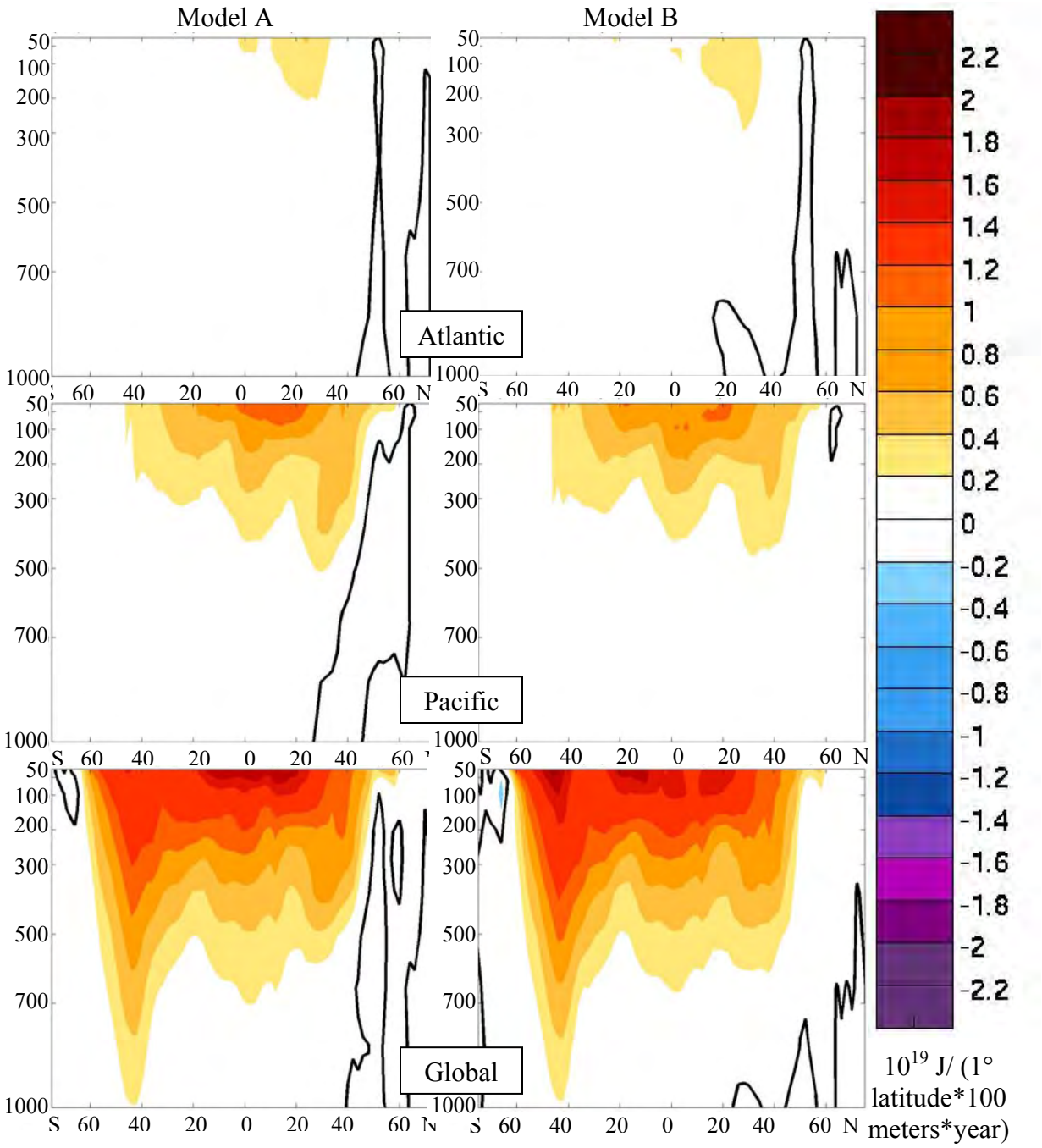


**Figure 61 - Zonally integrated ocean heat uptake in 1° latitude belts for 100m thick layers, average of years 1-5 to average of years 60-65 ($10^{19}$ J/(1° latitude*100 meters*year) ), Scenario 1 minus the control run. X-axis is latitude (80°S to 80°N), Y axis is depth (0-1000m). Note the contour range is quadruple of Figure 37. Heat uptake values are plotted at the midpoint of each 100-m layer.**

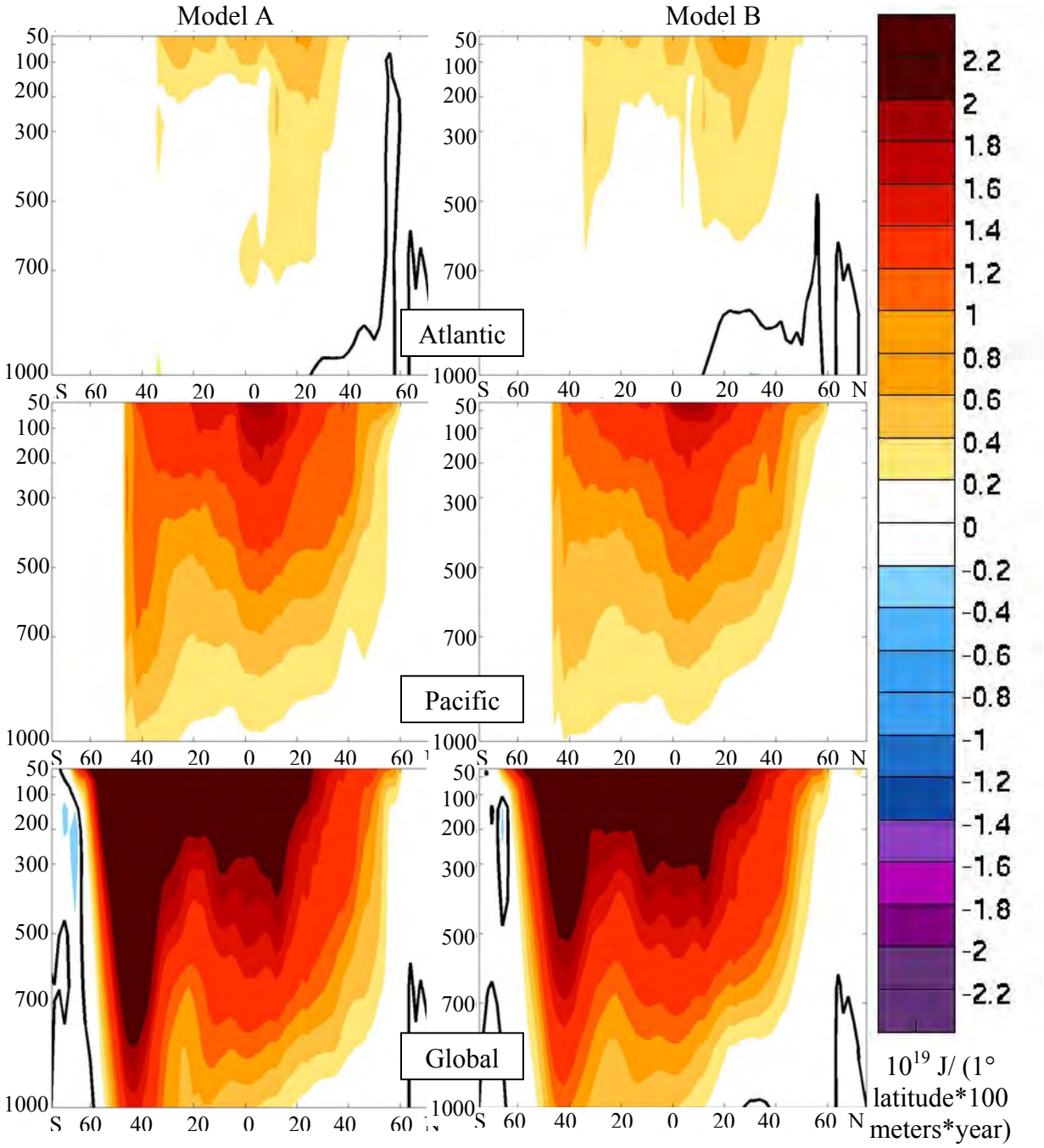


**Figure 62 - Zonally integrated ocean heat uptake in 1° latitude belts for 100m thick layers, average of years 65-70 to average of years 125-130 ($10^{19}$ J/(1° latitude*100 meters*year) ), Scenario 1 minus the control run. X-axis is latitude (80°S to 80°N), Y axis is depth (0-1000m). Note the contour range is quadruple of Figure 37. Heat uptake values are plotted at the midpoint of each 100-m layer.**

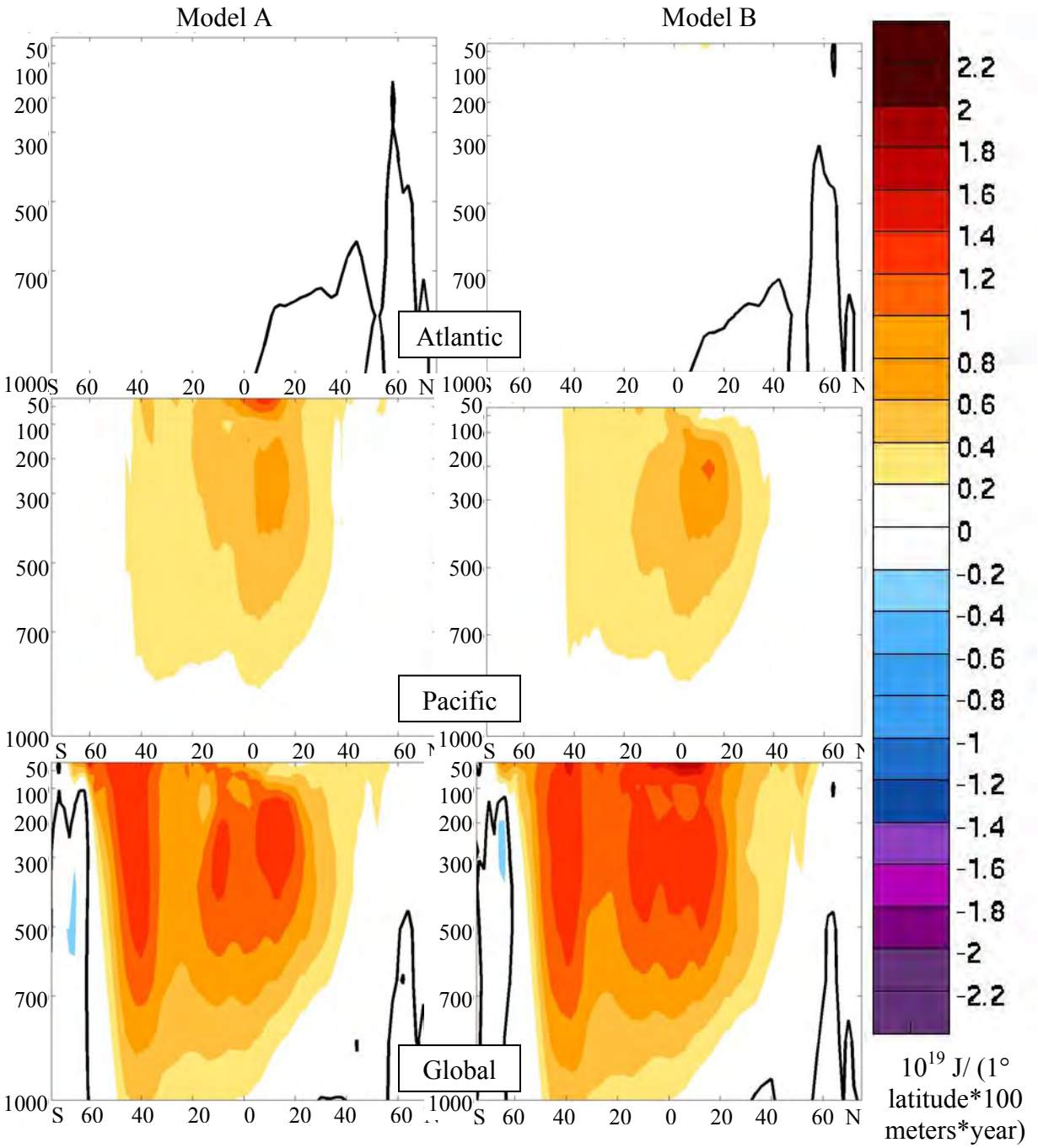


**Figure 63 – Difference image; Figure 62 minus Figure 61, ($10^{19}$ J/(1° latitude*100 meters*year) ). X-axis is latitude (80°S to 80°N), Y axis is depth (0-1000m). Note the contour range is quadruple of Figure 37. Heat uptake values are plotted at the midpoint of each 100-m layer.**

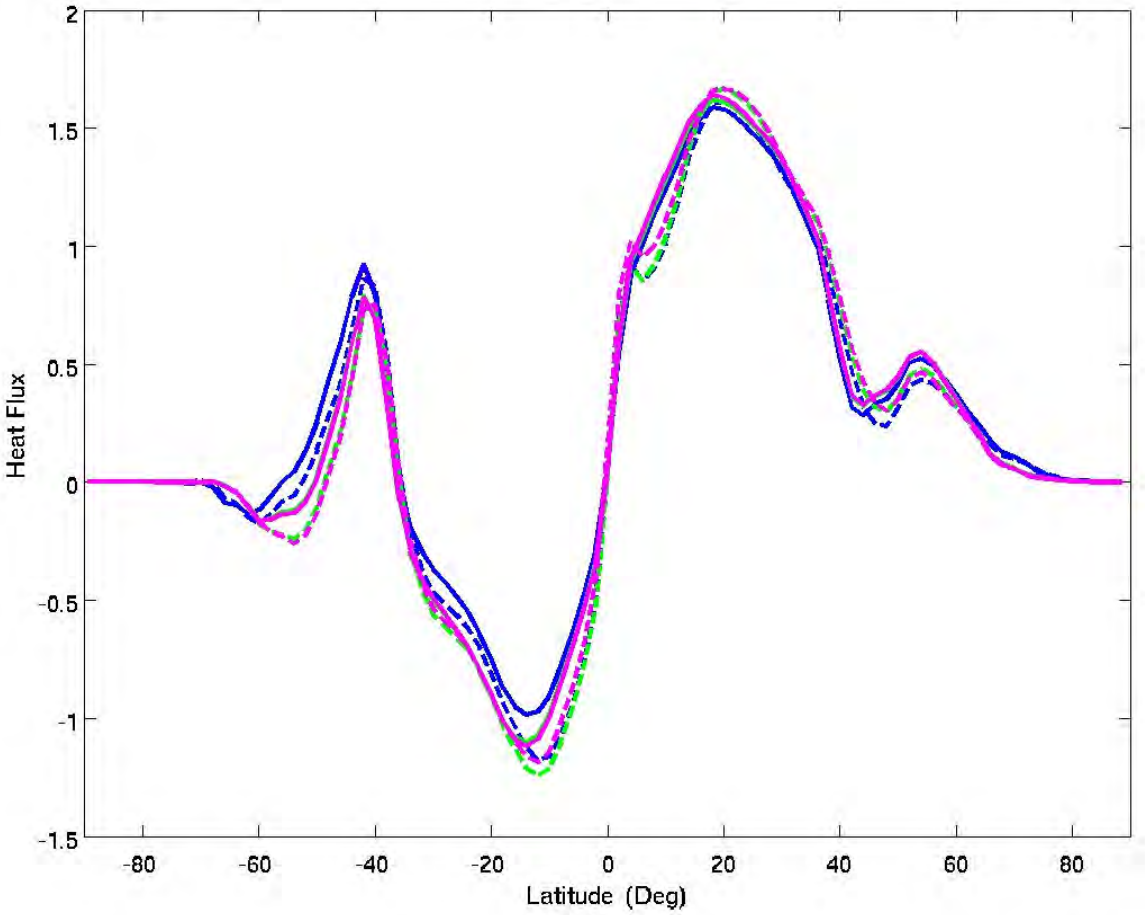


**Figure 64 - Meridional Heat Flux (PW), Scenario 1 minus the control run. Model A is in solid lines, Model B is blue lines. Average of Years 1-5 is pink, average of Years 65-70 is green, average of Years 125-130 is blue.**

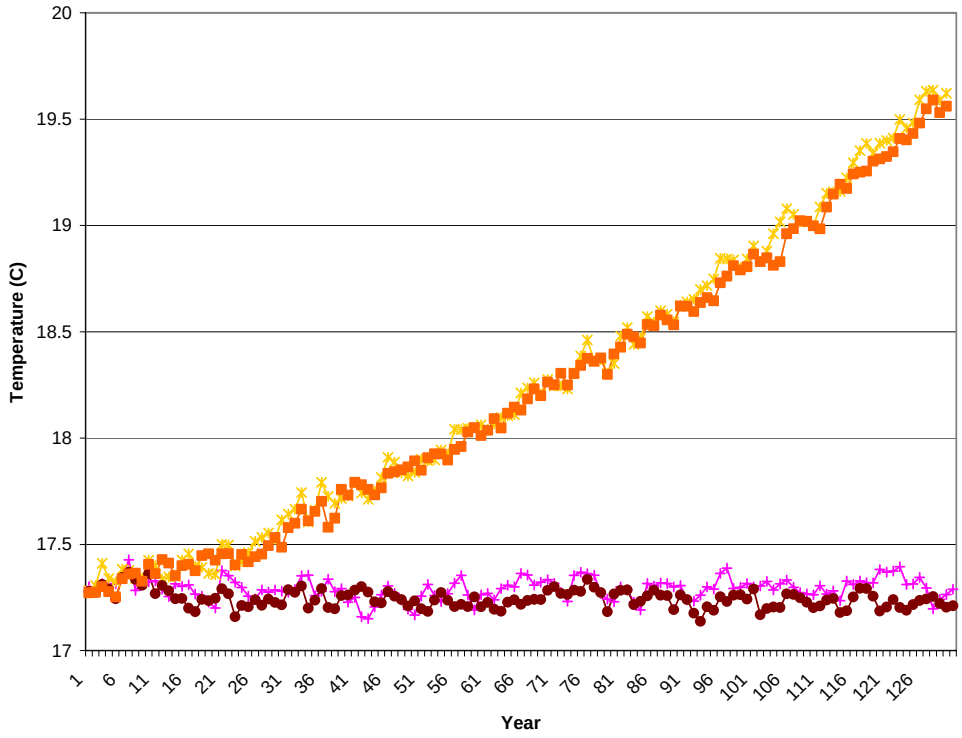


**Figure 65 – Globally averaged annually averaged sea surface temperature (C), Year 1 to 130. Model A control run is in magenta circles, Model B control run is in pink pluses, Model A Scenario 1 is in orange squares, Model B Scenario 1 per year run is in yellow stars.**

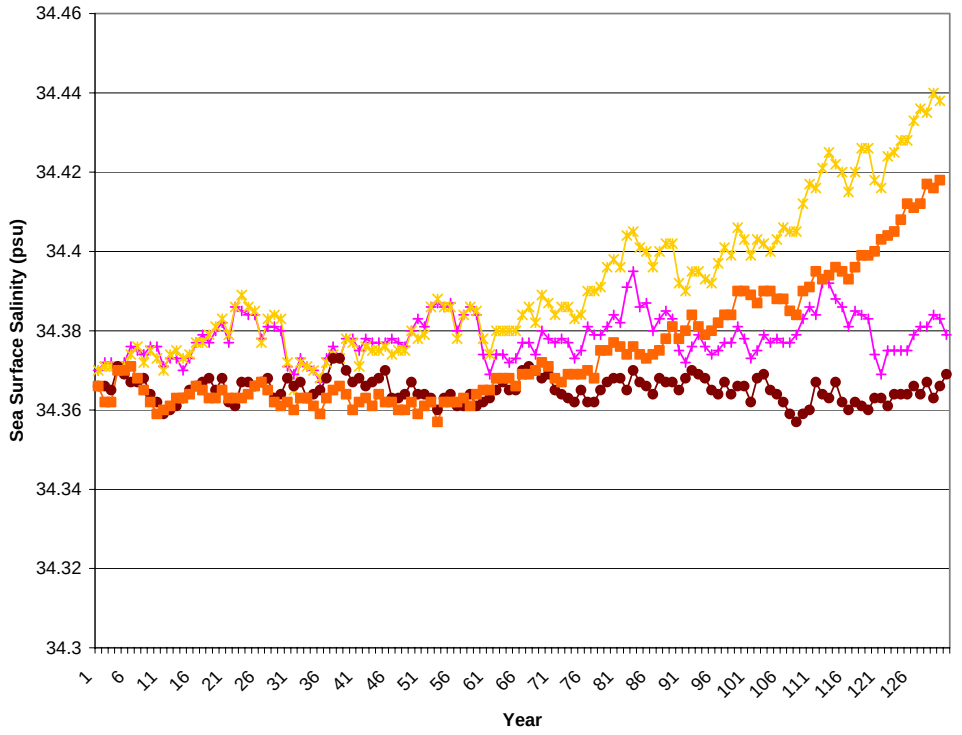


**Figure 66 – Globally averaged annually averaged sea surface salinity (psu) , Year 1 to 130. Model A control run is in magenta circles, Model B control run is in pink pluses, Model A Scenario 1 is in orange squares, Model B Scenario 1 per year run is in yellow stars.**

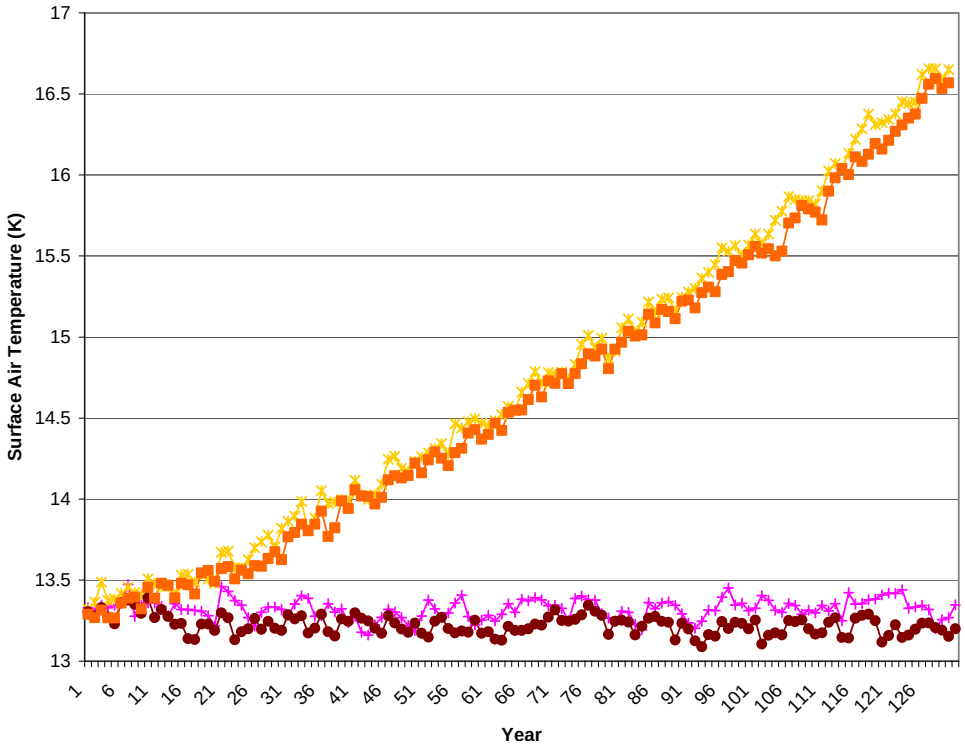


**Figure 67 – Globally averaged annually averaged surface air temperature (C) , Year 1 to 130. Model A control run is in magenta circles, Model B control run is in pink pluses, Model A Scenario 1 is in orange squares, Model B Scenario 1 per year run is in yellow stars.**

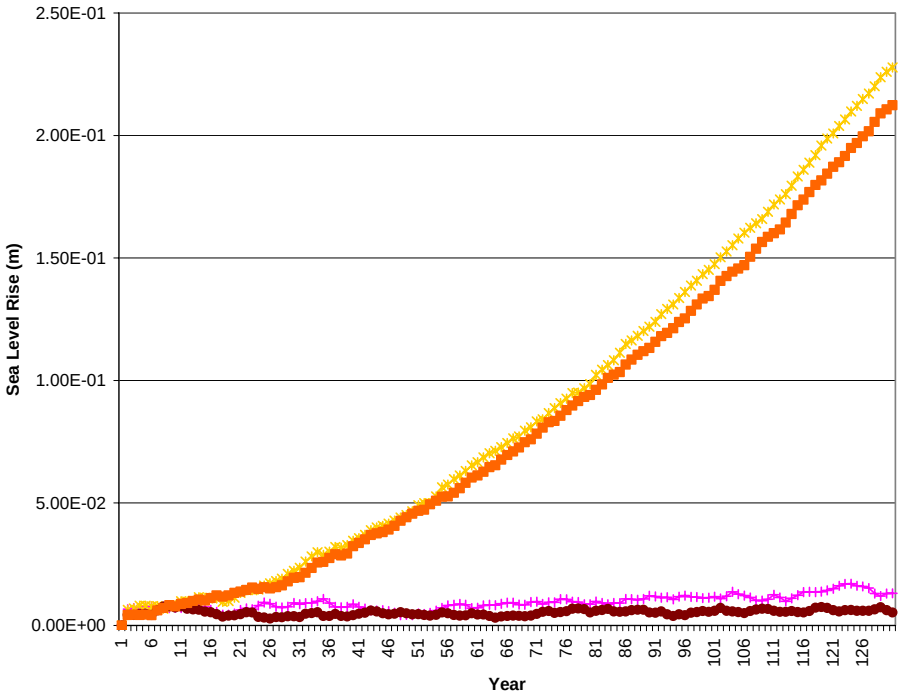


**Figure 68 – Globally averaged annually averaged sea level rise (m), Year 1 to 130. Model A control run is in magenta circles, Model B control run is in pink pluses, Model A Scenario 1 is in orange squares, Model B Scenario 1 per year run is in yellow stars.**

# REFERENCES


M. Babiker, J. Reilly, M. Mayer, R. Eckaus, I. Sue Wing, and R. Hyman. "The MIT Emissions Prediction and Policy Analysis (EPPA) Model: Revisions, Sensitivities, and Comparison of Results" MIT Joint Program on the Science & Policy of Global Change, Report No. 71, (2001).

T. P. Barnett, D. W. Pierce, and R. Schnur, 2001. "Detection of anthropogenic climate change in the world's oceans". *Science*, 292, 270-274.

T. P. Barnett, D. W. Pierce, K. AchutaRao, P. Gleckler, B. Santer, J. Gregory, and W. Washington, 2005. "Penetration of human-induced warming into the world's oceans". *Science*, 309, 284-287.

V. Bugnion, C. Hill, and P.H. Stone, 2006. "An Adjoint Analysis of the Meridional Overturning Circulation in an Ocean Model". *Journal of Climate*, 19, 3732-3750.

Canadian Centre for Climate Modeling and Analysis. "CCCma: CGCM1 and CGCM2 Runs Forcing, Equivalent CO2 Concentrations used in CCCma coupled global model." [http://www.cccma.ec.gc.ca/data/cgcm/cgcm_forcing.shtml].

J.A. Church, et al., 2001. "Changes in sea level". In: Climate Change 2001: The Scientific Basis. Contribution of Working Group I to the Third Assessment Report of the Intergovernmental Panel on Climate Change. [Houghton, J.T., et al. (eds.)]. Cambridge University Press: Cambridge, pp. 639–693.

M. Collins, C.M. Brierley, M. MacVean, B.B.B.Booth, G.R. Harris, 2007. "The Sensitivity of the Rate of Transient Climate Change to Ocean Physics Perturbations." *Journal of Climate,* 20, 2315-2320.

F. Dalan, P.H. Stone, I. Kamenkovich, and J. Scott, 2005. "Sensitivity of Climate to Diapycnal Diffusivity in the Ocean Part I: Equilibrium State". *Journal of Climate*, 18, 2460-2481.

S. Dutkiewicz, A. Sokolov, J. Scott, P. Stone, 2005. "A Three-Dimensional Ocean-Seaice-Carbon Cycle Model and its Coupling to a Two-Dimensional Atmospheric Model: Uses in Climate Change Studies." MIT Joint Program on the Science and Policy of Global Change, Report No.122.

K. Emanuel. Divine Wind: The History and Science of Hurricanes. Oxford University Press: New York, 2005.

K. Emanuel, 2001. "The contribution of tropical cyclones to the oceans' meridional heat transport". *Journal of Geophysical Research*, 106, 14xx-1481.

R. Ferrari, submitted 2006. "Eddy-mixed layer interactions in the ocean". Submitted

*Oceanography*.

R. Ferrari., and J. McWilliams, 2005. "Parameterization of Eddy Fluxes near Oceanic Boundaries". Submitted to *J of Climate*.

C.E. Forest, P. H. Stone, A. P. Sokolov, M. R. Allen, and M. D. Webster, 2002. "Quantifying uncertainties in climate system properties with the use of recent climate observations". *Science*, 295, 113–117.

C.E. Forest, P. H. Stone, A. P. Sokolov, 2005. "Estimated PDFs of climate system properties including natural and anthropogenic forcings". *Geophys. Res. Letters*, 33, L01705.

C.E. Forest, P. H. Stone, A. P. Sokolov, 2008. "Constraining Climate Model Parameters From Observed 20th Century Changes". *Tellus*, in press.

P. Gent, and J. McWilliams, 1990. "Isopycnal mixing in ocean circulation models". *J. Physical Oceanography*, 20: 150-155.

V. Gouretski and K.P. Koltermann, 2007. "How much is the ocean really warming?" *Geophys. Res. Let*., 34(L01610), doi:10.1029/2006GL027834.

J. M. Gregory, 2000. "Vertical heat transports in the ocean and their effect on time-dependent climate change". *Climate Dynamics*, 16, 501-515.

S. Griffies, 1998. "The Gent-McWilliams Skew Flux". *J. of Physical Oceanography*, 28, 831-841.

D. L. Hartmann. Global Physical Climatology. Academic Press: San Diego, 1994.

B. Huang, P. H. Stone and C. Hill, 2003. "Sensitivities of deep-ocean heat uptake and heat content to surface fluxes and subgrid-scale parameters in an ocean general circulation model with idealized geometry". *J. of Geophys. Research*, 108, 3015.

IPCC, 2007: Climate Change 2007: The Physical Science Basis. Contribution of Working Group I to the Fourth Assessment Report of the Intergovernmental Panel on Climate Change [Solomon, S., D. Qin, M. Manning, Z. Chen, M. Marquis, K.B. Averyt, M.Tignor and H.L. Miller (eds.)]. Cambridge University Press, Cambridge, United Kingdom and New York, NY, USA.

M. Ishii, M. Kimoto, K. Sakamoto, S. Iwasaki, 2006. "Steric Sea Level Changes Estimated from Historical Ocean Subsurface Temperature and Salinity Analyses". *Journal of Oceanography*, 62, 155-170.

I. S. F. Jones and Y. Toba. Wind Stress Over the Ocean. Cambridge University Press:

Cambridge, 2001.

A. Köhl and P. Heimbach, August 15, 2007. "A note on parameterizations of the drag coefficient". Internal MIT Document.

I. Kamenkovich, 2005. "Role of daily surface forcing in setting the temperature and mixed layer structure of the Southern Ocean". *Journal of Geophysical Research*, Vol 110 C07006, doi:10.1029/2004JC002610.

I. Kamenkovich, A. Sokolov, and P.H. Stone, 2002. "An efficient climate model with a 3D ocean and statistical-dynamical atmosphere". *Climate Dynamics*, 19, 585-598.

R. Korty, 2005. "On the maintenance of weak meridional temperature gradients during warm climates". PhD Thesis, MIT.

W. G. Large, J. C. McWilliams, S.C. Doney, 1994. "Oceanic Vertical Mixing: A Review and a Model with a Nonlocal Boundary Layer Parameterization". *Review of Geophysics*, 32, 363-403.

S. Levitus, J. Antonov, and T. Boyer, 2005. "Warming of the world ocean, 1955–2003". *Geophysical Research Letters,* 32, L02604.

M. S. Lozier, S. Leadbetter, R. Williams, W. Roussenov, M. Reed, and N. Moore, 2008. "The Spatial Pattern and Mechanisms of Heat-Content Change in the North Atlantic". *Science,* 319, 800.

J. Liu, J.A. Curry, and D.G. Martinson, 2004. "Interpretation of recent Antarctic sea ice variability". *Geophys. Res. Lett*., 31, L02205, doi:10.1029/2003GL018732.

J. Marshall, A. Adcroft, J.M. Campin, P. Heimbach, A. Molod, S. Dutkiewicz, H.Hill, M. Losch, B. Fox-Kemper, D. Menemenlis, D. Ferreira, E. Hill, M. Follows, C. Hill, C. Evangelinos, G. Forget, 2004. "MITGCM User Manual". *Internal Document,* MIT Department of EAPS.

J. Marshall, E. Shuckburgh, H. Jones, and C. Hill, 2006. "Estimates and Implications of Surface Eddy Diffusivity in the Southern Ocean Derived from Tracer Transport". *Journal of Physical Oceanography*, 36, 1806-1821.

M. Mayer, R. Hyman, J. Harnisch and J. Reilly. "Emissions Inventories and Time Trends for Greenhouse Gases and other Pollutants". MIT Joint Program on the Science & Policy of Global Change, Technical Note1, July 2000.

National Oceanic & Atmospheric Administration. "ESRL : PSD : NCEP/NCAR Reanalysis at CDC". [http://www.cdc.noaa.gov/cdc/reanalysis/reanalysis.shtml].Data on halo /disk30/reanal/NCEP-NCAR-reanalysis/dailyavgs/surface .

J. Pedlosky. Ocean Circulation Theory. Spring: Berlin, 1998.

J. Pexioto and A. Oort . Physics of Climate. Springer-Verlager: New York, 1992.

D. Pierce and T. Barnett, 2005. "Anthropogenic Warming of the Oceans: Observations and Model Results". *Submitted to J. of Climate.*

M. D. Powell, S. H. Houston, L. R. Amat, and N Morisseau-Leroy, 1998. "The HRD real-time hurricane wind analysis system". *J. Wind Engineer. and Indust. Aerodyn.* 77&78, 53-64

M. Redi, 1982. "Ocean Isopycnal Mixing by Coordinate Rotation". *J of Physical Oceanography*, 12, 1154-1158.

A.P. Sokolov, P.H.Stone, 1995. "Description and Validation of the MIT Version of the GISS 2-D Model." MIT Joint Program on the Science and Policy of Global Change, Report Number 2.

A.P. Sokolov, C.A. Schlosser, S. Dutkiewicz, S. Paltsev, D.W. Kicklighter, H.D. Jacoby, R.G. Prinn, C.E. Forest, J. Reilly, C. Wang, B. Felzer, M.C. Sarofim, J. Scott, P.H. Stone, J.M. Melillo and J. Cohen, July 2005. "The MIT Integrated Global System Model (IGSM) Version 2: Model Description and Baseline Evaluation". MIT Joint Program on the Science and Policy of Global Change, Report 124.

S. Sun and J. Hansen, 2003. "Climate Simulations for 1951-2050 with a Coupled Atmosphere-Ocean Model". *Journal of Climate,* 16, 2807-2826.

K. M. Trenberth, J. Olson, and W. G. Large, 1990. "The mean annual cycle in Global Ocean wind stress". *J. Phys. Oceanogr.*, 20, 1742-1760.

Trenberth, and J. M. Caron, 2001. "Estimates of meridional atmosphere and ocean heat transports". *Journal of Climate*, 14, 3433–3443.

M. Webster, C. Forest, J. Reilly, M. Babiker, D. Kicklighter, M. Mayer, R. Prinn, M. Sarofim, A. Sokolov, P. Stone and C. Wang. "Uncertainty Analysis of Climate Change and Policy Response". MIT Joint Program on the Science & Policy of Global Change, Report No. 95, December 2002.

D.S. Wilkes. Statistical Methods in the Atmospheric Sciences. Elsevier: Amsterdam, 2006.

J.K. Willis, D. Roemmich, B. Cornuelle, 2004. "Interannual variability in upper ocean heat content, temperature, and thermosteric expansion on global scales". *J. Geophys. Res.*, 109, C12036 doi:10.1029/2003JC002260.

C. Wunsch, R. Ferrari, 2004. "Vertical Mixing, Energy, and the General Circulation of the Oceans". *Annu. Rev. Fluid Mech.,* 36, 281-314.

C. Wunsch, P. Heimbach, 2008. "The Global Zonally Integrated Ocean Circulation (MOC) 1992-2006: Seasonal and Decadal Variability". Personal communication.

C. Wunsch, 2005. "The Total Meridional Heat Flux and Its Oceanic and Atmospheric Partition". *Journal of Climate*, 18, 4374-4380.

Stone & Yao, 1990. "Development of a Two-Dimensional Zonally Averaged Statistical-Dynamical Model. Part III: The Parameterization of the Eddy Fluxes of Heat and Moisture". *Journal of Climate*, 3, 725-740.